

Integrating remotely sensed hydrologic parameters into an index of sediment connectivity

Anna-Klara Ahlmer

June 2017

Supervisor:

Zahra Kalantari, KTH

Klas Hansson, Trafikverket

Examiner:

Ulla Mörtberg, KTH

Abstract

The expected increase in precipitation and temperature in Scandinavia, and especially short-time heavy precipitation, will increase the frequency of flooding. Urban areas are the most vulnerable, and specifically, the road infrastructure. The accumulation of large volumes of water and sediments on road-stream intersections gets severe consequences for the road drainage structures. The need for a tool to identify characteristics that impacts the occurrence of flooding, and to predict future event is thus essential.

This study integrates the spatial and temporal soil moisture properties into the research about flood prediction methods. Soil moisture data is derived from remote sensing techniques, with focus on the soil moisture specific satellites ASCAT and SMOS. Furthermore, several physical catchments descriptors (PCDs) are used to identify catchment characteristics that are prone to flooding and an inventory of current road drainage facilities are conducted. Finally, the index of sediment connectivity (IC) by Cavalli, Trevisani, Comiti, and Marchi (2013) is implemented to assess the flow of water and sediment within the catchment. A case study of two areas in Sweden, Västra Götaland and Värmland, that was affected by severe flooding in August 2014 are included.

The results show that the method with using soil moisture satellite data is promising for the inclusion of soil moisture data into estimations of flooding and the index of sediment connectivity.

Key words: *Flooding, road infrastructure, soil moisture, remote sensing, sediment connectivity*

Sammanfattning

De förväntade ökningarna i nederbörd och temperatur i Skandinavien, och speciellt extrem korttidsnederbörd, kommer att öka frekvensen av översvämningar. Urbana områden är de mest sårbara, och speciellt väginfrastrukturen. Ackumuleringen av stora volymer av vatten och sediment där väg och vattendrag möts leder till allvarliga konsekvenser för dräneringskonstruktionerna. Behovet av ett verktyg för att identifiera egenskaper som påverkar förekomsten av översvämningar, och för att förutsäga framtida händelser är väsentligt.

Studien integrerar markfuktighet både rumsligt och tidsmässigt i forskningen om metoder för översvänningsrisker. Markfuktighetsdata är inkluderat från fjärranalysteknik, med fokus på de specifika satelliterna för markfuktighet, ASCAT och SMOS. Vidare är flertalet faktorer (PCDs) inkluderade för att identifiera egenskaper i avrinningsområden som är benägna till översvämning samt en inventering av nuvarande vägdräneringskonstruktioner. Slutligen är ett index med sediment connectivity (Cavalli et al., 2013) implementerat för att se flödet av vatten och sediment inom avrinningsområdet. En fallstudie med två områden i Sverige, Västra Götaland och Värmland, som drabbades av allvarliga översvämningar i augusti 2014 är inkluderat.

Resultaten visar att metoden att använda markfuktighet från satellitdata är lovande för inkludering i uppskattningar av översvänningsrisk och i indexet med sediment connectivity.

Acknowledgements

I would like to thank the persons that contributed to the realization of this master thesis. At first, my supervisor Zahra Kalantari for her endless help and guidance, her input and contribution to this project. Her inspiration and devotion enhances the result of this study. I would also like to thank Alexander Koutsouris, Marika Wennbom and Guillaume Vigouroux for help with input data and useful discussions. Further, a special thanks to Marco Cavalli and Stefano Crema for their guidance, helpfulness, and hospitality during my stay at CNR in Padova, Italy.

I would also want to thank Klas Hansson and Eva Liljegren at Trafikverket for their feedback, contribution and interest in the topic. Furthermore, to the Bolin Centre for climate research for the funding of the project.

Finally, I would like to thank my mother, Ingela Ahlmer, for her invaluable help and support in the process.

Anna-Klara Ahlmer

June 2017

Table of contents

1 INTRODUCTION	1
1.1 Background	1
1.1.1 Climate change that affects flooding.....	1
1.1.2 Behaviour of the road infrastructure due to climate change.....	1
1.1.3 The influence of the road infrastructure on sediment transfer	3
1.2 Problem definition.....	4
1.3 Aim and objectives.....	4
2 LITERATURE REVIEW	5
2.1 Soil Moisture.....	5
2.1.1 The soil moisture content and affecting factors	5
2.1.2 Measuring soil moisture.....	6
2.2 Remote Sensing.....	7
2.2.1 Remote sensing in flood forecasting	7
2.2.2 Soil moisture retrieval from remote sensing technology	8
2.3 Sediment connectivity index (IC)	10
2.3.1 The concept of sediment connectivity	10
2.3.2 Previous studies in the subject of connectivity	11
3 METHOD	12
3.1 Case Study	12
3.1.1 Västra Götaland.....	13
3.1.2 Värmland.....	15
3.2 Precipitation data.....	16
3.2.1 Ground station measurements	16
3.2.2 Precipitation radar measurements	16
3.3 Choice of satellite data	17
3.3.1 ASCAT 25 km spatial resolution	17
3.3.2 ASCAT 1 km spatial resolution	18
3.3.3 SMOS	20
3.3.4 Satellite data processing.....	20
3.4 Sediment connectivity index (IC)	21
3.4.1 The index of sediment connectivity	21
3.4.2 Sediment connectivity calculations	22
3.5 Assumptions.....	23

4 RESULTS	24
4.1 Road drainage structures	24
4.2 Precipitation	25
4.2.1 Ground station measurements	25
4.2.2 Precipitation radar measurements	26
4.3 Satellite soil moisture values	28
4.3.1 Comparison between satellites	28
4.3.2 Results ASCAT 25 km	29
4.3.3 Results ASCAT 1 km	31
4.3.4 Results SMOS	32
4.4 Sediment connectivity results	33
4.4.1 The different IC calculations.....	33
4.4.2 Site specific results of IC	35
5 DISCUSSION	37
5.1 Comparison between PCDs, precipitation and soil moisture	37
5.1.1 Västra Götaland.....	37
5.1.2 Värmland.....	37
5.1.3 Summary	38
5.2 Sediment connectivity index.....	38
5.3 Comparison of flood prediction methods	39
5.4 Application and validation of remote sensing data	39
5.4.1 Application difficulties	39
5.4.2 Validating issues.....	40
5.4.3 Soil moisture retrievals from satellite data	41
5.5 Limitations and possibilities with the methods used.....	42
5.5.1 Limitations	42
5.5.2 Possibilities	43
CONCLUSION	44
RECOMMENDATIONS	45
REFERENCES	46
APPENDIX	55
APPENDIX A. PCD overview.....	55
APPENDIX B. Sediment connectivity index calculations.....	57
APPENDIX C. Road drainage constructions from BaTMan	60
APPENDIX D. Soil moisture values ASCAT 25km, ASCAT 1km and SMOS 50km	61
APPENDIX E. IC results	62

List of figures

Figure 1. The different soil zones, where A and B represent two distinct volumes of soil moisture (Seneviratne et al., 2010).....	6
Figure 2. Study areas in southwest Sweden	12
Figure 3. Study area of Värmland and Västra Götaland with flooded and non-flooded points	13
Figure 4. E6 flooded in Västra Götaland (Bohuslänningen, 2014-08-21)	14
Figure 5. Railway embankment at Bohusbanan damaged (Småröd) (Bohuslänningen, 2014-08-21)...	14
Figure 6. Soil type and land use for Västra Götaland with flooded and non-flooded points, roads and watersheds.....	14
Figure 7. Lagmansgatan collapsed due to the heavy precipitation (SverigesRadio, 2014-08-21).....	15
Figure 8. Östra Ringvägen was flooded (SVT nyheter Värmland, 2014-08-23).....	15
Figure 9. Soil type and land use for Värmland with flooded and non-flooded points, roads and watersheds.....	16
Figure 10. Definition of the index of sediment connectivity. Modified by (Crema, Schenato, Goldin, Marchi, & Cavalli, 2015) from the original index by (Borselli et al., 2008)	21
Figure 11. Culverts under E6 at Hogsbotorpsmotet. Retrieved from Google Maps. Image taken in October 2009, before the event.	24
Figure 12. Stone culvert under E18 at IKEA, Värmland. Retrieved from Google Maps. Image taken in May 2011, before the event.....	24
Figure 13. Precipitation per 15 minutes. 21st of August for Värmland and 19th of August for Västra Götaland, with large amounts of precipitation during 15 minutes.	27
Figure 14. Correlation between the ASCAT 25 km resolution, ASCAT 1 km resolution and SMOS satellite. The location shown is IKEA, Värmland.....	28
Figure 15. Soil moisture content from ASCAT 25 km resolution satellite for Västra Götaland and Värmland (EUMETSAT, 2017). The values are the 19th of August for Västra Götaland and the 21st of August for Värmland. Each pixel corresponds to 25 km.....	30
Figure 16. Soil moisture content from ASCAT 1 km resolution satellite (HSAF, 2017). Soil moisture values for each passing of the satellite the 21st of August at Kristinehamn, Värmland.....	32
Figure 17. IC calculations with IC (Cavalli et al.,2013) and soil moisture for the catchment of Östra Ringvägen, Värmland. A, IC Combined (Cavalli et al., 2013) and soil moisture 25km for the whole catchment. B, IC Combined (Cavalli et al., 2013) and soil moisture 25km for the flooded points. C, IC Combined (Cavalli et al., 2013) and soil moisture 1km for the flooded points. D, Soil moisture from ASCAT 25km. E, Soil moisture from ASCAT 1km. F, Soil moisture from ASCAT 1km for the flooded points.....	36
Figure 18. SedInConnect 2.3 dialogue window (Crema et al., 2015).....	57

List of tables

Table 1. Summary of several sensors, their characteristics and previous studies.....	9
Table 2. Main characteristics of sensors with better temporal resolution	10
Table 3. Main characteristics of ASCAT and ASAR with operation modes of ScanSAR (EUMETSAT, 2010)	19
Table 4. Ground station measurements. The stations Uddevalla and Heden are used for Västra Götaland and Kristinehamn and Väse for Värmland (SMHI, 2017c). The marked columns are the starting day of the flooding.	26
Table 5. Precipitation Västra Götaland during the evening of the 19th of August 2014. Derived from the 15 minutes radar precipitation data of Berg et al. (2016). The highest measured values are in red text.	26
Table 6. Precipitation Värmland during the night to the 21st of August 2014. Derived from the 15 minutes radar precipitation data of Berg et al. (2016). The highest measured values are in red text. ...	27
Table 7. ASCAT 25km soil moisture (EUMETSAT, 2017). Relative soil moisture values the days before, and the first day of flooding for Västra Götaland and Värmland. The marked columns are the day of flooding.	29
Table 8. Radar precipitation (Berg et al., 2016) and ASCAT 25km soil moisture (EUMETSAT, 2017). Västra Götaland: Precipitation evening the 19th, soil moisture 19th of August. Värmland: Precipitation the night 20–21st, soil moisture 21st of August.....	31
Table 9. ASCAT 1 km Soil moisture content at flooded points the 20th and 21st of August 2014 in Värmland	32
Table 10. Soil moisture from the SMOS satellite (ESA, 2017) for Västra Götaland and Värmland. Blank columns are no data.	33
Table 11. Result of Sediment Connectivity calculations with soil moisture (SM).	34

Word List

ASCAT = A radar scatterometer onboard the MetOp satellites. Measures soil moisture in C-band with a spatial resolution of 25 km and a temporal resolution of 1,5 day. Measures relative soil moisture (EUMETSAT, 2017).

BaTMan = A database from Trafikverket that manage, monitor and provides information about bridges, tunnels and other constructions in relation to roads. Constructions below 2000 mm in span width are not included (Trafikverket, 2015).

Drainage density = Measures how much a catchment is drained by stream channels. Defined as the total length of streams divided with the catchment area (Kalantari, Nickman, Lyon, Olofsson, & Folkesson, 2014).

PCDs = Physical catchment descriptors developed to describe road and catchment features and are divided into three main categories considering soil type, land use and topography (Kalantari et al., 2014).

Relative soil moisture = An estimation of the water saturation of the topsoil layer is presented in relative units between 0-100 %, comparing the wettest and the driest conditions (Gruber, Wagner, Hegyiová, Greifeneder, & Schlaffer, 2013).

Remote sensing = The science of deriving information about areas or objects from a distance, i.e. from satellites. It collects data through detecting the energy that the Earth reflects (Lillesand, Kiefer, & Chipman, 2015).

Sediment Connectivity = is the degree of linkage within a catchment between sources of sediment and downstream areas (Cavalli et al., 2013).

SMOS = The Soil Moisture and Ocean Salinity mission. A satellite that measures soil moisture in L-band with a spatial resolution of 50 km and a temporal resolution of 2,5-3 days. Measures volumetric soil moisture (EO, 2017).

Soil moisture = Soil moisture can refer to different kinds, but the most common and also used here, is the near-surface soil moisture and accounts for the surface soil moisture in the top centimeters and not the root zone soil moisture (Kerr et al., 2010).

SWI = Soil Water index is the moisture conditions at different depths of the soil (Copernicus, 2017).

TWI = Topographical wetness index, indicates the ability of a point in an area to develop saturated conditions by water accumulation in a catchment (Kalantari et al., 2014).

Volumetric soil moisture = The ratio between volume of water and volume of soil, measured in the unit m^3/m^3 (Kerr et al., 2010; Seneviratne et al., 2010).

1 INTRODUCTION

1.1 Background

This chapter gives a background to the subject where climate change, the behavior of the road infrastructure and issues with sediment transfer is assessed.

1.1.1 Climate change that affects flooding

Global warming is now proceeding faster than before, which is with large probability due to increased pressure from human activities. Scandinavia, and thus Sweden, are expected to face a higher temperature increase than the global average with an increase of 3-5 degrees in 2080 compared to 1960-1990. The precipitation patterns will also increase in Sweden during winter, spring and autumn (Holgersson et al., 2007). SMHI (2012) concludes that the frequency of heavy precipitation will increase together with an estimated increase in intensity of 10-15% by the end of the century. Although, the dispersion between climate modeling scenarios are large with indications of increases by more than 40% to unchanged intensity.

Climate change will most likely increase the intense short-term precipitation, i.e. rainfall with a duration of hours or less, due to a warmer atmosphere that holds more water vapor and thus prerequisites for intense precipitation. An intensification of the precipitation would have consequences for the runoff in urban areas, considering the large impervious surfaces that limits the ability of infiltration (Bates, Kundzewicz, Wu, & Palutikof, 2008; Lenderink & van Meijgaard, 2008; Olsson & Foster, 2013). The projected increase in runoff is around 20% until 2090 compared to 1980-1999 for Scandinavia and Sweden (Bates et al., 2008). The Green paper report (European Commission, 2007) identified Scandinavia as one of the most vulnerable areas due to the large increases in precipitation. While Holgersson et al. (2007) identified the western parts of Sweden as the area with largest increase of runoff and a significant increase of 100 year flows.

The development of floods is dependent on several factors; Precipitation patterns (intensity, volume and timing), drainage basin conditions (saturation level, soil character), wetness, urbanization and the presence of embankments, reservoirs and dams. A lack of response areas and human activities at flood plains further enhance the risk of flood damage. Flooding is also dependent on the degree of saturation. Changes of precipitation and evapotranspiration rates changes the soil moisture content, which in turn changes the infiltration, groundwater recharge and runoff ratios (Nigel et al., 2001). Several studies conclude that initial soil moisture conditions can be the difference between minor and huge effects of flooding (Berthet, Andréassian, Perrin, & Javelle, 2009; Brocca, Melone, & Moramarco, 2008; Crow, Bindlish, & Jackson, 2005). Accurate and timely data of soil moisture is thus essential for an enhanced flood prediction (Kerr et al., 2010).

Studies show that climate change most likely already have had an impact on the intensity and frequency of floods (Bates et al., 2008). Twice as many flood events per decade has occurred between 1996-2005 compared to 1950-1980, with a fivefold increase of economic losses during the same time. This is mainly due to population increase, economic growth, changes in land use and development in vulnerable areas (Kron & Berz, 2007).

1.1.2 Behaviour of the road infrastructure due to climate change

Several studies conclude that climate change will have significant impacts on the road infrastructure (Bates et al., 2008; Holgersson et al., 2007; Kalantari & Folkesson, 2013). The

road infrastructure is affected by high stream flows, precipitation, temperature, sea levels rise, wind and ice coatings. The increased precipitation, stream flows and snow melting enhances flooding, landslides and erosion, and thus creates damage on roads, embankments and bridges. Prolonged precipitation can raise the ground water level, create higher pore pressure in the soil and hence affect the slope stability. With increased risk of erosion and high flows, the impacts on low lying roads, underpasses and drums becomes problematic (Nordlander, Löfling, & Andersson, 2007).

The expected climate change with increased precipitation, runoff and frequency of storms will enhance the flood risk. In addition, population growth and economic wealth put further demands on the urban landscape and creates more infrastructure at risk (Suarez, Anderson, Mahal, & Lakshmanan, 2005). Urban areas are vulnerable to environmental changes, and particularly the infrastructure which has long lifetimes and high investment costs (European Commission, 2007; Kalantari & Folkesson, 2013) and with the expansion closer to coastal areas and watercourses the risk of flooding increases further (Holgersson et al., 2007). Furthermore, the road infrastructure also has an impact on the hydrological responses with consequences for drainage patterns and the natural landscape (Tague & Band, 2001; Wemple, Swanson, & Jones, 2001). Consideration of urban areas in the flood prediction research is therefore important, as changes in land use and more impermeable surfaces has a large effect on the soils capacity to accumulate water and thus avoid surface runoff (Brimicombe, 2009; Olsson & Foster, 2013; Vägverket, 2008).

The infrastructure today is not adapted for future changes in the climate (European Commission, 2007). Drainage facilities, such as bridges and culverts, in Sweden are in most parts dimensioned for 50-year flows (Vägverket, 2002). Although, according to Vägverket (2008) some adjustments of the dimensioning have been performed. However, the basis for these adjustments are simple static corrections and not representable changes in land use and climate conditions (Hansson, Hellman, Grauert, & Larsen, 2010; Kalantari et al., 2015). Changes in climate puts pressure on the current hydraulic structures and enhances the risk of failure (Brimicombe, 2009). The degree of saturation is dependent on infiltrating precipitation, and through cracks in the roads, the water infiltrates, changes the saturation level and the soil suction, which in turn affects the behavior of the road (Erlingsson, Brencic, & Dawson, 2009). To target maintenance issues and accident risks, it is essential to understand changes in climate and land use, and furthermore, how they affect the infrastructure (Brimicombe, 2009).

The infrastructure in a society is a capital asset and is a condition for an effective and productive economy. Disturbances thus has both direct and indirect costs through restoration, accidents, diversion of traffic, increased pressure on other modes of transportation, increased travel times, fuel consumption and emissions (European Commission, 2007). The European Commission (2007) estimate that maintenance costs from stresses due to weather account for 30-50%, and 10% of this is related to heavy rainfall and flooding of the costs of the road infrastructure. Furthermore, Vägverket (2002) concluded that restoration costs of 200 rainfall events in Sweden between 1994-2001 cost 600-700 million SEK, and if also counting indirect costs an additional 70 million SEK was included. Adaptation of the existing infrastructure, research and development of new climate-resilient infrastructure is thus important (European Commission, 2007; Koetse & Rietveld, 2012). The research by Hughes, Chinowsky, and Strzepak (2010) show that the cost for adapting the infrastructure only accounts for 1-2% of the total costs, and the expected increase in investment cost is thus not unreasonable high.

In a report about climate adaptation of road constructions, operation and maintenance by Arvidsson et al. (2012), they argue that the ability to a fast adaptation is restricted by the infrastructure dependency, time demanding planning processes, long lifetimes and large socio-economical costs. There is a complex relationship between the climate and the road constructions which complicates the process of identifying impacting factors. Characteristics of road material, hydraulic conditions and the drainage effectivity are some parameters that are affected by climate and thus should be considered. Temperature and moisture patterns affect the road behavior and alternate its life span. The vulnerability can be lowered by locating areas with prerequisites for sensitivity to weather events and implement appropriate measurements (Arvidsson et al., 2012; Bates et al., 2008).

1.1.3 The influence of the road infrastructure on sediment transfer

Topography has an important role in the movement of sediment, and is emerged from natural driving forces. However, human activities, like agriculture, mining and road constructions can directly or indirectly affect the topography as large amounts of soil is replaced which has consequences for the geomorphological landscape (Tarolli & Sofia, 2016). Flows of water and sediment follow the flow paths gravitational, moving from hillslopes downwards to channels and further in to the stream network. The road infrastructure appears to have an effect on debris flows and floods, thus changing dynamics in the landscape (Jones, Swanson, Wemple, & Snyder, 2000). It can alter the movement of precipitation that produce floods and the road network can act as an extended part of the stream drainage network. Most consequences will occur downstream along individual road-stream crossings (Jones et al., 2000).

The geomorphic processes and the road network interacts in several ways; a decreased infiltration and rerouted flow paths increases the surface runoff, rerouted flow paths also lead to new channels exposed to sediment delivery and thus erosion, and the road network might enhance the consequences of for example vegetation removal (Wemple et al., 2001). Wemple et al. (2001) show that the basin-wide sediment production is increased because of roads, and that roads function as both a depositional site and initiation for sediment and water movements. It also highlights the natural hydrological factors as important and to consider the slope, age of the road, and the underlined bedrock. The geomorphic processes are influenced by roads, and is strongly affected by the location of the road, construction practices, rainfall characteristics and basin geology. They conclude that the highest risk of sediment storage was on roads located on valley-floors due to low adjacent landforms and that old roads with medium slope gathers most sediment during storms. Roads can thus have an effect on the connectivity of the catchment (Croke, Mockler, Fogarty, & Takken, 2005).

Water is an important environmental and constructional constraint in the planning, maintenance, operation, design and construction of roads, and can influence the operational costs, the bearing capacity of pavement and a safe traffic flow. Roads interact with water in several ways as the water from the recharge area can intercept the road (Erlingsson et al., 2009). Roads can be a barrier for moving sediment and water (Fryirs, 2013), and the presence of road infrastructure might influence the duration and size of the flooding, drying wetlands and create fragmented habitats. Culverts and other road structures maintain inundation patterns, however, as the road network is developed more impacts on duration and extent of the flooding are observed together with changed water levels (Beevers, Douven, Lazuardi, & Verheij, 2012).

In a low-land catchment with full forest coverage, only 5% of the rainfall is estimated to be runoff due to the impede of the vegetation that creates time for infiltration into the ground. The amount for agricultural land is 30%. Furthermore, in urban environments with drainage systems, 95% is transported to surface water bodies, which creates a quicker water road compared to the natural route with percolation into the ground and vegetation obstacles. Thus creating higher maximum flows than a non-urban area would (Santinho Faisca et al., 2009).

1.2 Problem definition

The expected climate changes in Sweden with increased precipitation and occurrence of extreme events will have impacts on the road infrastructure. Holgersson et al. (2007) identified the western parts of Sweden as especially prone to increases in runoff, an area that in 2014 was affected by severe flooding with large consequences for Västra Götaland and Värmland. Movement of large amounts of water and sediment damaged drainage structures and it is thus essential to identify road-stream intersections that are in risk of future flooding.

Problems occur when roads cross a catchment, and the upstream watercourses are concentrated in a single drainage facility (e.g. a culvert or pipe), to pass under the road. This concentration of runoff modifies the normal flow and leads to increased erosion over a large distance if the stream bed is not adapted for these newly implemented hydraulic conditions. If the runoff exceeds the capacity of the drainage facility, the road will act as a dam and induce flooding (Brencic, Dawson, Folkesson, Francois, & Leitao, 2009).

To investigate catchment characteristics that influence the flood probability at road-stream intersections can contribute in maintenance issues, improve planning processes, and reduce the vulnerability to flooding. Previous research by Kalantari et al. (2014), Michielsen, Kalantari, Steve, and Liljegren (2016) and Cantone (2016) focus on these issues and the goal is to further develop a method for identification of flood prone areas. The addition of soil moisture as a contributing factor is not included in these previous studies, and will hence be acknowledged with inclusion of remote sensing techniques for soil moisture retrieval. The importance of sediment and water transport for the risk in a catchment are assessed, and an extension of the work by Cantone (2016) with the inclusion of sediment connectivity (IC) is performed. The concept of sediment connectivity is further explained in section 2.3.

1.3 Aim and objectives

This study aims to integrate spatial and temporal soil moisture properties in the index of sediment connectivity (IC) by Cavalli et al. (2013).

The objectives to consider are:

- Application of soil moisture satellite imagery in IC to assess sediment connectivity at the catchment scale
- Investigate temporal and spatial characteristics that affects soil moisture
- Combine the results of previous studies in the areas and identify similarities and differences
- Develop a reliable tool for predicting flood risk along transport infrastructure for decision makers (Trafikverket)

The Swedish transport administration (Trafikverket) has developed a strategy for climate adaptation (Trafikverket, 2016), where evaluation and identification of risk areas in the current road network are one key area. This research aims to contribute to this area and is a part of the continuous acquisition of knowledge in the climate impact research.

2 LITERATURE REVIEW

2.1 Soil Moisture

In this section the soil moisture content is defined and affecting factors are discussed. Literature about how soil moisture is measured is assessed and the development through remote sensing technology presented.

2.1.1 The soil moisture content and affecting factors

The soil moisture content (SMC) can be referred to the amount of water in the pores and most often it refers to the water in the unsaturated soil zone. The volume of the soil consists of approximately 50% mineral and organic content, and the other half of pores (Barrett & Petropoulos, 2012; Hillel, 1998; Seneviratne et al., 2010). Soil moisture can refer to different kinds, but the most common and also used here, is the near-surface soil moisture and accounts for the surface soil moisture in the top centimeters and not the root zone soil moisture (Kerr et al., 2010).

The soil moisture content depends on several factors and are very variable both spatially and temporally. The soil texture, especially the particle size, determines the holding capacity of the water. Soil with large particles retain less moisture due to gravitational infiltration of water through open spaces and thus infiltrates more. Accordingly, water flows faster through sand than silt and clay, as smaller grain size generally has lower permeability (Larsson, 2008; Petropoulos, Griffiths, Dorigo, Xaver, & Gruber, 2013). The infiltration capacity (soil permeability) and the type of rock underneath affect the catchment runoff. Larger amounts of permeable soils, for example coarse sand and gravel, has lower probability of flooding due to higher infiltration capacity and lower soil moisture content. Finer material, for example silt and peat, that has low hydraulic conductivity and high capacity of soil moisture retention has a higher probability of flooding (Kalantari et al., 2014; Petropoulos et al., 2013).

Climate affects the soil moisture through humidity, temperature, precipitation, solar illumination and wind. The soil moisture content (SMC) is generally increased with more precipitation, but the variety of type and intensity also affects the SMC. Moderate precipitation during a longer time penetrate the soil and increases the soil moisture, while short term, intense precipitation rather creates flash floods due to restricted ability for the soil to absorb the rain fast enough. Temperature also affects soil moisture as higher temperatures increases the evaporation and thus lower the content of soil moisture, and lower temperatures means less evaporation and preservation of moisture. Another factor that affects the soil moisture is the topography. Both elevation and slope influences the SMC, and the infiltration and runoff characteristics. Areas with higher elevation have lower soil moisture and low lying areas have higher soil moisture. This is due to gravity as water flows downwards, and that also explains why steeper slopes hold less soil moisture than flat surfaces. Land cover also affects the soil moisture and the evapotranspiration. Areas with more vegetation has more organic ground cover that creates a protection for the surface soil from evaporation and thus more soil moisture can be retained. While less vegetated areas expose the soil to evaporation (Barrett & Petropoulos, 2012; SMAP, 2017).

Lakshmi, Jackson, and Zehrhuhs (2003) tried to show a relationship between soil moisture and temperature. Their results showed that an increase in surface temperature corresponds to a decrease in soil moisture. However, observations and conclusions about soil moisture and temperature are difficult as both factors are temporally variable seen to seasonal and annual scales, and also spatially variable, depending on land cover, land use and soil type.

2.1.2 Measuring soil moisture

The exact definition of soil moisture is dependent on the relevant context, i.e. whether it is absolute, relative or in indirect terms and it is also dependent on the storage (Seneviratne et al., 2010). The most common expressions of soil moisture are volumetric soil moisture or gravimetric (by weight) (Kerr et al., 2010). Often only a part of the soil moisture is measureable and relevant, which advocates consideration to a given soil volume (Figure 1). The soil moisture content differs vertically and horizontally, and therefore differs regarding soil volumes. This is highly relevant for the choice of measurement method as it might only provide estimates of the top centimeters, as with remote sensing technology (Seneviratne et al., 2010). Thus is volumetric soil moisture, the ratio between volume of water and volume of soil (unit m^3/m^3), the most commonly used in remote sensing (Kerr et al., 2010).

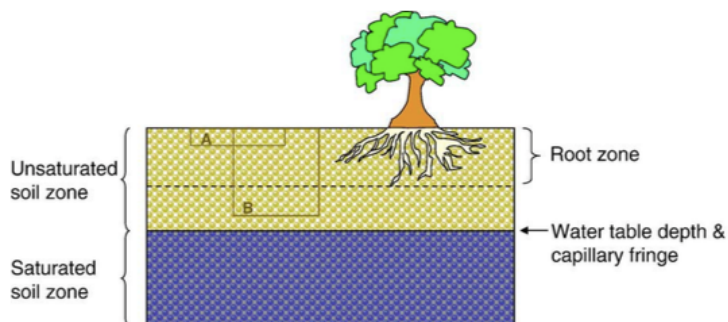


Figure 1. The different soil zones, where A and B represent two distinct volumes of soil moisture (Seneviratne et al., 2010)

In hydrology and land surface practices the volumetric soil moisture θ is often defined as $[\text{mm}_{\text{H}_2\text{O}}/\text{mm}_{\text{soil}}]$ in the soil volume V , which provide the equation (Seneviratne et al., 2010):

$$\theta = \left(\frac{\text{volume of water in } V}{V} \right)$$

On wet soils and catchments with saturated soils (e.g. near watercourses and in low-land areas), overland flow will occur more quickly and be more extensive. The spatial distribution of soil moisture is thus important to determine infiltration potential, floods and erosion possibilities and in turn impacts on the landscape, streams and infrastructure (Petropoulos et al., 2013). The amount of water in the top soil layer affect several processes at the land surface, among others hydrological, geomorphic, atmospheric and biological processes, and the requirement for soil moisture observations are essential for improving modelling and research (Wagner et al., 2013). The soil moisture content is included in some global climate models to give an indication of changes, although with a very coarse spatial resolution (Nigel et al., 2001).

Soil moisture is an important parameter in several processes on earth. The exchange of energy and mass, controlling incoming radiant energy through transpiration and evaporation of plants, affects the surface runoff or infiltration, groundwater recharge rates and climate effects (Barrett & Petropoulos, 2012; Seneviratne et al., 2010) However, the spatial and temporal heterogeneity limits the ability to measure the soil moisture over large areas. A lot of techniques have been developed to be able to measure the soil moisture content and as the remote sensing techniques are developed more options reveals. During the last decades, several approaches using space born remote sensing has developed where microwave, optical or thermal infrared (TIR) sensors has been used (Barrett & Petropoulos, 2012; Kerr et al., 2010).

Measurements of soil moisture was first based on shortwave measurements where the basis was that wet soil is darker in color and thus distinguishable. However, vegetation cover, atmospheric effects and cloud cover reduced the sensitivity and the method failed. Another method was based on the latent heat effect where wet soils are cooler and have higher thermal inertia than dry soils. Although, this method had problems inherent to optical remote sensing as atmospheric effects (like wind) drastically changed the temperature of the soil. The water content is related to the dielectric constant of soils, which microwave systems measure and focus was then rearranged to include radar, radiometers and scatterometers. The lack of atmospheric and cloud effects, the ability to penetrate vegetation and operate in darkness created better prerequisites for representative measurements of soil moisture. Furthermore, a new approach was developed that relies on gravity field measurements from space. This is based on the fact that changes in mass on short time scales are linked to the amount of water. However, this includes also the water table, in vegetation, atmosphere and in lakes, so the relationship with water storage should be validated and further explored. The project Gravity Recovery and Climate Experiment (GRACE) is currently working with this method (Kerr et al., 2010)

2.2 Remote Sensing

In this section the remote sensing technique in flood forecasting and in measuring soil moisture content is assessed. Advantages and disadvantages with different sensors are discussed in relation to the requirements for hydrological applications.

2.2.1 Remote sensing in flood forecasting

To be able to produce accurate flood forecasts, the estimates of the hydrological conditions are essential. Soil moisture affects the infiltration and runoff and is therefore an important parameter in flood modelling to get a more robust result. Unfortunately, measurements of soil moisture at appropriate scales for hydrological applications are a challenge. Within a catchment, several ground measurements of the soil profiles can be conducted, but it is difficult over larger areas. One alternative is to use remote sensing methods which instead of point values can provide soil moisture estimates over a large continuous area at global scale. Although, large pixel sizes, low temporal resolution and limited depths of the microwave signal might be an obstacle in hydrological applications. However, depending on the type of application or area, i.e. in regions without adequate monitoring of hydrological parameters, satellite based estimates might be important (Gruber et al., 2013).

The requirements for soil moisture observations are a soil moisture accuracy of $0.04 \text{ m}^3/\text{m}^3$ or better, a spatial resolution of less than 50 km (preferable lower), a revisit time of 1-2 days are optimal to be able to determine soil hydraulic properties, and a reasonable time acquisition (Kerr et al., 2010).

Passive and active microwave sensors have been identified as those with most consistent temporally and spatially retrieval of soil moisture (Barrett & Petropoulos, 2012), however, certain limitations occur. Passive sensors are affected by cloud cover, which is a frequent occurring during flood events due to precipitation. Cloud removal methods thus must be applied to achieve any useful data. Although, passive sensor has been used in several flood studies due to other advantages like abundant spectral features of multi-spectral imagery and its long temporal availability, which is suitable for evaluating long-term effects of flooding (Zhang, Zhu, & Liu, 2014). Active sensors have the ability to penetrate clouds, and thus derive information during precipitation events, but the long revisit time restricts the use for

rapid responses. However, several active sensors have been launched (i.e. COSMO-SkyMed, TerraSAR-X and Envisat ASAR) with higher temporal and spatial resolution and thus enhances the conditions for effective flood monitoring (Pierdicca, Pulvirenti, Fascetti, Crapolichio, & Talone, 2013; Pulvirenti, Chini, Pierdicca, Guerriero, & Ferrazzoli, 2011; Zhang et al., 2014).

Wang, Colby, and Mulcahy (2002) tried to develop an efficient method for mapping flood extent using Landsat data. Cloud cover, dense vegetation and the long revisit time (16 days) limited the study and they found that Landsat alone could not identify the flooded areas. Refice et al. (2014) used COSMO-SkyMed with a high resolution of 3 meters for flood modelling with good results. However, the large cost of the data is an issue for the usability.

2.2.2 Soil moisture retrieval from remote sensing technology

The volumetric soil moisture content can be measured by in situ ground stations. However, these are generally very sparse and variations spatially are not retrieved, thus global coverage are not achieved. Remote sensing technique is a tool to monitor soil moisture from microwave bands to provide measurements at different scales, both temporal and spatial (Fascetti, Pierdicca, Pulvirenti, & Crapolichio, 2014). Indirect measurements of the thermal inertia in thermal infrared spectral bands can provide volumetric soil moisture content. However, remote sensing measurements of microwave bands can provide a direct sensitivity. The retrieval depends on large differences between the dielectric constant of water and dry soil as the soil moisture content influences the soil electrical permittivity (Pierdicca et al., 2013).

Passive microwave remote sensing sensors (radiometers) measures the naturally emitted microwave radiation and is dependent on sufficient energy to measure the signal. The active microwave sensors (scatterometers) provide its own energy and measures the ratio between transmitted and received electromagnetic radiation (radar backscattering). The spatial resolution is the same for passive and active sensors, but the active sensor has a better temporal resolution which meets the requirements of a few days revisit time for soil moisture retrieval. C-band (5.3 GHz) can with advantage be used for soil moisture mapping, and successful studies including both passive and active sensors have been identified. For example, the passive AMSR-E and the active scatterometers ERS, ENVISAT and ASAR (Pierdicca et al., 2013).

Although, perturbing factors, such as vegetation cover and atmospheric effects, affects the retrieval on higher frequencies more significantly and L-band (1.4 GHz) has therefore been proven to be the most suitable spectral range for observing soil moisture due to low sensitivity to vegetation and a larger penetration into the soil (Kerr, 2007). Passive sensors are also not as responsive to soil roughness as active backscattering (Pierdicca et al., 2013). From this, the first microwave radiometer completely adapted for soil moisture was launched in 2009 by the European Space Agency (ESA). The Soil Moisture and Ocean Salinity (SMOS) satellite is an L-band interferometric radiometer (MIRAS), that has a temporal resolution of 2-3 days and a spatial resolution of 40 km (Albergel et al., 2012).

Moran, Peters-Lidard, Watts, and McElroy (2004) evaluate the spectral measurements for surface soil moisture and compare optical, microwave and radar approaches. Optical sensors and thermal imaging radar (TIR) has a fine spatial resolution, covers large areas and there are several satellite sensors available. However, the penetration of the surface is minimal (~1 mm), cloud cover and vegetation blocks the measurements and the relation to soil moisture is therefore weak. The microwave sensors show a strong relation to soil moisture retrieval,

penetrates the surface down to 5 cm, has a broad coverage and is not affected by cloud cover. Although, the coarse spatial resolution is a disadvantage together with disturbances primarily from vegetation biomass and surface roughness. Synthetic aperture radar (SAR) was until recently, limited by a coarse revisit time, but with the development of different sensors, high temporal frequencies are now possible together with a fine spatial resolution. It has a suitable penetration depth of 5 cm, not affected by clouds and show a strong relation to soil moisture. As with microwave sensors, the disturbances are from surface roughness and to some extent vegetation. Hence, Moran et al. (2004) suggests SAR sensors as the best approach for spatially distributed soil moisture at the watershed scale. Several SAR sensors are listed in Table 1 with their characteristics and references to previous studies.

Table 1. Summary of several sensors, their characteristics and previous studies

Sensor	Start date	Band	Type	Spatial resolution	Temporal resolution	Previous studies
Sentinel 1 (SAR)	2014	C-band	SAR	5-20 meter	12 days	(Gruber et al., 2013; Hornacek et al., 2012; Petropoulos, Ireland, & Barrett, 2015; Wagner, Sabel, Doubkova, Bartsch, & Pathe, 2009)
TerraSAR-X (SAR)	2007	X- or C-band	SAR	0,5-18 meter	11 days	(Baghdadi, Aubert, & Zribi, 2012)
Cosmo Skymed (SAR)	2008	X-band	SAR	1-100 meter	12 hours	(Pulvirenti et al., 2011; Refice et al., 2014)
Radarsat (SAR)	1995 and 2007	C-band	SAR	3-100 meters	24 days	(Bonn & Dixon, 2005; Hassaballa, Althuwaynee, & Pradhan, 2014)
Envisat ASAR	2002 and 2012 (?)	C-band	SAR	30 meters	3 days	(Saran, Sterk, Nair, & Chatterjee, 2014)
Landsat 7/8	2013	X-band	Passive sensor (OLI and TIRS)	30 meters	16 days	(Wang et al., 2002; Zhang et al., 2014)

Hydrological applications require a good temporal resolution as the revisit time limits the ability to use soil moisture data in operational flood forecasting models if the data is not available when needed. A lot of the current sensors allow retrieval of data around 10-35 days, which might not be adequate for applications in hydrology (Kornelsen & Coulibaly, 2013; Moran et al., 2004). The major advantage of SAR sensors when working with soil moisture is the fine spatial resolution, which should be put in relation to low temporal and radiometric resolution. This has developed platforms like SMOS, SMAP, ASCAT and AMSR-E as a complement with lower retrieval error, near real time capabilities, and 1-3 days temporal resolution, but coarse spatial resolution (Table 2) (Albergel et al., 2012; Barrett & Petropoulos, 2012; Brocca et al., 2017; Kornelsen & Coulibaly, 2013; Lacava et al., 2012; Petropoulos et al., 2015).

Table 2. Main characteristics of sensors with better temporal resolution

Sensor	Start date	Band	Type	Spatial resolution	Temporal resolution	Previous studies
ASCAT	2007	C-band	Active Radar Scatterometer	25 km	1,5 day	(Albergel et al., 2012; Barrett & Petropoulos, 2012; Bartalis et al., 2007; Brocca et al., 2017; Brocca et al., 2011; Gruber et al., 2013; Lacava et al., 2012)
SMOS	2009	L-band	Passive interferometric radiometer	50 km	2-3 days	(Albergel et al., 2012; Kerr et al., 2010; Lacava et al., 2012; Parrens et al., 2012; Piles et al., 2014)
AMSR-E	2012	C-band	Passive Microwave radiometer	25 km	1 day	(Brocca et al., 2011; Lacava et al., 2012; Njoku, Jackson, Lakshmi, Chan, & Nghiem, 2003)
SMAP	2015	L-band	Radiometer	36 km	2-3 days	(Entekhabi et al., 2010; Lakshmi, 2013)

The coarse spatial resolution is a disadvantage when applying on local areas, however, that can be overseen by the temporal resolution of a few days, and the opportunities for near real time applications. Data from the ASCAT sensor was the first with near real time capabilities and data can be provided 130 minutes after retrieval, which enhances the ability to monitor flooding while they occur (Albergel et al., 2012; Brocca et al., 2017). The need for finer spatial resolution has started the development to disaggregate large scale products to enable usage in small-scale catchments, where the disaggregation of the ASCAT 25 km resolution product to a 1 km product is one option (Wagner et al., 2013)

2.3 Sediment connectivity index (IC)

In this chapter, the concept of sediment connectivity is presented, its definition and previous research in the area of connectivity.

2.3.1 The concept of sediment connectivity

Connectivity is referred to as the internal connections and linkages in networks, and is applied in several fields of Environmental and Earth science (Bracken & Croke, 2007). In case of extreme precipitation, the flow of water occurring on the surface might bring sediments, trees and stones with it and eventually cause problems with obstruction of drainage facilities such as culverts, bridges and ditches. The transport of sediment and water has consequences environmentally, but also economically and for society in both direct and indirect ways. The connectivity and the interactions in the catchment is thus important to consider.

The sediment connectivity index is developed by Cavalli et al. (2013) from a geomorphometric index originally by Borselli, Cassi, and Torri (2008). The definition of sediment connectivity (IC) is *“The degree of linkage which controls sediment fluxes throughout landscape, and, in particular, between sediment sources and downstream areas, is a key attribute in the study of sediment transfer processes in mountainous catchments”* (Cavalli et al., 2013 pp.31). How a given part of the catchment work as a source of sediment is based on the spatial characterization of the connectivity patterns, and that defines the paths of sediment transfer. The intent is to find the potential connectivity in a catchment and evaluate connections between hillslopes and storage areas, i.e. sinks, with the connection of sediments between the outlet of the catchment and the hillslope considered (Cavalli et al.,

2013). The sediment connectivity index proposed by Cavalli et al. (2013) focus on the influence of topography and is derived from a Digital Elevation Model (DEM). It does not for example take vegetation cover into account, however, additional maps of other factors can be included as weights in the calculation.

The intention of IC is to represent the linkage between parts of the catchment, and evaluate potential connections between hillslopes and the interesting features that are considered, i.e. channel networks, catchment outlets, road intersections or storage areas like lakes (sinks). Two different aspects are considered: (1) the delivery of sediments across the whole drainage system (i.e. the connection of sediment between outlets of the catchment and hillslopes), and (2) coupling-decoupling between selected targets or sinks and hillslopes. The main issues that are addressed are with the first (1), what the probability that sediment from a certain source will reach the outlet of the catchment, and second (2), what the probability is that eroded sediment from hillslopes will reach the target of interest (Cavalli, Crema, & Marchi, 2014).

2.3.2 Previous studies in the subject of connectivity

To assess the subject of identifying and assessing flood risks in relation to infrastructure, a number of studies have also included landscape morphology and connectivity features in relation to flood risk over large scales (Borselli et al., 2008; Cavalli et al., 2013; Gay, Cerdan, Mardhel, & Desmet, 2016; Trevisani & Cavalli, 2016).

Earlier studies by Bracken and Croke (2007) focuses on hydrological connectivity, i.e. how water is linked in catchments and the generation of catchment runoff response, which can be connected to sediment connectivity. Components that affect the catchment connectivity is defined as the climatic environment, especially dependent on the distribution, intensity and duration of precipitation, catchment characteristics, slope, vegetation, surface roughness, land management and antecedent conditions. The intensity and duration of storms and precipitation are essential for creating connectivity, the timing of high intensity rainfall can be crucial and also light rainfall as it wets the catchment and if followed by high intensity rainfall the generation of runoff is rapid and losses by transmission low, which enhances connected flows. Infiltration is important in the runoff generation as the connectivity depends on whether runoff can infiltrate or if it moves on the surface (Bracken & Croke, 2007). The antecedent conditions impact the spatial patterns of runoff and infiltration, and depends on the soil moisture and saturation levels. When the soil moisture content increases, the probability of increased connection between runoff sources also increases, and thus the connectivity (Fitzjohn, Ternan, & Williams, 1998).

Bracken, Turnbull, Wainwright, and Bogaart (2015) worked with sediment connectivity as a conceptual framework, while Fryirs, Brierley, Preston, and Kasai (2007) created the connect of (dis)connectivity which describes the limiting factors that blocks the sediment transport. Baartman, Masselink, Keesstra, and Temme (2013) focused on showing how complex environments lead to a decreased connectivity. Thus can the complex landscape and landform impediment might be disconnecting features that decreases the sediment transport (Baartman et al., 2013; Fryirs et al., 2007). Several studies identify surface roughness, vegetation cover (spatial and density) and rainfall intensity and duration as the most influencing factors for connectivity (Keesstra, Kondrlova, Czajka, Seeger, & Maroulis, 2012; López-Vicente, Quijano, Palazón, Gaspar, & Navas, 2015).

An increasing interest in issues concerning sediment connectivity created a need for a development of a tool to assess sediment transport at the catchment scale (Baartman et al.,

2013; Fryirs, 2013). The potential to use quantitative estimates of sediment connectivity and relate it to databases of sediment sources is an important step towards improving risk and hazard assessment. This integrated approach enhances the possibility to evaluate both availability of sediment but also the potential for the sediment to reach a specific target (Cavalli et al., 2014).

In the study made by Cavalli et al. (2013) their result indicates higher IC values for the middle and lower parts of the basin, with highest values by the catchment outlet. However, gullies and deep channels at the upper parts of the catchment also indicates high IC values. The results also show a correlation between the shape of the catchment and the connectivity patterns, as the catchment with a circular shape allows for a high and homogenous connection between steep slopes and the catchment outlet, and thus having higher IC values. Also Messenzehl, Hoffmann, and Dikau (2014) use the sediment connectivity index and found that the highest values are in the lower part of the basin, with a clear decline further upslope. Although, a degree of overestimation of the connectivity have been found in this study. However, they conclude that GIS approaches like IC are valuable when investigation properties of sediment movement, especially on the basin scale.

The connectivity index by Cavalli et al. (2013) evaluates the connection between selected targets where sediment is gathered and hillslopes. In this study the targets are the road network to assess the potential risk of sediment and water transfer towards the road infrastructure.

3 METHOD

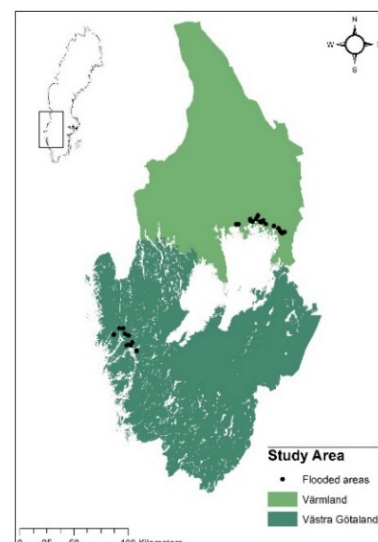
This section starts with an explanation of the two study areas in detail, before it addresses the methods and the data input. The soil type and land use maps are obtained from Geodata (2015). The shapefile “jordart, grundlager (JG2)” has been reclassified into seven classes: clay, gravel, peat, rock, sand, till and water, by the methodology proposed by (Michielsen, 2015). The land use map is produced by the Swedish mapping, cadastral and land registration authority (Lantmäteriet), and have been reclassified into six classes: agriculture, forest, grassland, other, urban area and water.

After the case study, the precipitation data is assessed, followed by a chapter about the choice of satellite sensor, and finally a description of the sediment connectivity index (IC).

3.1 Case Study

This project will be conducted through a case study of two areas in the southwest part of Sweden, Västra Götaland and Värmland (Figure 2), that has been affected by severe flooding in August 2014.

Figure 2. Study areas in southwest Sweden



A number of flooded points are investigated, and several non-flooded areas have also been selected for the study, which are adapted from the choice by (Michielsen, 2015). All selected points, flooded and non-flooded, can be seen in Figure 3, for respectively study area.

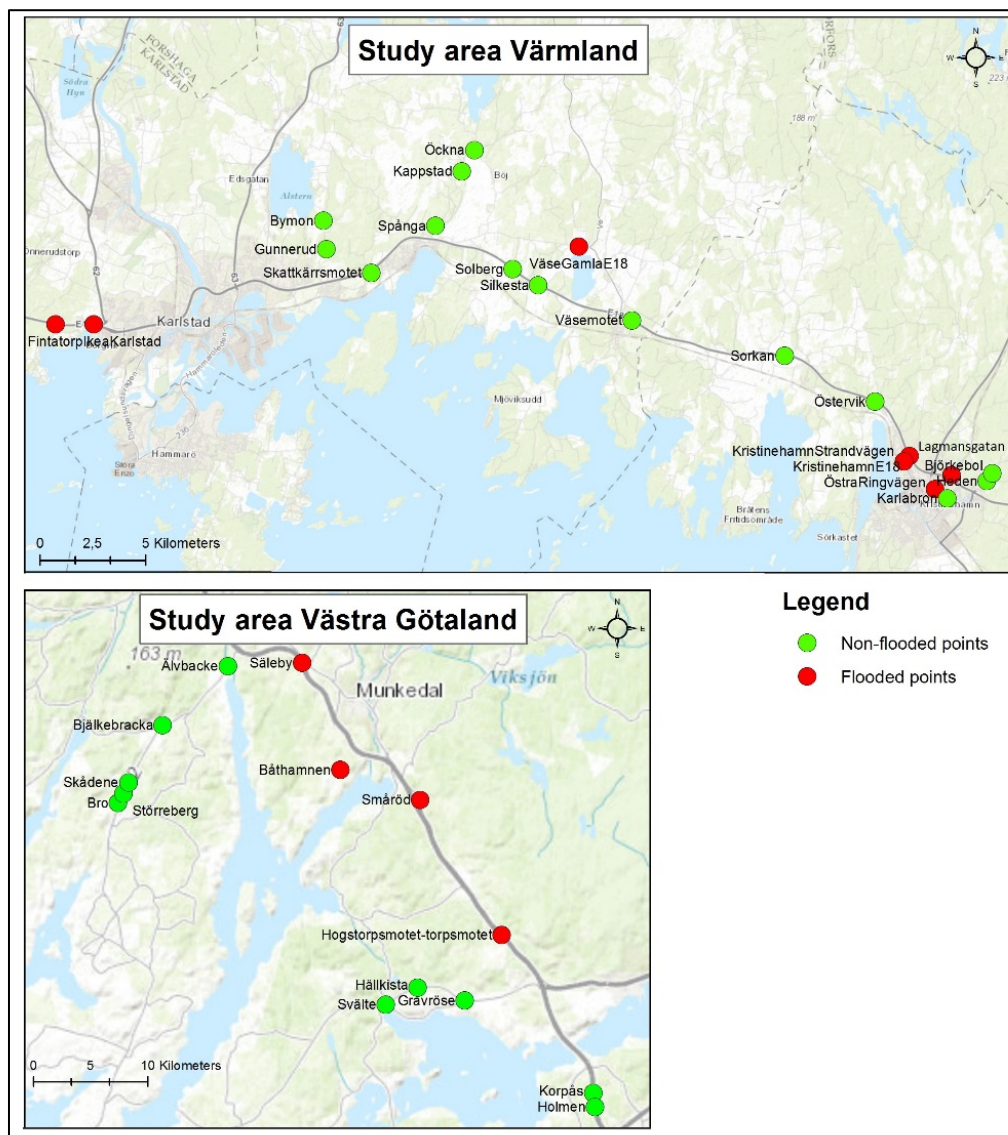


Figure 3. Study area of Värmland and Västra Götaland with flooded and non-flooded points

3.1.1 Västra Götaland

Västra Götaland is an area that has been identified as prone to flooding due to a future increase in precipitation and a history of intense short term precipitation events (Holgersson et al., 2007). Heavy rainfall hit the area the 19th and 20th of August 2014 with multiple flood events as a result, and with severe consequences for roads, railways, buildings, and for society by traffic delays, pressure on other modes of transportation and electricity problems (Bohusläningen, 2014-08-21; SVT, 2014-08-21).

Parts of the E6 highway were flooded and between the 19th and 20th the road was closed between Torpsmotet and Hogstorpsmotet, and between Håby and Munkedal, due to large amounts of water on the road (Figure 4) (SVT, 2014-08-21). Also the railway, Bohusbanan, between Gothenburg and Strömstad was affected by the rainfall. Up to 20 meter of railway embankments was entirely washed away in Småröd and Kråkeröd (Figure 5) (Svenska Dagbladet, 2014-08-20; SVT, 2014-08-20).



Figure 4. E6 flooded in Västra Götaland (Bohuslänningen, 2014-08-21)



Figure 5. Railway embankment at Bohusbanan damaged (Småröd) (Bohuslänningen, 2014-08-21)

The soil type in Västra Götaland is apart from water, characterized by rock (35%) and clay (33%), and forest is the main land use in this area, followed by agriculture (Figure 6). A correlation between urban areas and clay or till can be seen, and also large amounts of clay nearby roads. Impervious surfaces together with clay will result in more runoff compared to forest areas with the capacity to restrain water. Several of the flooded areas are also located close to agriculture, which might alter the flow path of the water. More information about soil type and land use per catchment can be found in Appendix A.

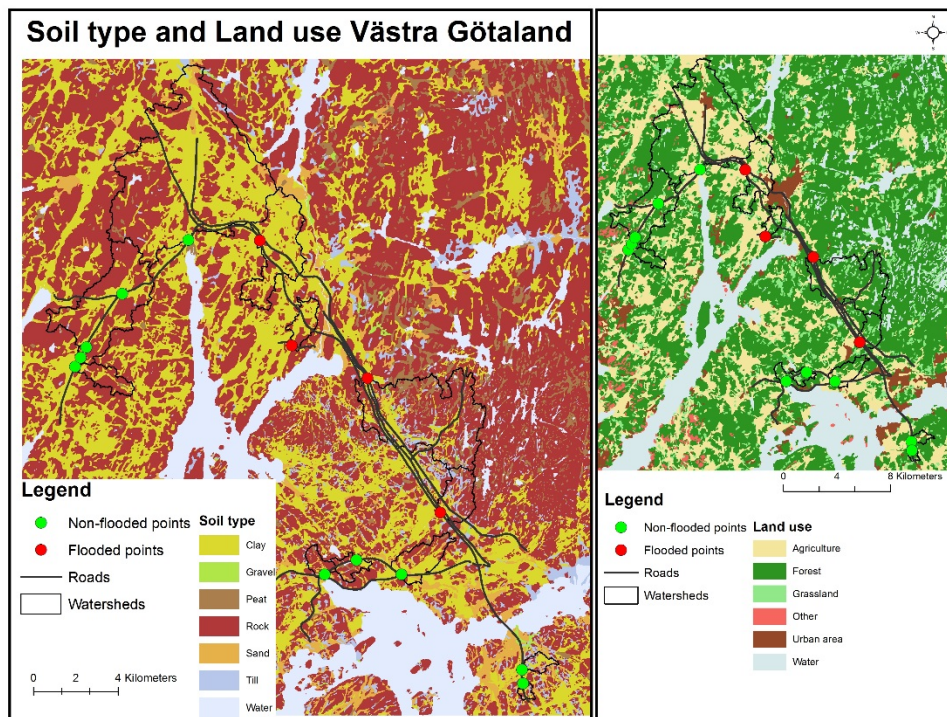


Figure 6. Soil type and land use for Västra Götaland with flooded and non-flooded points, roads and watersheds

3.1.2 Värmland

The area of Värmland was affected by severe flooding from the 21st to the 25th of August 2014, that had consequences for the road infrastructure. The E18 highway close to Kristinehamn was closed as nearly 100 mm of precipitation fell in a short time span during the night to the 21st of August (Sveriges Radio, 2014-08-21). Several other areas around Kristinehamn, Karlstad and Ölme was also affected by large amounts of water that impacted the road structure, facilities for draining and the drinking water. Roads collapsed and all road and train traffic was interrupted, both locally and long distance trains (Nya Kristinehamnsposten, 2014-08-21). The highway E18 was also closed off around Karlstad, between Skutbergsmotet and Bergviksmotet, close to IKEA and Fintatorp, due to large amounts of water on the road (SVT nyheter Värmland, 2014-08-23). The area around Väse was among the most affected and road 571, the old E18, was destroyed (Nya Kristinehamnsposten, 2014-08-21).

In Kristinehamn was Lagmansgatan heavily affected and collapsed completely (Figure 7) (Sveriges Radio, 2014-08-21). Also Rådmansgatan, Mariebergsmotet, Strandvägen and Östra Ringvägen (Figure 8) was flooded (Sveriges Radio, 2014-08-21; SVT, 2014-10-14).



Figure 7. Lagmansgatan collapsed due to the heavy precipitation (Sveriges Radio, 2014-08-21)



Figure 8. Östra Ringvägen was flooded (SVT nyheter Värmland, 2014-08-23)

The soil type in Värmland is, apart from water, mainly till (21%), clay (14%) and rock (15%). The land use is mainly forest and agriculture with urban areas in the larger cities of Karlstad and Kristinehamn (Figure 9). A correlation can be seen where urban areas tend to have till and sand as soil type, which to some extent have a better drainage of water than clay. However, large amounts of impervious surfaces increase the surface runoff. More information about soil type and land use per catchment can be found in Appendix A.

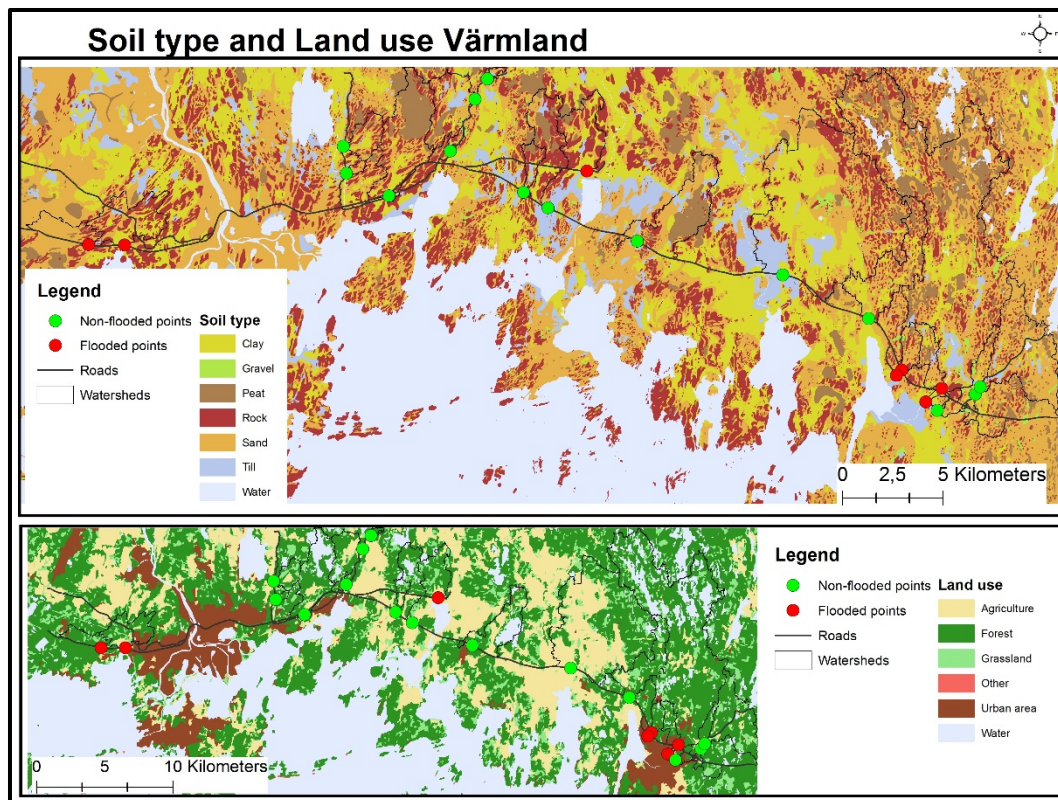


Figure 9. Soil type and land use for Värmland with flooded and non-flooded points, roads and watersheds

3.2 Precipitation data

The precipitation is collected from two different sources. At first the ground station measurements of two stations in each area are included (SMHI, 2017c) and secondly, the radar measurements by Berg, Norin, and Olsson (2016).

3.2.1 Ground station measurements

The ground stations used in Västra Götaland are placed in Uddevalla and Heden. The flooded areas are located in the middle of these stations and an average of their precipitation measurements was therefore calculated. The stations used in Värmland are placed in Kristinehamn and Våse, where areas closest to each station is represented by that station. Areas in Kristinehamn is thus represented by the Kristinehamn station and areas between Våse and Karlstad by the station in Våse.

3.2.2 Precipitation radar measurements

To perform hydrological forecasting, real time precipitation data is a requirement. However, data retrieval might be problematic due to high temporal (sub-daily) and spatial resolution (less than 10-20 km) requirements. A method to merge high temporal resolution radar composite with coarser gridded gauge data is presented by Berg et al. (2016). This results in a data set with long-term spatial properties, but with inclusion of spatial and temporal details from radar data as ground truth precipitation measurements are combined with high resolution radar data.

The radar data used is from the operational system, NORDRAD, which provides spatial information and high temporal resolution. 12 C-band Ericsson Doppler radars create the radar network, which scan every 15 minutes at 10 different tilt angles. The spatial resolution is 2x2 km. The developed data set is called HIPRAD (High-resolution Precipitation from gauge-

adjusted weather RADar). Several corrections are performed in the post-processing to increase the quality of the measurements; corrections to reduce reflectivity from topography by a beam blockage correction, satellite cloud observations to remove radar echoes in non-cloud areas, and corrections of range-dependent bias using rain gauges. If 15-minute radar observations are missing, this is corrected by interpolation of neighboring time intervals. The time stamp defines the end of the measured period with accumulated values for 15 minutes (Berg et al., 2016).

The precipitation data from radar measurements by Berg et al. (2016) was downloaded in NetCDF format and processed in Matlab to extract latitude and longitude coordinates. The point layer was then imported to ArcMap 10.5 and converted into raster format. A classification into 6 different classes has been performed for visualization. The precipitation values for each 15-minutes period in the relevant days has thereafter been summarized into table 5 and 6.

3.3 Choice of satellite data

Several satellites have prerequisites to extract soil moisture values. However, hydrological applications, and especially soil moisture extraction, require a temporal resolution of a few days, which limits the adequate satellites. All satellites under investigation can be seen in Table 1 and 2. However, the ones that have been evaluated as most suitable for the aim of the study is the ASCAT sensor, where both the 25 km spatial resolution product and the 1 km product has been assessed, and furthermore the SMOS satellite. In this section the chosen satellites are presented.

3.3.1 ASCAT 25 km spatial resolution

The radar scatterometer ASCAT on the MetOp satellites uses a push-broom scanning mode and six side-looking antennas that scan $+45^\circ$ and -45° . Each antenna has a swath of 550 km with a 670 km gap between them. Global coverage for Europe can be obtained in approximately 1.5 days from the launch in 2012 and onwards. This global surface soil moisture product is distributed by EUMETSAT and has a spatial resolution of 12.5 and 25 km respectively (Brocca et al., 2011; EUMETSAT, 2010).

The sensor uses C-band, which has a frequency of 5.255 GHz and a wavelength of 7.5-3.8 cm, which thus allows for monitoring of the top soil layer (0.5-2 cm). The MetOp scatterometers provides the opportunity to derive soil moisture information with a relatively direct approach because of the microwaves high sensitivity to water content in the surface layer. With increasing content of water there is an evident increase in the soil dielectric constant, especially in low frequency regions (1-10 GHz). However, other factors like vegetation and surface roughness also affects the scattering. The sensor design of the MetOp scatterometers are unique and allows for direct accounting for the influencing effects of vegetation, surface roughness and dielectric properties. The viewing capability is a multi-incidence angel which enable separation of factors influencing the backscatter coefficient, and the good radiometric accuracy decrease the noise level (HSAF, 2017; Wagner et al., 2013).

The high temporal resolution of 1.5 day, the multi-angel capability, the continuous measurements and the near real time capabilities of the ASCAT sensor makes it the most suitable for monitoring soil moisture changes (Brocca et al., 2017). Wagner et al. (2013) summarizes the ASCAT satellite as better than current passive microwave sensors and as particular advances and useful in hydrological modelling and numerical weather prediction. Anderson et al. (2012) concludes that the backscatter measurements are stable over time with

annual changes of 0.02 dB (decibel), which makes the ASCAT satellite very well suited for observing soil moisture changes. One concern with the ASCAT satellite is the wavelength in C-band which is considered to be less effective due to reduced sensitivity of soil moisture when the vegetation amount is higher compared to the longer wavelength of L-band. Although, the high radiometric accuracy and therefore the signal-to-noise ratio is sufficient to achieve high retrieval accuracy. The accuracy of the sensor is $0.05 \text{ m}^3\text{m}^{-3}$ (Wagner et al., 2013).

The data acquisition for equatorial and mid-latitude regions are in the descending phase 9:30 and in the ascending 21:30 (± 1 hour). With the two swaths of the satellite that results in a daily global coverage of approximately 82%. Gaps are largest near the equator, and best coverage are achieved over the poles ($>65^\circ$). The irregular spatial coverage also makes the temporal coverage irregular as different amounts of acquisitions are retrieved per day. Two acquisitions per day can be achieved, or more over the poles, at a specific location, but the next day no acquisitions might be retrieved. These irregularities are a constraint of the current available ASCAT data, although, interpolation of measurements can be an option, thus with more uncertainty (Wagner et al., 2013). However, the near real time capabilities of 130 minutes after sensing is a huge advantage in flood monitoring (Albergel et al., 2012).

An estimation of the water saturation of the topsoil layer is presented in relative units between 0-100 %, comparing the wettest and the driest conditions. The soil moisture content m_s , is estimated using σ^0 as the backscatter to be inverted, σ^0_{wet} the backscatter measurements when wet and σ^0_{dry} when dry (Wagner et al., 2013).

$$m_s = \frac{\sigma^0 - \sigma^0_{\text{dry}}}{\sigma^0_{\text{wet}} - \sigma^0_{\text{dry}}}$$

The values are in decibels (dB) at 40° incidence angle and varies in time and space. This degree of saturation can be transformed to volumetric soil moisture content Θ by adding the soil porosity ϕ to determine values with the unit m^3m^{-3} .

$$\Theta = m_s \cdot \phi$$

Water enhances the soil dielectric constant with around 10 times between dry and wet soils, and with an increasing soil moisture the dielectric constant increases and thus the backscatter that are measured. The backscatter variations in densely vegetated areas are small and hence the soil moisture sensitivity is lower (<2 dB), leading to high retrieval error. Agricultural and grassland areas have the highest sensitivity (between 8-12 dB), thus resulting in the best estimates of soil moisture content. The soil moisture retrieval is strongly impacted in case of open water, frozen soils or snow cover (Brocca et al., 2011; Wagner et al., 2013).

The algorithm used is the TU-Wien change detection model that retrieves relative changes in soil moisture and indirectly takes land cover and surface roughness into account (Barrett & Petropoulos, 2012; Wagner, Lemoine, Borgeaud, & Rott, 1999; Wagner, Lemoine, & Rott, 1999). The basic assumptions of the algorithm include a linear relationship between the backscattering and the soil moisture content, the land cover and roughness are stable in time at the spatial scale, vegetation influence on seasonal scale and the backscatter are dependent on the incidence angle (Brocca et al., 2017; Wagner et al., 2013).

3.3.2 ASCAT 1 km spatial resolution

A small-scale surface soil moisture product has been developed with 1 km spatial resolution. This product is disaggregated and re-sampled from the original 25 km product as a tool for

hydrological processes and measures the top 0-2 cm of the soil. The conversion process includes a parameter database and a pre-computed fine-mesh layer that contains information about backscatter and scaling characteristics. This information is derived from finer resolution SAR images provided from Envisat ASAR while operating in ScanSAR global monitoring mode (Brocca et al., 2017; EUMETSAT, 2017; Wagner et al., 2013; Wagner et al., 2008). Main characteristics of ASCAT and ASAR can be seen in Table 3.

Table 3. Main characteristics of ASCAT and ASAR with operation modes of ScanSAR (EUMETSAT, 2010)

ASCAT	Advanced Scatterometer			
Satellites	MetOp-A, MetOp-B, MetOp-C			
Status	Operational - Utilised in the period: 2006 to ~ 2021			
Mission	Sea surface wind vector. Also large-scale soil moisture			
Instrument type	Radar scatterometer - C-band (5.255 GHz), side looking both left and right. 3 antennas on each side			
Scanning technique	Two 550-km swaths separated by a 700-km gap along-track. 3 looks each pixel (45, 90 and 135° azimuth)			
Coverage/cycle	Global coverage in 1.5 days			
Resolution	Best quality: 50 km – standard quality: 25 km – basic sampling: 12.5 km			
Resources	Mass: 260 kg - Power: 215 W - Data rate: 42 kbps			
ASAR	Advanced Synthetic Aperture Radar - SAR mode			
Satellite	Envisat			
Status	Operational - Utilised in the period 2002 to ~ 2013			
Mission	High-resolution all-weather multi-purpose imager for ocean, land and ice			
Instrument type	Imaging radar - C-band SAR, frequency 5.331 GHz, multi-polarisation and variable pointing/resolution			
Scanning technique	Side-looking, 15-45° off-nadir, swath 100 to 405 km, depending on operation mode - See table			
Coverage/cycle	Global coverage in 5 day for the 'global monitoring' mode (if used for 70 % of the time); in longer periods for other operation modes, up to 3 months			
Resolution	30 m to 1 km, depending on operation mode - See table			
Resources	Mass: 832 kg - Power: 1400 W - Data rate: 100 Mbps			
Operation mode	Resolution	Swath	Field of regard	Polarisation
Stripmap	30 m	100 km	485 km	HH or VV
ScanSAR alternating pol	30 m	100 km	485 km	VV/HH, HH/HV, VV/VH
ScanSAR wide swath	150 m	405 km	405 km	HH or VV
ScanSAR wide swath	150 m	405 km	405 km	HH or VV
ScanSAR global monitoring	1 km	405 km	405 km	HH or VV
Wave	30 m	5 x 5 km ² imagettes sampled at 100 km intervals		HH or VV

The global coverage of the original 25 km product is reduced to only apply for Europe in the disaggregated 1 km product. The spatial coverage is dependent on the Envisat ASAR coverage and due to conflicting operating modes, some areas are not fully covered. However, this is currently being developed. The effective resolution is therefore controlled by the original product and the lowest representative resolution could be 25 km. The resolution is affected by the availability and by the disaggregation parameters effectiveness, which in some areas are of deficient quality (EUMETSAT, 2010; Wagner et al., 2008). The 1 km soil moisture product is distributed through H-SAF and is available since August 2009 for Europe (HSAF, no year).

Temporal dynamics of the soil moisture are assumed to be similar across scales, which enable a linear model for the relationship between regional and local scale measurements where soil moisture at 1 km scale can be derived from the 25 km product using (Wagner et al., 2013):

$$m_s^{1km}(t, x, y) = c_{ASAR}(x, y) + d_{ASAR}(x, y)m_s^{25km}(t)$$

where m_s^{1km} is the estimated soil moisture at 1 km by the coordinates (x,y) and m_s^{25km} is the 25 km soil moisture at time t . Time series of backscatter from ASAR creates the coefficients c_{ASAR} and d_{ASAR} that are the scaling parameters. Considering that the downscaling parameters by ASAR are static, i.e. the temporal information is still derived from the original 25 km product, the value of the 1 km product is not yet clear. Nevertheless, it provides interpretation of soil moisture information at much finer resolution which makes it valuable in applications where the spatial distribution is more important than the temporal dynamics (Wagner et al., 2013).

3.3.3 SMOS

The SMOS (Soil Moisture and Ocean Salinity) Mission was launched the second of November 2009 by ESA as a science mission to increase the understanding of the Earth's water cycle, where soil moisture is a key variable. It was the first space born mission with the purpose of retrieving soil moisture (Kerr et al., 2010).

The spatial resolution is 50 km and the revisit time 2-3 days (EO, 2017; Kerr et al., 2010; Parrens et al., 2012). It has a sun-synchronous orbit and measures at an altitude of 757 km. SMOS is an interferometric radiometer, L-band (1.42 GHz), that measures soil moisture content through surface emission at the top 5 cm of the soil (Albergel et al., 2012). With lower frequencies, it is expected that vegetation and other perturbation effects have less impact (Lacava et al., 2012). L-band measurements thus limit the atmospheric contribution, and cloud cover and atmospheric water has insignificant effects. In vegetated areas, the L-band is more sensitive to soil moisture compared to higher frequencies. The accuracy is $0.04 \text{ m}^3 \text{ m}^{-3}$ (Kerr et al., 2010; Parrens et al., 2012). The ascending and descending orbits passes at 6 A.M and 6 P.M equator crossing time on days for retrieval (Kerr et al., 2010).

The SMOS level 2 soil moisture product contains soil moisture data, surface temperature, brightness temperature, roughness parameter and a dielectric constant. The algorithm is a function between the brightness temperature from the modeling of the surface (including knowledge about soil texture and land cover) and actual angular measurements. The brightness temperature is used to derive surface soil moisture (EO, 2017; Kerr et al., 2010; Leroux et al., 2014). Large dielectric contrast can be identified between dry soil and water, and the soil emissivity depend on the moisture content (EO, 2017). The SMOS algorithm consists of a radiative transfer model which identifies each land use class and quantifies the contribution of these (see Kerr et al. (2012) for further information about the algorithm). Difficulties in the estimations using microwave radiometry are presence of vegetation that add its own emission and weakens the existing soil emission. Topography and large water bodies may also affect the soil moisture retrieval (Parrens et al., 2012), and there is no retrieval if the main land use is water (Leroux et al., 2014). However, the L-band has high sensitivity to soil moisture and minimal surface roughness and atmospheric disturbances (EO, 2017). Although, radio frequency interferences (RFI) can disturb and perturbed the microwave emission at some places and hence affect the retrieval of soil moisture from SMOS (Albergel et al., 2012; Pierdicca et al., 2013).

3.3.4 Satellite data processing

The ASCAT soil moisture at 25 km Swath Grid data was downloaded as raw level 1 data in NetCDF format from EUMETSAT (EUMETSAT, 2017). The data was processed in Matlab to make it compatible before import to ArcMap 10.4. The point layer was imported through x/y data and converted to raster format. In the conversion to raster the MEAN was used to get an average value of the points within every cell. One raster layer per day was extracted to be used for comparison, and if a catchment was located over two 25 km cells, the average value of both cells was used. It was then classified into 10 different classes for visualization.

The ASCAT 1 km soil moisture data (SM-OBS-2 Small-scale surface soil moisture by radar scatterometer) was downloaded in BUFR format from HSAF (HSAF, 2017). It was converted to NetCDF with a python code to be compatible before import to ArcMap 10.4 and conversion into raster format. The data was clipped to only cover the flooded areas, and all layers with no data was removed. Due to overlapping bands and the side-looking antenna, images from several times per day could be extracted. The values extracted are from the point

of flooding, and not the entire catchment area, which can affect the resulting values. It was classified into 8 different classes for visualization.

Level 2 soil moisture data in NetCDF format from the SMOS satellite was downloaded from ESA (ESA, 2017). To process the data, the SNAP toolbox version 5.0.0 has been used (Step-ESA, 2017). The values are extracted for the whole catchment, and due to the large spatial resolution the catchment are in the same cell.

3.4 Sediment connectivity index (IC)

This section explains how the sediment connectivity index is calculated through its formulas and later which parameters that have been used in this study.

3.4.1 The index of sediment connectivity

From the approach of Borselli et al. (2008), the sediment connectivity (IC) was developed with the original definition as:

$$IC = \log_{10} \left(\frac{D_{up}}{D_{dn}} \right)$$

where D_{up} and D_{dn} are the upslope and downslope components (Figure 10).

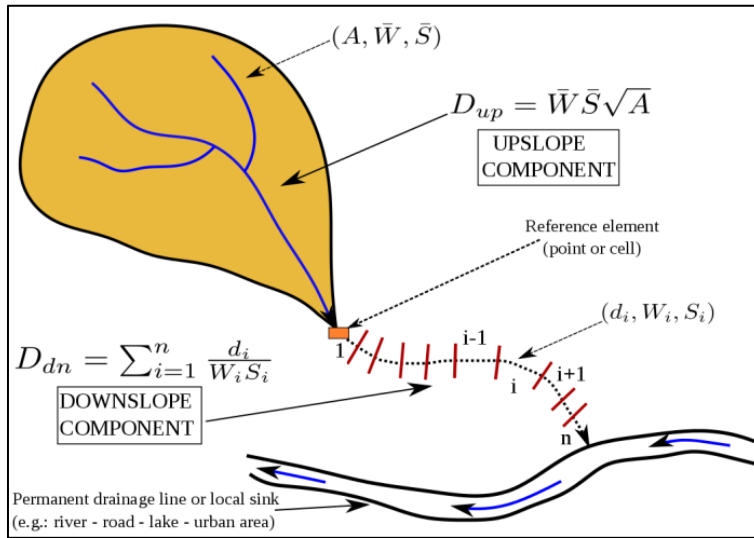


Figure 10. Definition of the index of sediment connectivity. Modified by (Crema, Schenato, Goldin, Marchi, & Cavalli, 2015) from the original index by (Borselli et al., 2008)

D_{up} is the upslope component that characterizes by the downward route of sediment produced upslope, and is defined as:

$$D_{up} = \bar{W} \bar{S} \sqrt{A}$$

W is the average weighting factor of the contributing area upslope, S is the average slope gradient of the contributing area upslope (measured in m/m) and A is the upslope contributing area (m^2).

D_{dn} is the flow path length that a particle travels to arrive to the target or sink, and is defined as:

$$D_{dn} = \sum_i \frac{d_i}{W_i S_i}$$

d_i is the flow path length along the i^{th} cell in accordance with the steepest downslope direction (m), W_i is the weighting factor and S_i is the slope gradient of the i^{th} cell. The connectivity increases with larger IC values, and is defined in $[-\infty, +\infty]$.

Cavalli et al. (2013) revised the IC index to some extent changing the slope factor, the contributing area and the weight factor. To avoid infinities of the slope gradient in the D_{dn} calculation, a lower limit of 0.005 m/m was set in the original model by Borselli et al. (2008), however, Cavalli et al. (2013) added an upper limit of 1 m/m to limit bias due to extremely high IC values that can occur on steep slopes.

The contributing area was in the original model computed by the single-flow direction algorithm, while the revised IC model uses the multiple flow D-infinity approach (Tarboton, 1997). This change was due to the advantages of being able to capture the real flow paths, instead of being restricted to eight directions as the single-flow direction method. It also considers the cell-size of the channel width better, as the single-flow direction method makes sequences of single cells and thus underestimating the width of the channels, while D-infinity algorithm takes the whole cross section into consideration and thus gives a more representative pattern.

The last modification of the model is the weighting factor W . Borselli et al. (2008) based the weighting factor on soil surface and local land use. However, in the revised version (Cavalli et al., 2013) topographic surface roughness, i.e. roughness index (RI) is instead used as the weighting factor, and is based on the standard deviation of the residual topography at a few meter scale. This creates the advantage that only a DTM is needed as input. The difference between the original DTM at 2.5 m resolution and a version that takes the average DTM values on a 5 x 5 cell window that is moved across the topography grid creates the roughness index:

$$RI = \sqrt{\frac{\sum_{i=1}^{25} (x_i - x_m)^2}{25}}$$

Where 25 is the processing cells within the moving window, x_i is a specific cells value of the residual topography within the moving window and x_m is the mean of the 25 cells included in the window. Furthermore, the new weighting factor is defined as:

$$W = 1 - \left(\frac{RI}{RI_{MAX}} \right)$$

Where RI_{max} is the highest possible value of the roughness index (RI).

3.4.2 Sediment connectivity calculations

The sediment connectivity was calculated using the software SedInConnect 2.3 (Crema, Schenato, Goldin, Marchi, & Cavalli, 2015), which is a stand-alone application and open source. Sediment connectivity can also be computed using the Sediment connectivity toolbox in ArcGIS. The input data was processed in ArcMap 10.5 before it was used in SedInConnect. The input data consists of a Digital Elevation Model (DEM), 2 m resolution, that is reconditioned to remove artificial dams, lakes and road-stream intersections that block the original flow of water through the implementation of cross-sections into the DEM. It is therefore corrected for culverts and sinks that affect the water flow and thus creates a more realistic road of transport of sediment and water through the landscape. The target in the calculations are a layer with roads that consists of a 4-meter buffer, corresponding the width of the road. The soil moisture data used as a weight in the calculations are the ASCAT 25 km data and the ASCAT 1 km data, and has first been processed in ArcMap before implementation in the sediment connectivity index. In visualization and representing the

results, the sediment connectivity values have been divided into 5 classes according to natural breaks.

The different calculations performed and the weighting factors are presented in detail in Appendix B.

3.5 Assumptions

This project is based on previous research in the field and the same case study areas has been used. A number of physical catchment descriptors (PCDs) are applied from the work by Kalantari et al. (2014), and later by Michielsen et al. (2016), and modified with soil moisture and precipitation values (Appendix A). The sediment connectivity calculations are based on the same input data that Cantone (2016) used, to be able to compare the results. The same base material has thus been applied in this study to enable analysis of how soil moisture contributes to the development of a reliable flood prediction method.

Further assumptions include the exclusion of some flooded points in the IC calculations due to being located within the same catchment as another point (Cantone, 2016). The soil moisture values for the IC calculations are the 19th of August 2014 for Västra Götaland and 21st of August for Värmland, as these days were the starting point of the flooding.

Temperature affects the soil moisture content as warmer temperatures results in less soil moisture due to evapotranspiration. However, in this case the temperature differences are 1 degree at the most, which is judged not to affect the result.

The soil type layer from the Swedish Geological Institute is measured below 0,5 m depth, not the top soil cover (SGU, 2016). The satellite data measures the top 5 cm of the soil cover, which means that the soil moisture content cannot be completely compared with the soil layer from SGU. Furthermore, the top soil cover in Sweden consists of 75% moraine (SGI, 2016).

4 RESULTS

In this section the results of the study are presented. At first an overview of existing road drainage structures at the study sites are presented, continuing with the precipitation data, the soil moisture extracted from satellite data and finally the results from the sediment connectivity calculations.

4.1 Road drainage structures

An inventory of road drainage structures has been done for the flooded areas using Trafikverkets database BaTMan. A database that manage, monitor and provides information about bridges, tunnels and other constructions in relation to roads. Constructions below 2000 mm in span width are not included (Trafikverket, 2015). Google Maps is used as a complement to locations where no culverts or bridges are registered in BaTMan, to see if there are smaller drainage structures visible. The table with all road drainage structures can be found in Appendix C.

In Västra Götaland 4 out of 5 flooded areas lack a larger road bridge. At Hogsbotorpsmotet culverts can be identified through Google Maps (Figure 11), although, no outlet of the 4 visible culverts can be seen. However, these are expected to exist. The only flooded location with a bridge is Säleby, while 5 of the non-flooded areas have a larger bridge registered.

Out of 8 flooded areas in Värmland, 6 is missing a larger road bridge. Smaller culverts are visible at 3 of these locations, but with questionable standard and size. At Ikea, a stone culvert that are somewhat overgrown can be identified from Google Maps (Figure 12). At the non-flooded points 7 bridges are registered.



Figure 11. Culverts under E6 at Hogsbotorpsmotet. Retrieved from Google Maps. Image taken in October 2009, before the event.



Figure 12. Stone culvert under E18 at IKEA, Värmland. Retrieved from Google Maps. Image taken in May 2011, before

The area of Värmland had received large amounts of precipitation also before the event which saturated the surrounding peatlands and enhanced the flood risk of the coming rainfall event. Projected precipitation the week after the event did not reach Kristinehamn, which would have affected already damaged roads and culverts further. In Kristinehamn, and especially the locations Lagmansgatan, Östra Ringvägen and Rådmansgatan, that are connected with the same watercourse was largely affected. In this area also upstream dams and passing storm water flows got consequences, together with a culvert owned by the municipality upstream from the road E18 that had restricted flow (Styffe, 2017-05-19). Dimensioning of culverts upstream and downstream affect each other, and according to Appendix C the occurrence and sizes of the road constructions differs in this area. There are no larger bridges or culverts at Lagmansgatan, and only a small culvert at Kristinehamn E18.

The road bridge at Rådmansgatan with 4 m span width was built in 2012, but was flooded in 2014, which indicates a too low dimensioning when being built only 2 years before. Östra Ringvägen is located the most downstream and that road bridge had a 5 m span width. However, it was flushed away during the event, and is today replaced by a new one with twice the dimension (SVT, 2014-10-14).

Other measures have been made by Trafikverket to prevent similar future events and to reduce potential consequences. At Väse Gamla E18 the existing small culverts was newly installed when the event happened, which made them more sensitive as material and grass cover was not yet established as with older constructions. However, new dimensioning of culverts at that location is under investigation (Styffe, 2017-05-19). In Ölme, located between Kristinehamn and Karlstad along the affected E18, Trafikverket has investigated the placement and capacity of the pumps to avoid similar situations again. In Broby (road 766 and 768), located north of Ölme and E18, tree culverts were placed laterally under the road. This is the wrong way of installing road constructions, and these are now replaced by a bridge with larger dimension (Styffe, 2017-05-19).

4.2 Precipitation

The precipitation is collected from two different sources. At first the ground station measurements of two stations in each area are included (SMHI, 2017c) and secondly, the radar measurements by Berg et al. (2016).

4.2.1 Ground station measurements

According to SMHI ground station measurements the precipitation amount in Västra Götaland in August 2014 was 218 mm for Uddevalla station and 179 mm for Heden station. Considering the last 10 years of monthly precipitation these are the highest recorded numbers. For Uddevalla station the average precipitation between year 2004-2013 is 105 mm and for Heden 111 mm. Uddevallas precipitation of 218 mm in August 2014 is thus more than twice the average the last 10 years. The precipitation was highest the 19th of August, which is the day of the occurred flooding, with an average precipitation of 31,6 mm including both stations. Highest numbers were recorded in Uddevalla with 49 mm the 19th (SMHI, 2017c).

The precipitation in Värmland in August 2014 was 290 mm for Väse station and 168 mm for Kristinehamn station. The average precipitation per month the last 10 years is 97 mm for Väse and 102 mm for Kristinehamn. The precipitation of 290 mm in Väse during August 2014 is thus high compared to the average of 97 mm per month. On the 20th of August 2014 the precipitation was 59,7 mm and the 23rd 61,9 mm, which is more than an average month in the

area (SMHI, 2017c). The precipitation the days before the flooding and the starting day of the flooding is presented in Table 4.

Table 4. Ground station measurements. The stations Uddevalla and Heden are used for Västra Götaland and Kristinehamn and Våse for Värmland (SMHI, 2017c). The marked columns are the starting day of the flooding.

Precipitation		Unit: mm							
		16-aug	17-aug	18-aug	19-aug	20-aug	21-aug		
Västra Götaland	Flooded	1 Hogstorpstötet	4,70	15,35	7,55	31,60	10,15	14,60	
		2 Småröd	4,70	15,35	7,55	31,60	10,15	14,60	
		3 Säleby	4,70	15,35	7,55	31,60	10,15	14,60	
		4 Båthammen	4,70	15,35	7,55	31,60	10,15	14,60	
	Non-Flooded	5 Älvbacken	4,70	15,35	7,55	31,60	10,15	14,60	
		6 Bro	4,70	15,35	7,55	31,60	10,15	14,60	
		7 Gravröse	4,70	15,35	7,55	31,60	10,15	14,60	
		8 Hällkista	4,70	15,35	7,55	31,60	10,15	14,60	
		9 Holmen	4,70	15,35	7,55	31,60	10,15	14,60	
		10 Korpås	4,70	15,35	7,55	31,60	10,15	14,60	
		11 Störreberg	4,70	15,35	7,55	31,60	10,15	14,60	
		12 Svalte	4,70	15,35	7,55	31,60	10,15	14,60	
Värmland	Flooded	13 Ikea	15,00	7,90	7,10	15,10	59,70	14,10	
		14 Fintatorp	15,00	7,90	7,10	15,10	59,70	14,10	
		15 Våse Gamla E18	15,00	7,90	7,10	15,10	59,70	14,10	
		16 Strandvägen	0,90	9,90	5,10	7,00	21,10	13,00	
		17 Kristinehamn E18	0,90	9,90	5,10	7,00	21,10	13,00	
		18 Lagmansgatan	0,90	9,90	5,10	7,00	21,10	13,00	
		19 Östra Ringvägen	0,90	9,90	5,10	7,00	21,10	13,00	
		Non-Flooded	20 Skattkärrstötet	15,00	7,90	7,10	15,10	59,70	14,10
			21 Solberg	15,00	7,90	7,10	15,10	59,70	14,10
	22 Silkesta		15,00	7,90	7,10	15,10	59,70	14,10	
	23 Karlabron		0,90	9,90	5,10	7,00	21,10	13,00	
	24 Sorkan		0,90	9,90	5,10	7,00	21,10	13,00	
	25 Väsemotet		15,00	7,90	7,10	15,10	59,70	14,10	
	26 Björkebol		0,90	9,90	5,10	7,00	21,10	13,00	
	27 Heden		0,90	9,90	5,10	7,00	21,10	13,00	
	28 Byrmon		15,00	7,90	7,10	15,10	59,70	14,10	
	29 Gunnerud		15,00	7,90	7,10	15,10	59,70	14,10	
	30 Kappstad	15,00	7,90	7,10	15,10	59,70	14,10		
	31 Öckna	15,00	7,90	7,10	15,10	59,70	14,10		
32 Östervik	0,90	9,90	5,10	7,00	21,10	13,00			
33 Spånga	15,00	7,90	7,10	15,10	59,70	14,10			

4.2.2 Precipitation radar measurements

The precipitation in Västra Götaland was low during the day of the 19th, but started to increase around 17:30 and was ongoing until 21:15. From 20:00 the precipitation amounts increase a lot locally. At 20:15 Hällkista receives 21,4 mm in 30 minutes, which is close to the definition of a skyfall, which according to SMHI (2017a) is a minimum of 50 mm in one hour or at least 1 mm in one minute. In 2 hours the precipitation was 36,3 mm. Interesting here is that despite the extreme precipitation in Hällkista, the area was not flooded. Småröd, Högsbotorp and Båthammen that also received large amounts during a short period was flooded (Table 5).

Table 5. Precipitation Västra Götaland during the evening of the 19th of August 2014. Derived from the 15 minutes radar precipitation data of Berg et al. (2016). The highest measured values are in red text.

Unit: mm		19-aug																	SUM
VÄSTRA GÖTALAND		17:30	17:45	18:00	18:15	18:30	18:45	19:00	19:15	19:30	19:45	20:00	20:15	20:30	20:45	21:00	21:15	21:30	
Flooded	Hogstorpstötet	0,0	0,4	2,4	2,5	1,0	0,4	0,5	0,7	0,8	2,6	5,0	5,4	2,9	2,6	1,0	0,0	0,0	28,1
	Småröd	0,0	0,0	0,0	0,3	0,5	0,9	2,3	4,1	4,1	1,9	1,0	0,9	0,1	0,0	0,0	0,0	0,0	16,0
	Säleby	0,0	0,0	0,0	0,0	0,9	0,3	0,5	1,1	1,6	1,8	1,0	0,4	0,0	0,0	0,0	0,0	0,0	7,4
	Båthammen	0,0	0,0	0,0	0,4	1,2	4,6	5,1	5,5	4,2	2,5	1,5	1,1	0,9	0,0	0,0	0,0	0,0	26,9
Non-Flooded	Älvbacken	0,0	0,0	0,0	0,2	0,4	0,1	1,1	0,8	0,6	0,7	0,6	0,0	0,0	0,0	0,0	0,3	0,0	4,8
	Bro	0,0	0,0	0,0	3,5	6,2	4,6	3,2	2,2	1,1	0,2	0,0	0,0	0,0	0,0	0,0	0,0	0,0	21,1
	Gravröse	3,1	5,6	3,1	0,5	0,3	0,2	0,2	0,3	0,4	0,4	0,3	2,0	5,1	4,0	1,0	0,1	0,0	26,5
	Hällkista	0,4	1,6	1,6	0,9	0,8	0,7	0,4	1,2	2,7	2,3	3,0	10,5	10,9	4,7	0,9	0,0	0,0	42,6
	Holmen	1,4	1,6	1,0	0,7	0,7	0,4	0,1	0,2	0,5	0,5	0,1	0,2	0,4	1,2	4,9	4,5	0,0	18,3
	Korpås	2,3	1,1	0,8	0,3	0,1	0,1	0,2	0,2	0,5	0,6	0,2	0,3	1,3	1,5	5,4	3,0	0,0	17,8
	Störreberg	0,0	0,0	0,2	0,7	1,2	0,7	0,2	0,3	0,2	0,1	0,0	0,0	0,0	0,0	0,0	0,0	0,0	3,6
	Svalte	1,4	0,8	0,6	0,4	0,8	0,7	0,3	0,3	0,3	0,4	0,2	1,0	1,0	0,3	0,2	0,0	0,0	8,5

The precipitation in Värmland started at 23:30 the 20th of August and continued during the night to the 21st. The largest amounts hit Solberg and Silkesta with 46,9 mm and 42,6 mm respectively. Solberg had the largest precipitation with 42,2 mm during 2 hours (between 01:30 and 03:30) and 26,1 mm during one hour. Which can be compared with SMHI's definition of a skyfall (SMHI, 2017a), but according to that definition the event was not a skyfall. In total up to 60 mm of precipitation has been reported during the 20th to the 21st, and 40 mm fell during a few hours in the night according to Table 6.

Table 6. Precipitation Värmland during the night to the 21st of August 2014. Derived from the 15 minutes radar precipitation data of Berg et al. (2016). The highest measured values are in red text.

Unit:	20-aug		21-aug																SUM		
mm	VÄRMLAND																				
	23:30	23:45	00:00	00:15	00:30	00:45	01:00	01:15	01:30	01:45	02:00	02:15	02:30	02:45	03:00	03:15	03:30	03:45	04:00		
Flooded	Ikea	0,0	0,0	0,0	0,1	0,1	0,1	0,0	0,0	0,0	0,0	0,0	0,0	0,0	0,0	0,0	0,0	0,0	0,0	0,0	0,3
	Fintatorp	0,0	0,0	0,0	0,1	0,1	0,0	0,0	0,0	0,0	0,0	0,0	0,0	0,0	0,0	0,0	0,0	0,0	0,0	0,0	0,2
	Väse Gamla E18	0,0	0,0	0,1	0,6	0,5	0,1	0,2	0,9	2,4	3,9	4,3	4,2	3,6	3,6	3,8	2,2	0,8	0,6	0,6	32,2
	Strandvägen	0,7	1,1	1,2	1,9	2,8	3,2	2,6	1,9	1,8	2,0	2,8	2,5	1,3	1,6	1,7	0,6	0,4	0,4	0,2	30,9
	Kristinehamn E18	0,6	0,7	0,9	0,7	1,4	2,5	1,6	2,4	2,5	0,8	1,9	2,0	0,8	0,5	0,5	0,3	0,1	0,2	0,2	20,4
	Lagmansgatan	3,1	3,0	1,1	2,6	3,3	3,6	3,2	2,1	0,7	0,1	1,8	2,0	0,5	0,5	0,4	0,2	0,1	0,2	0,2	29,1
	Östra Ringvägen	2,7	2,6	2,1	3,5	2,0	1,6	2,4	1,6	0,3	0,0	1,3	1,4	0,4	0,6	0,5	0,3	0,2	0,3	0,3	24,3
Non-Flooded	Skattkärrsmotet	0,0	0,0	0,0	0,0	0,4	0,5	0,9	1,5	0,7	2,1	2,0	0,0	0,5	1,6	1,9	1,0	0,5	0,6	0,5	14,7
	Solberg	0,0	0,0	0,0	0,0	0,3	0,4	0,6	1,1	0,9	5,6	9,4	6,2	4,2	6,4	6,0	3,1	1,4	0,6	0,7	47,0
	Silkesta	0,0	0,0	0,1	0,4	0,2	0,1	0,2	1,3	2,3	6,6	6,6	3,7	5,2	6,5	4,5	2,1	1,4	0,7	0,8	42,7
	Karlabron	2,4	1,9	2,1	3,3	2,1	2,5	3,4	2,2	0,5	0,4	1,5	1,6	0,6	0,5	0,2	0,2	0,2	0,2	0,2	25,8
	Sorkan	0,0	0,1	0,1	0,2	1,6	3,5	5,9	5,4	2,1	2,2	2,0	0,9	1,0	0,9	0,5	0,2	0,3	0,3	0,3	27,4
	Väsemotet	0,0	0,0	0,1	0,2	0,4	2,5	2,8	3,1	2,7	1,0	1,4	1,4	1,0	0,3	0,3	0,2	0,7	1,1	0,7	19,9
	Björkebol	1,0	0,8	0,4	1,2	1,9	2,2	1,7	2,0	2,1	0,9	0,8	1,2	0,7	0,3	0,3	0,3	0,2	0,2	0,2	18,6
	Heden	1,2	0,8	1,4	2,4	2,1	2,6	2,9	2,2	1,8	1,3	1,3	1,4	0,7	0,3	0,1	0,1	0,2	0,2	0,2	23,4
	Bymon	0,0	0,0	0,0	0,0	0,0	0,0	0,2	0,3	0,2	0,1	0,2	0,2	0,3	0,2	0,2	0,2	0,2	0,2	0,1	2,7
	Gunnerud	0,0	0,0	0,0	0,0	0,0	0,1	0,2	0,3	0,2	0,1	0,2	0,2	0,3	0,2	0,2	0,2	0,2	0,2	0,1	2,7
	Kappstad	0,0	0,0	0,0	0,2	0,1	0,0	0,0	0,2	0,3	0,2	0,4	0,5	0,3	0,2	0,3	0,2	0,2	0,1	0,1	3,2
	Öckna	0,0	0,0	0,0	0,0	0,0	0,0	0,0	0,1	0,2	0,1	0,2	0,2	0,2	0,1	0,2	0,2	0,2	0,2	0,1	1,9
	Östervik	0,1	0,7	1,2	2,1	3,0	3,0	2,5	5,6	6,1	2,6	1,0	0,7	1,8	1,8	1,0	1,9	1,9	0,6	0,3	37,8
	Spånga	0,0	0,0	0,0	0,0	0,1	0,1	0,1	0,3	0,2	1,9	3,4	1,6	0,5	1,3	1,2	0,6	0,4	0,4	0,5	12,6

Figure 13 show the distribution of rainfall the 21st of August at 02.00 AM for Värmland and 19th of August 20:15 for Västra Götaland, where several points of interest had large amounts of precipitation during 15 minutes.

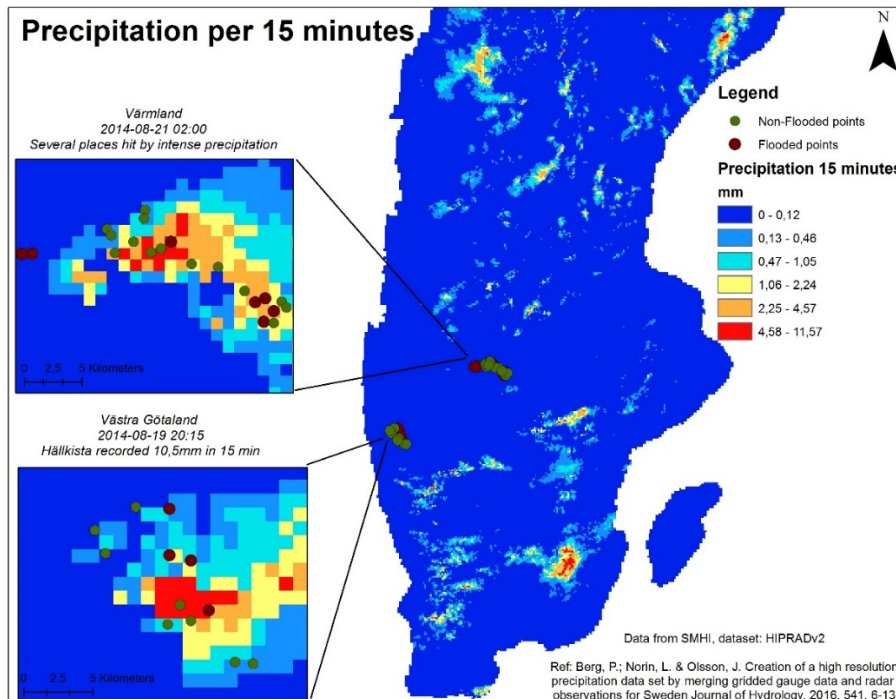


Figure 13. Precipitation per 15 minutes. 21st of August for Värmland and 19th of August for Västra Götaland, with large amounts of precipitation during 15 minutes.

4.3 Satellite soil moisture values

In this section the results from the satellite soil moisture data from ASCAT 25 km resolution, ASCAT 1 km resolution and SMOS is presented. A comparison between the satellites has been performed to validate the results.

4.3.1 Comparison between satellites

The 3 satellites used in this study are the ASCAT 25 km resolution, ASCAT 1 km resolution and the SMOS satellite. In regards of the soil moisture values extracted from the satellites a comparison to validate them has been made in Figure 14. Since the ASCAT soil moisture product is degree of saturation representing a relative value of the driest and wettest conditions in each cell, and the SMOS dataset is volumetric soil moisture in m^3/m^3 a conversion by a linear transformation can be made (Fascetti et al., 2014).

$$\frac{SMC_{ASCAT} - \min(SMC)}{\max(SMC) - \min(SMC)} = \frac{SMI_{ASCAT}}{100}$$

However, in this case has the SMOS values only been multiplied with 100 to show the correlation between them. The ASCAT 1 km and the SMOS satellite miss data some days which explains the missing values in the diagram (Figure 14).

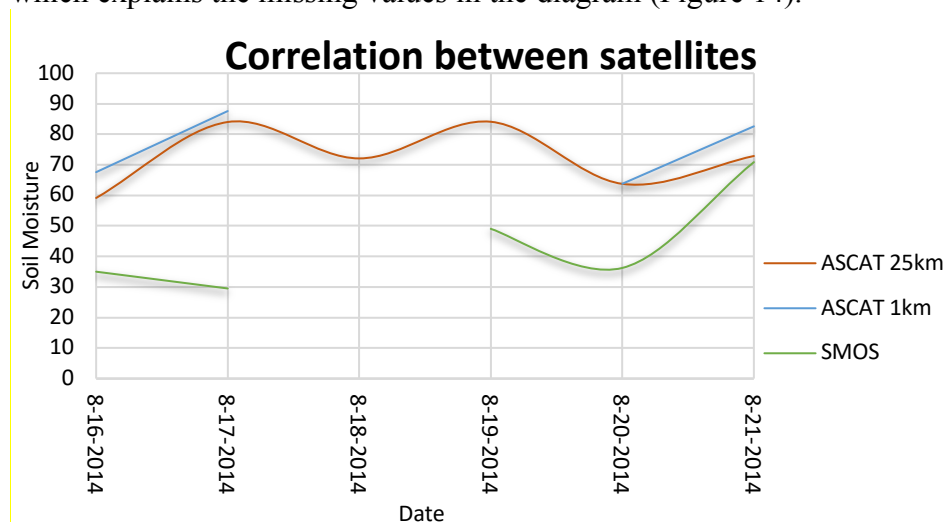


Figure 14. Correlation between the ASCAT 25 km resolution, ASCAT 1 km resolution and SMOS satellite. The location shown is IKEA, Värmland

Figure 14 show that the three different satellites approximately follow the same pattern. Most prominent is the raise in values after the high rainfall the night between the 20th and 21st, that has a high degree of correlation. The ASCAT 25 km and ASCAT 1 km is based on the same base data, as the 1 km product is a disaggregated version of the 25 km. In a comparison between these two the 1 km product has somewhat higher soil moisture values. Which also agrees when looking at all locations the 21st of August in Värmland, where the 1 km product has higher average soil moisture values (90,5%) than the 25 km product (79,6%) (see Appendix D). This could be an overestimation of the values in the 1 km product.

In the average values of ASCAT 1 km, Solberg has a soil moisture content of 100% in 11 out of 21 measurements (Appendix D), which is questionable. It has 100% even on days with 0 mm of precipitation. The results for the 1 km product of Solberg is therefore excluded from average calculations. Also the location Karlabron differs a lot from the rest with extremely low values as it has half the soil moisture values of the other sites, and has therefore also been excluded from average measurements considering the 1 km product.

Another factor affecting the choice of satellite is the amount of No Data. The SMOS satellite has a lot of No Data with 52% missing values for Värmland and 56% for Västra Götaland. The ASCAT 1 km has 44% missing values during the dates of interest for Värmland and no values at all for Västra Götaland. This is due to the differences in temporal resolution and the disaggregating effects concerning the ASCAT 1 km product. Therefore, is the ASCAT 25 km product valued as most useful in this context. All soil moisture values during the studied period for all 3 satellites can be found in Appendix D.

4.3.2 Results ASCAT 25 km

The days before the flooding Västra Götaland received some medium amounts of precipitation before the heavier precipitation of the 19th (Table 4). The soil moisture content increases during these days before the flooding with the peak values on the 19th of 70,73% soil moisture, and 61,58% in average for the whole area (Table 7). On the 20th the soil moisture content went down (a decrease of 10-20%), to increase again the 21st. There was a small increase in precipitation between the days, 10,15 mm the 20th and 14,6 mm the 21st. The near 20% drop in soil moisture content between the 19th and the 20th could be due to less precipitation 31,6 mm the 19th and 10,15 mm the 20th.

Table 7. ASCAT 25km soil moisture (EUMETSAT, 2017). Relative soil moisture values the days before, and the first day of flooding for Västra Götaland and Värmland. The marked columns are the day of flooding.

Soil moisture		ASCAT 25 km % Relative soil moisture						
		16-aug	17-aug	18-aug	19-aug	20-aug	21-aug	
Västra Götaland	Flooded	1 Hogstorpshotet	47,48	57,25	61,35	70,73	51,45	61,10
		2 Småröd	47,48	57,25	61,35	70,73	51,45	61,10
		3 Sälaby	32,08	47,77	42,82	52,75	38,79	48,89
		4 Båthamnen	37,16	44,70	41,84	50,58	40,81	57,95
	Non-Flooded	5 Älvbacken	32,08	47,77	42,82	52,75	38,79	48,89
		6 Bro	42,23	41,63	40,86	48,40	42,82	67,01
		7 Gravrose	47,48	57,25	61,35	70,73	51,45	61,10
		8 Hällkista	47,48	57,25	61,35	70,73	51,45	61,10
		9 Holmen	47,48	57,25	61,35	70,73	51,45	61,10
		10 Korpås	47,48	57,25	61,35	70,73	51,45	61,10
		11 Störreberg	37,16	44,70	41,84	50,58	40,81	57,95
		12 Svälte	44,86	49,44	51,11	59,56	47,14	64,01
Värmland	Flooded	13 Ikea	59,15	84,02	72,10	84,10	63,77	72,89
		14 Fintatorp	64,44	80,79	67,70	84,15	65,63	75,58
		15 Väse Gamla E18	66,50	79,73	74,50	91,41	69,83	77,74
		16 Strandvägen	60,70	75,46	64,64	81,54	65,44	86,58
		17 Kristinehamn E18	60,70	75,46	64,64	81,54	65,44	86,58
		18 Lagmansgatan	60,70	75,46	64,64	81,54	65,44	86,58
	Non-Flooded	19 Östra Ringvägen	67,28	75,46	70,77	90,13	70,67	84,59
		20 Skattkärrshotet	59,15	84,02	72,10	84,10	63,77	72,89
		21 Solberg	59,15	84,02	72,10	84,10	63,77	72,89
		22 Silkesta	66,50	84,02	74,50	91,41	69,83	77,74
		23 Karlabron	60,70	75,46	64,64	81,54	65,44	86,58
		24 Sorkan	67,28	75,46	70,77	90,13	70,67	84,59
		25 Väsemotet	67,28	75,46	70,77	90,13	70,67	84,59
		26 Björkebol	60,70	75,46	64,64	81,54	65,44	86,58
27 Heden	60,70	75,46	64,64	81,54	65,44	86,58		
28 Bymon	59,15	84,02	72,10	84,10	63,77	72,89		
29 Gunnerud	59,15	84,02	72,10	84,10	63,77	72,89		
30 Kappstad	59,15	84,02	72,10	84,10	63,77	72,89		
31 Öckna	59,15	84,02	72,10	84,10	63,77	72,89		
32 Östervik	67,28	75,46	70,77	90,13	70,67	84,59		
33 Spånga	59,15	84,02	72,10	84,10	63,77	72,89		

Generally, there are much higher soil moisture content in Värmland compared to Västra Götaland (Table 7). The flooding started at the 21st of August in Värmland, however, the peak values of over 90% soil moisture occurred the 19th of August in the area of Väse (Väse Gamla E18, Väsemotet, Silkesta, Sorkan and Östervik), and also at a location close to Kristinehamn (Östra Ringvägen) whose watershed area goes up towards Väse as well. The soil moisture content was high in all of the area on the 19th as the average was 85,2%, this despite the fact that the precipitation was relatively low. Interesting here is that several of the areas was not flooded despite the high soil moisture content.

Most precipitation fell on the evening of the 20th and the night to the 21st with 59,7 mm at Våse and 21,1 mm in Kristinehamn (Table 6), which correspond with the higher values of soil moisture on the 21st compared to the 20th. However, this was still lower than the 19th, although, the high values then might have saturated the soil and enhanced the conditions for flooding on the 21st. Nevertheless, the high amounts of precipitation should have had a larger effect considering the much higher soil moisture values some days earlier with less precipitation. The precipitation was lower in Kristinehamn than in Våse, which not correspond with the higher soil moisture values in Kristinehamn. All areas in Kristinehamn has till as main soil type (Appendix A), and are located in urban areas with a lot of impermeable surfaces. Furthermore, comparing this to the areas in Våse, where the precipitation was much higher but the soil moisture content lower, the soil types varies between rock, peat, sand and till.

A visualization of the soil moisture can be seen in Figure 15, with the days of the flooding chosen for each study area.

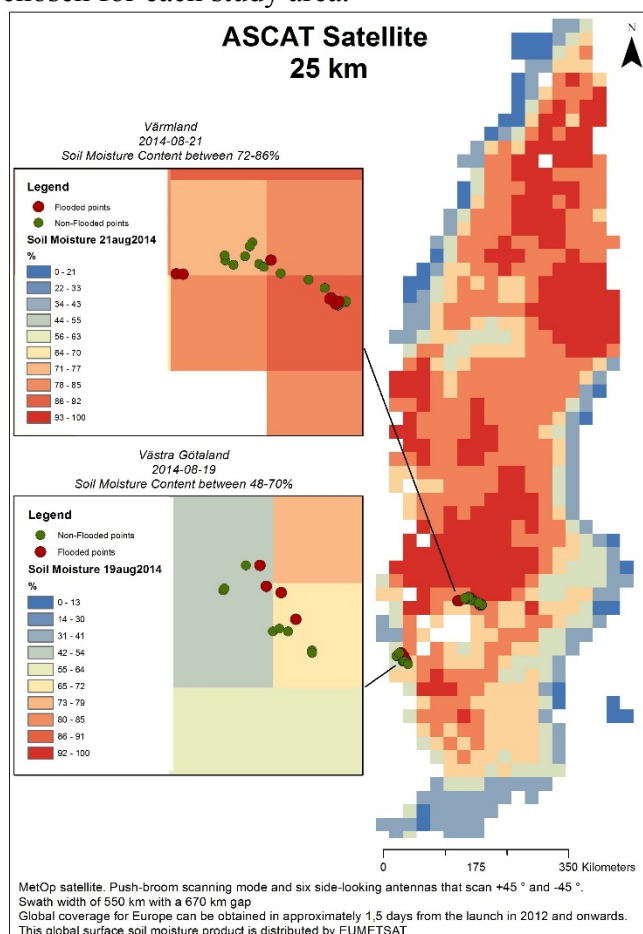


Figure 15. Soil moisture content from ASCAT 25 km resolution satellite for Västra Götaland and Värmland (EUMETSAT, 2017). The values are the 19th of August for Västra Götaland and the 21st of August for Värmland. Each pixel corresponds to 25 km.

In a comparison between the soil moisture content and the 15 minutes precipitation data (Berg et al., 2016), a good correlation can be seen (Table 8). Higher precipitation results in most cases to a larger increase in soil moisture. The exception is Solberg and Silkesta in Värmland with over 40 mm of precipitation, but a smaller increase in soil moisture, and Båthamnen in Västra Götaland with 26,92 mm of precipitation but a lower soil moisture than areas with the same precipitation amounts.

Table 8. Radar precipitation (Berg et al., 2016) and ASCAT 25km soil moisture (EUMETSAT, 2017). Västra Götaland: Precipitation evening the 19th, soil moisture 19th of August. Värmland: Precipitation the night 20–21st, soil moisture 21st of August

Precipitation and ASCAT 25km soil moisture		Soil moisture			
		Precipitation mm	%		
Västra Götaland	Flooded	1 Hogstörpsmotet	28,07	70,73	
		2 Småröd	15,99	70,73	
		3 Säleby	7,42	52,75	
		4 Båthammen	26,92	50,58	
	Non-Flooded	5 Älvbacken	4,78	52,75	
		6 Bro	21,06	48,40	
		7 Gravröse	26,90	70,73	
		8 Hällkista	42,61	70,73	
		9 Holmen	18,69	70,73	
		10 Korpås	19,55	70,73	
		11 Störreberg	3,61	50,58	
		12 Svälte	9,42	59,56	
Värmland	Flooded	13 Ikea	0,30	72,89	
		14 Fintatorp	0,15	75,58	
		15 Väse Gamla E18	32,24	77,74	
		16 Strandvägen	30,89	86,58	
		17 Kristinehamn E18	20,44	86,58	
		18 Lagmansgatan	29,09	86,58	
		19 Östra Ringvägen	24,27	84,59	
		Non-Flooded	20 Skattkärrsmotet	14,71	72,89
			21 Solberg	46,95	72,89
	22 Silkesta		42,66	77,74	
	23 Karlabron		25,75	86,58	
	24 Sorkan		27,43	84,59	
	25 Väsemotet		19,94	84,59	
	26 Björkebol		18,58	86,58	
	27 Heden		23,37	86,58	
	28 Bymon		2,65	72,89	
	29 Gunnerud		2,71	72,89	
	30 Kappstad		3,15	72,89	
	31 Öckna	1,86	72,89		
	32 Östervik	37,80	84,59		
33 Spånga	12,57	72,89			

4.3.3 Results ASCAT 1 km

The ASCAT 1 km product has no data for Västra Götaland during the period of interest. This is most likely due to the closeness to water (which is excluded) and due to the disaggregating effect when downscaling from 25 km to 1 km. Soil moisture information is only available if there is a sufficient temporal correlation among the local and regional backscatter information. The downscaling approach uses static parameters (from SAR data), it is thus the temporal variation of the 25 km product that drives the 1 km product, and the soil moisture information is scaled down linearly for each grid point (Wagner et al., 2008). The 1 km product is thus useful for spatial distribution at a higher spatial scale, but not sufficient when investigating temporal dynamics.

Since the satellite passes both in the ascending and the descending phase, and with side-looking antennas measurements can be done several times during a day (Table 9 and Figure 16). This is useful to see how the soil moisture content is changing during the day. The highest soil moisture content is recorded on the morning of the 21st of August. This correlates with the large amounts of precipitation that fell between the 20th and the 21st. The soil moisture content has an average of 90,5% on the morning of the 21st. The soil moisture content is generally lower later on the day, which most likely is due to evapotranspiration. However, it also depends on the precipitation patterns during the day. At some locations in Värmland the soil moisture content increases in the evening which is due to increased precipitation amounts during the afternoon. Although, the extremely large amounts of precipitation fell on the night between the measure at 18:57 the 20th and the measure at 08:45 the 21st, which correlates with the soil moisture increase between those measurements (Table 9).

Table 9. ASCAT 1 km Soil moisture content at flooded points the 20th and 21st of August 2014 in Värmland

Soil Moisture ASCAT 1 km		20-aug	21-aug	21-aug	21-aug	21-aug
		Time: 18:57 %	Time: 08:45 %	Time: 10:24 %	Time: 18:36 %	Time: 20:15 %
Flooded	Ikea Karlstad	63,80	82,60	80,70	78,60	77,40
	Fintatorp	61,90	69,00	72,20	71,20	69,70
	Våse Gamla E18	83,10	95,00	No Data	86,70	90,80
	Kristinehamn Strandvägen	72,00	86,10	No Data	70,00	74,00
	Kristinehamn E18	71,50	85,60	No Data	76,00	80,40
	Lagmansgatan	59,40	71,80	71,10	63,30	67,20
	Östra Ringvägen	57,30	69,00	No Data	61,20	64,90

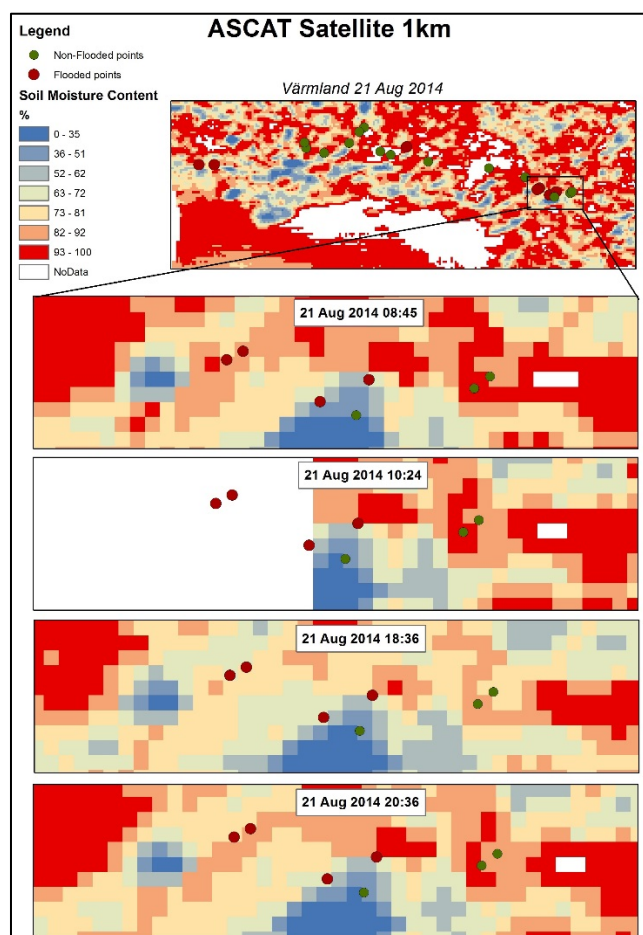


Figure 16. Soil moisture content from ASCAT 1 km resolution satellite (HSAF, 2017). Soil moisture values for each passing of the satellite the 21st of August at Kristinehamn, Värmland.

4.3.4 Results SMOS

The results from the SMOS satellite are in volumetric soil moisture, however, a correlation can still be seen between the relative values of the ASCAT satellite. The SMOS satellite contains a lot of no data values due to the higher temporal resolution of 2-3 days (Table 10), which makes it harder to interpret the results. Although, the values follow the same trend as the values from the ASCAT satellite, as there is an increase the 19th of August in Västra Götaland and in the 21st in Västra Götaland. This can also be seen in Figure 14 where the comparison between the satellites show a good correlation of the values.

Table 10. Soil moisture from the SMOS satellite (ESA, 2017) for Västra Götaland and Värmland. Blank columns are no data.

Soil moisture		SMOS 50km						
		Unit: m ³ m ⁻³ Volumetric soil moisture						
		16-aug	17-aug	18-aug	19-aug	20-aug	21-aug	
Västra Götaland	Flooded	1 Hogstörpsmotet	0,20			0,01		0,26
		2 Småröd	0,11			0,31		0,50
		3 Sälaby	0,11			0,31		0,50
		4 Båthamnen	0,11			0,31		0,50
	Non-Flooded	5 Alybacken	0,11			0,31		0,50
		6 Bro						0,24
		7 Gravröse				0,01		0,26
		8 Hällkista				0,01		0,26
		9 Holmen	0,20	0,04	0,10	0,11		0,16
		10 Korpås	0,20	0,04	0,10	0,11		0,16
		11 Störreberg						0,24
		12 Svälte				0,01		0,26
Värmland	Flooded	13 Ikea	0,35	0,30		0,49	0,36	0,71
		14 Fintatorp	0,35	0,30		0,49	0,36	0,71
		15 Väse Gamla E18	0,33	0,30		0,44	0,55	0,64
		16 Strandvägen						
		17 Kristinehamn E18						
		18 Lagmansgatan						
	Non-Flooded	19 Östra Ringvägen						
		20 Skattkärrsmotet	0,33	0,30		0,44	0,55	0,64
		21 Solberg	0,33	0,30		0,44	0,55	0,64
		22 Silkesta	0,33	0,30		0,44	0,55	0,64
		23 Karlabron						
		24 Sorkan						
		25 Väsemotet	0,33	0,30		0,44	0,55	0,64
		26 Björkebol						
		27 Heden						
		28 Bymon	0,33	0,30		0,44	0,55	0,64
		29 Gunnerud	0,33	0,30		0,44	0,55	0,64
		30 Kappstad	0,33	0,30		0,44	0,55	0,64
		31 Öckna	0,33	0,30		0,44	0,55	0,64
32 Östervik								
33 Spånga	0,33	0,30		0,44	0,55	0,64		

4.4 Sediment connectivity results

From the calculations in SedInConnect 2.3 the following IC result was obtained. The input DEM for all calculations is the reconditioned DEM with no lakes and is corrected for culverts and sinks, so that the water pathway is more realistic and can cross the road, and no false accumulations of water and sediment. The input target is for all calculations the roads with a 4-meter buffer. All background calculations and further instructions of the calculations, see Appendix B.

4.4.1 The different IC calculations

Here follows a short description of each calculation and all results can be seen in Table 11. Higher values indicate high capacity of sediment delivery and thus connected catchments, while low values correspond to catchments that are less connected.

IC by (Cavalli et al., 2013) with reconditioned DEM

This calculation is based on the weight of the Roughness index (RI), as the original method of Cavalli et al. (2013). It is highly dependent on the topography of the area and follows the patterns of changed slopes. There are higher IC values for steeper areas, and lower values for flat surfaces.

IC weighted on soil moisture 25 km

This calculation has the ASCAT 25 km resolution soil moisture layer as a weighting factor instead of the roughness index. When comparing with IC by Cavalli et al. (2013), it can clearly be seen that all IC values are lower when soil moisture is the weight.

IC combined (Cavalli et al., 2013) and soil moisture 25 km

This calculation combines the weighting factor of roughness index with the weighting factor of soil moisture 25 km. Namely, a combination of the two previous IC calculations. The

difference between the IC results only weighted on soil moisture and the combined one with surface roughness is minimal.

IC weighted on soil moisture 1 km

This calculation instead uses the ASCAT 1 km resolution soil moisture layer as a weighting factor. This calculation is only performed for Värmland, as no data exists for Västra Götaland from the 1 km product. Here there are larger differences between the catchments in soil moisture content as the spatial resolution of the pixels are smaller. Generally, there are higher IC values for the 1 km calculation compared to the 25 km calculation. However, the difference is in average 0.03, which is very small.

IC combined (Cavalli et al., 2013) and soil moisture 1 km

This calculation combines the weighting factor of roughness index and the weighting factor of soil moisture 1 km. This calculation is only performed for Värmland, as no data exists for Västra Götaland from the 1 km product. Again, the values are somewhat lower for the combined calculation than with only the soil moisture as weighting factor.

Table 11. Result of Sediment Connectivity calculations with soil moisture (SM).

Sediment connectivity (IC)		Location	IC Cavalli, AgreeDEM	IC SM 25km	IC Cavalli and SM 25km	IC SM 1km	IC Cavalli and SM 1km	
			IC Max values	IC Max values	IC Max values	IC Max values	IC Max values	
Västra Götaland	Flooded	1 Hogstorpsmotet	2,39	2,22	2,21			
		2 Småröd	2,55	2,38	2,37			
		3 Säleby	2,38	2,16	2,15			
		4 Båthammen	2,26	2,05	2,04			
	Non-Flooded	5 Älvbacken	2,63	2,39	2,39			
		6 Bro	2,48	2,20	2,19			
		7 Gravröse	2,34	2,16	2,15			
		8 Hällkista	2,17	1,96	1,95			
		9 Holmen	1,50	1,34	1,33			
		10 Korpås	2,08	1,91	1,90			
		11 Störreberg	2,65	2,39	2,38			
		12 Svälte	2,33	2,11	2,10			
Värmland	Flooded	13 Ikea	2,00	1,89	1,88	1,91	1,90	
		14 Fintatorp	1,85	1,74	1,73	1,76	1,75	
		15 Väse Gamla E18	0,21	0,18	0,12	0,24	0,18	
		16 Strandvägen	2,05	1,99	1,97	1,98	1,97	
		17 Kristinehamn E18	-4,09	-4,18	-4,23	-4,16	-4,21	
		18 Lagmansgatan	-5,49	-5,59	-5,63	-5,59	-5,64	
		19 Östra Ringvägen	2,75	2,69	2,68	2,71	2,70	
		Non-Flooded	20 Skattkärrsmotet	2,13	2,03	2,02	2,07	2,07
			21 Solberg	1,72	1,63	1,62	1,66	1,65
	22 Silkesta		2,10	2,01	2,00	2,07	2,06	
	23 Karlabron		2,31	2,25	2,24	2,26	2,25	
	24 Sorkan		2,64	2,57	2,56	2,62	2,61	
	25 Väsemotet		2,01	1,94	1,93	2,00	1,99	
	26 Björkebol		-4,70	-4,82	-4,85	-4,83	-4,85	
	27 Heden		0,58	0,53	0,50	0,42	0,40	
	28 Bymon		1,99	1,88	1,87	1,94	1,93	
	29 Gunnerud		1,70	1,59	1,58	1,67	1,66	
	30 Kappstad	0,94	0,85	0,83	0,93	0,92		
	31 Öckna	1,60	1,50	1,48	1,54	1,53		
32 Östervik	2,34	2,27	2,26	2,30	2,29			
33 Spånga	1,68	1,58	1,57	1,65	1,64			

4.4.2 Site specific results of IC

The catchment of Östra Ringvägen is interesting from several perspectives. When analyzing the IC results, it can be identified that the catchment of Östra Ringvägen is the one with the highest IC values in all calculations (Table 11). This is most likely due to the large slope of 4,4%, which is the main factor that influences the roughness index in IC by Cavalli et al. (2013) and by the high soil moisture content.

The main soil type is till (42%) and peat (22%), while the land use is mainly forest. However, the lower part of the catchment, where the flooding occurred, is urban areas with the highway E18 passing. In the catchment of Östra Ringvägen several road-stream intersections became flooded, and as earlier mentioned in chapter 4.1 about the road drainage structures, both the bridge at Östra Ringvägen and at Rådmansgatan was destroyed in the flood event.

There is a clear distinction between the high and low IC values as the high values are in the lower part of the catchment, closer to the road (Figure 17A). A comparison between the combined results IC (Cavalli et al., 2013) and soil moisture 25 km and the combined 1 km result show similar results for the entire catchment, with only 0.02 difference (Table 11). However, when looking at the lower part of the catchment where the flooding occurred some differences can be identified (Figure 17, B and C). There are higher IC values between Rådmansgatan and Östra Ringvägen in the 25km results (B) than in the 1 km results (C). This is most likely due to the differences in soil moisture content from the extraction, where the soil moisture content is higher in the 25 km product than in the disaggregated 1 km product. The soil moisture values can be seen in figure 17D, E and F.

Östra Ringvägen catchment IC and Soil Moisture

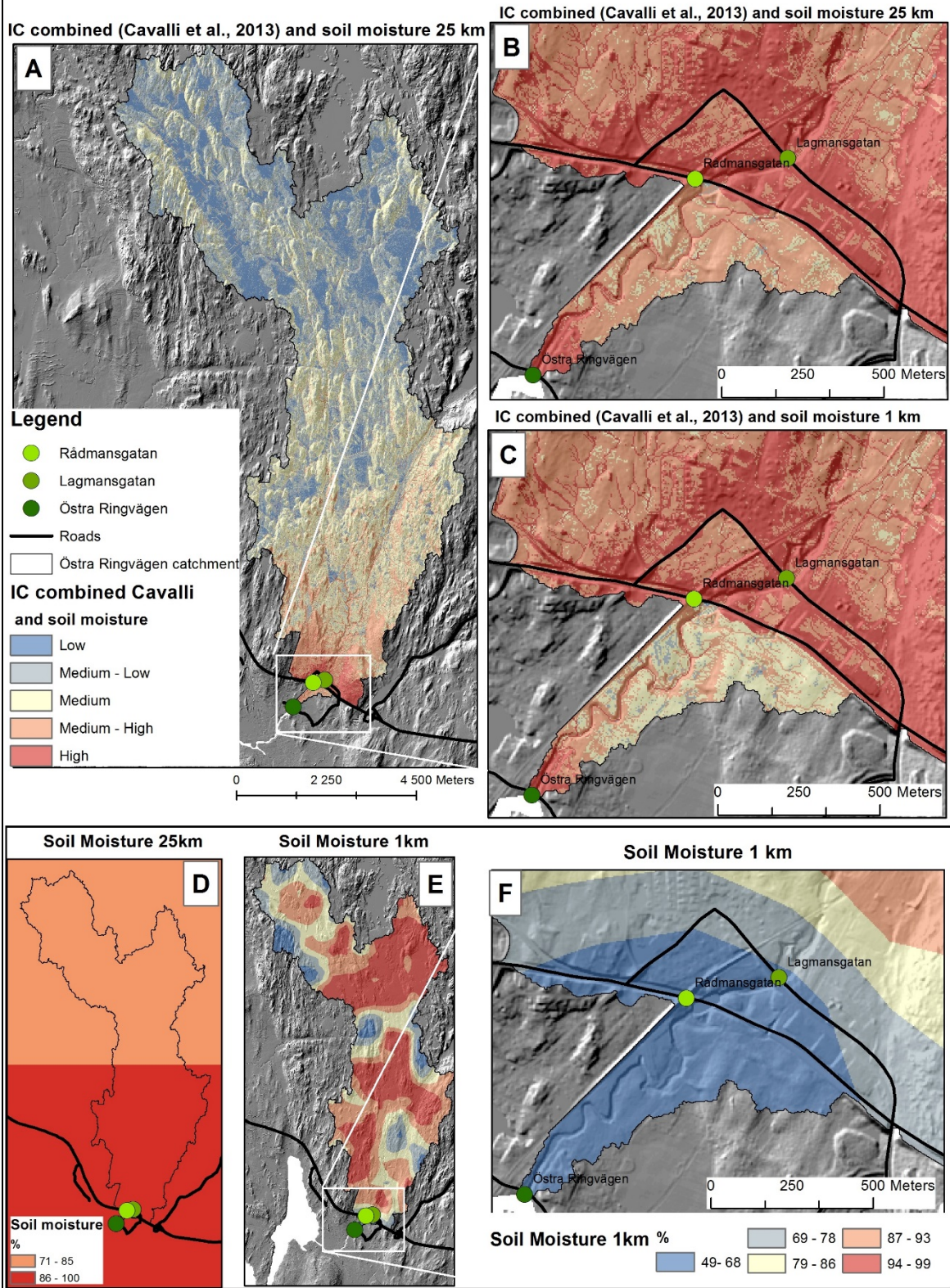


Figure 17. IC calculations with IC (Cavalli et al., 2013) and soil moisture for the catchment of Östra Ringvägen, Värmland. A, IC Combined (Cavalli et al., 2013) and soil moisture 25km for the whole catchment. B, IC Combined (Cavalli et al., 2013) and soil moisture 25km for the flooded points. C, IC Combined (Cavalli et al., 2013) and soil moisture 1km for the flooded points. D, Soil moisture from ASCAT 25km. E, Soil moisture from ASCAT 1km. F, Soil moisture from ASCAT 1km for the flooded points

5 DISCUSSION

This section analyzes the results of the study. At first, a comparison between PCDs, precipitation and soil moisture is performed. Secondly, a discussion about the results from the sediment connectivity calculations, followed by a comparison between different methods. Further, a discussion about the validation and application of satellite data and finally limitations and possibilities with the methods used.

5.1 Comparison between PCDs, precipitation and soil moisture

This chapter discuss the different physical catchment descriptors (PCDs) that have been investigated, connects it to soil moisture and includes a discussion about the contribution to the flooding. The soil moisture values used in the discussion is from the ASCAT 25 km resolution satellite as it is valuated as the most reliable one considering temporal and spatial resolution, and the comprehensive research using it. All values are from Appendix A, if nothing else is stated.

5.1.1 Västra Götaland

Västra Götaland has rock and clay as dominating soil types, and forest and agriculture as main land uses. Two of the flooded areas, Säleby and Båthammen has higher percentage of agriculture with 59% and 41% respectively, and clay as dominating soil with 71% and 60% respectively. These areas have lower soil moisture than the average, however, the fine grain size of the clay should be able to keep a higher soil moisture. The two other flooded areas in Västra Götaland, Hogstorpsmotet and Småröd has rock as main soil type and forest as land use. These areas have higher soil moisture, and one reason for this could be that the roots of the trees keep moisture to a larger extent. However, there is no difference in average soil moisture or precipitation between flooded and non-flooded areas.

All flooded areas have relatively small catchment size, higher slope values and around the same drainage density. The non-flooded areas have one large catchment, Älvbacken, which also has a high drainage density. The large catchment of Älvbacken could have been in risk of flooding, but the precipitation was low and thus the soil moisture. Furthermore, the road-stream intersection also had a larger bridge that lead the water under the road (Appendix C).

5.1.2 Värmland

Four out of seven flooded areas have till as the dominant soil type and a low percentage of clay. These areas are all located in the central Kristinehamn. Two of the other flooded areas has rock as the dominant soil type and clay as second, and the last flooded area has 78% sand. All areas are dominated by forest and has a high soil moisture content between 73 and 86% the 21st of August. There is only a small difference in average soil moisture considering both flooded and non-flooded areas, where the flooded areas have 3% more soil moisture.

Two of the flooded areas in Värmland had very large catchments, Lagmansgatan (59km²) and Östra Ringvägen (63km²). Although, these areas have somewhat lower drainage density than the rest of the flooded areas in Värmland (17 m/ha compared to the average of 19,8 m/ha). Several of the flooded points have large slopes compared to the non-flooded areas. The non-flooded areas have generally smaller catchment size, except Sorkan with 46km², and a lower average drainage density of 16 m/ha. The non-flooded catchment Sorkan is interesting to consider as it has a large catchment size, relatively high drainage density of 17,8 m/ha, 1% slope, clay and till as main soil type and agriculture as land use. It has a high soil moisture of

84,5% and received 26 mm of precipitation during 3 hours. According to these conditions it should have been flooded, however, a large bridge is located by the road-stream intersection which leads away the water (Appendix C).

5.1.3 Summary

From the comparison between the flooded and non-flooded areas seen to PCDs, precipitation and soil moisture several conclusions can be made. Although, the small amount of areas investigated decreases the validity of the result.

- Larger slope generates more flooding. The average for the flooded catchments in Värmland is 2,59% slope, and 1,33% for non-flooded. For Västra Götaland the flooded catchments have 1,25% and the non-flooded 0,98%.
- Larger drainage density generates more flooding. The flooded areas in Värmland has 3 m/ha more drainage density than the non-flooded. The number for Västra Götaland is 2 m/ha more drainage density for the flooded.
- Larger catchments size might lead to more flooding, but noting certain as too few catchments are included. It applies for Värmland, but not Västra Götaland in this case.
- No conclusion can be made from the soil type as all areas, flooded or non-flooded, in general has till or clay as main soil type. Same applies for the land use where almost all catchments have forest, both flooded and non-flooded.
- The precipitation is in average the same for flooded and non-flooded areas. Less precipitation can lead to flooding.
- More precipitation gives in most cases higher soil moisture values, but that might not generate more flooding.

The precipitation amounts in Västra Götaland, and thus the soil moisture content, was low the days before the flooding. These small amounts should not have made the soil saturated before the increase in precipitation the 19th that caused the flooding. However, depending on the soil type and other preconditions in the catchment, several days with precipitation might had an impact when the intense rainfall occurred, and thus creating the flood.

Kristinehamn in Värmland had high soil moisture content, although a somewhat lower precipitation, but a lot of impermeable surfaces and a lack of sufficient road drainage structures. This was most likely the reason for the flooding in this area. In several cases could the occurred flooding rather depend on sediment and water that have impeded culverts than the amounts of precipitation. With the clogging of culverts by sediment, the consequences with increased precipitation gets severe impacts. Furthermore, the high IC values of this catchment (Chapter 4.4.2) also indicates that large amounts of water and sediment can be transported through the catchment.

5.2 Sediment connectivity index

To use the index of sediment connectivity in flood prediction studies contribute with a relative evaluation of how sediment is moving within a catchment depending on the used input factors. It is a method to identify parts of the catchment that works as storage, or as discharge areas, to assess the risk of accumulation. Although, it is not an absolute measurement. Higher values of IC indicate a higher capacity of sediment delivery and more connected catchments, and thus more water and sediments that flows towards the outlet with clogging of drainage facilities as a result. It is therefore interesting to investigate whether the sediment connectivity reflects the occurrence of the flooding in 2014.

The flooded areas in Västra Götaland has high IC values, however, several of the non-flooded also has high values. The IC values in Värmland are much lower, despite the fact that the slope and the soil moisture content in general are higher there compared to Västra Götaland. Although, low IC values can also mean a risk as water and sediment then accumulate at specific locations. It can be concluded that the addition of soil moisture to the original IC calculations by Cavalli et al. (2013), somewhat lowers the IC (Table 11).

5.3 Comparison of flood prediction methods

In this section a comparison between the results of this study and earlier results from the research by Michielsen (2015) and Cantone (2016) is conducted.

When comparing the IC results between this study and the one by Cantone (2016) the results show a good correlation (Appendix E). However, there are some issues with the comparison for a few locations as the values are different and do not correlate. The reason to this is unknown at the moment, however, it might depend on the chosen layer for the catchment statistics. It is mainly the areas of Kristinehamn E18, Lagmansgatan and Björkebol that has large minus values, while all other areas have positive values. Nevertheless, it is a low percentage of error, but it still affects the reliability of the result. When comparing the IC by Cantone (2016), which includes precipitation, land use and soil type as weighting factor (column IC_q in Appendix E), and the soil moisture as weighting factor in the IC results of this study, it can be concluded that the soil moisture increases the IC values. However, the general trend of which areas that are identified with high values are almost exactly the same (Appendix E).

When comparing the identified flood prone areas based on IC and soil moisture, with the statistical results of the PCD calculation by Michielsen (2015), a good correlation can be seen. The catchment area of Östra Ringvägen (Chapter 4.4.2 and Figure 16), had the highest IC results and high soil moisture values, and the 3 flooded points within the catchment was also identified as in high risk of flooding by Michielsen (2015). This further contributes and enhances the development of a reliable flood prediction tool.

5.4 Application and validation of remote sensing data

This chapter discuss the difficulties with the application and validation of remote sensing data and addresses the possibilities with working with soil moisture data.

5.4.1 Application difficulties

To applicate satellite soil moisture data into for example flood prediction involves some difficulties concerning scientific and technical challenges. Many small and medium scale applications, considers the coarse resolution of 25-50 km that many of the soil moisture specific satellites, like ASCAT and SMOS, provides to not be sufficient. The first challenge thus includes to change the perception about the usefulness of these products and take them into account (Wagner et al., 2013). For example, studies made by Brocca et al. (2012) show that soil moisture data from ASCAT efficiently can be employed in small and medium catchments in flood prediction despite the coarse spatial resolution. The problem is to achieve a higher spatial resolution while maintaining a high temporal resolution. The disaggregation techniques that use external information to redistribute the soil moisture to a better spatial resolution is one promising approach (Kerr et al., 2010). For example, the ASCAT product that has been disaggregated from 25 km to a 1 km product or studies that disaggregate SMOS data (Merlin, Chehbouni, Kerr, & Goodrich, 2006; Merlin, Walker, Chehbouni, & Kerr, 2008;

Piles et al., 2014). However, the long-term availability of data also has an important role and in an application viewpoint the high temporal resolution of these sensors is a great advantage.

A general problem for remote sensing data is the presence of vegetation and its seasonal variability, and in cases of dense canopies the soil moisture retrievals will be less accurate. Surface roughness have an impact, topography that affects the angular measurements, snow and frozen soils induce some signals and urban areas are not fully assessed considering its emissivity (Kerr et al., 2010). For the SMOS satellite also the influence of radio frequency interferences (RFI) can have an impact of the retrieving result (Albergel et al., 2012; Kerr et al., 2010; Pierdicca et al., 2013). Another obstacle is that the presence of water within a measured pixel must be known to get an acceptable accuracy, although, water is variable and can change due to seasons, weather conditions and human activity (Kerr et al., 2010). Open water, with no disturbance of wind that generates roughness, acts like a mirror where no backscatter signal is generated, which is good for the retrieval of soil moisture (Gruber et al., 2013). If the water area is small compared to the area of the scatterometer footprint, it should not impact the retrieval of soil moisture. Nevertheless, in areas with large amounts of water, the soil moisture values will be affected (Bartalis, Naeimi, Hasenauer, & Wagner, 2008).

Furthermore, problems with validating different studies is a consequence from the lack of practices and standards when handling satellite data and thus no agreed values for retrieval errors. Which in turn causes problems for users when deciding which data is most suitable for the specific application. Currently available remote sensing measurements of soil moisture can for example only measure the top surface layer and some applications may require information about the entire unsaturated zone. If root zone soil moisture is required, in a depth of 1-1,5 m, satellite data are not sufficient. For observations of root zone soil moisture, the SWI (Soil Wetness Index) can instead be applied (Brocca et al., 2010). Especially in cases of low certainty of the initial conditions of soil moisture, can ASCAT together with SWI improve flood modelling. To use even lower frequencies could be an approach, but the spatial resolution would then be inappropriate and reduce its usability. Another indirect method could be assimilation of ground surface measurements and simulations (Kerr et al., 2010; Wagner et al., 2013).

5.4.2 Validating issues

Validation of the results obtained by remote sensing is challenging. At first, issues with sensing depth and scaling properties impede the interpretation. Secondly, soil moisture is a parameter that is highly variable in time and space, thus creating difficulties in comparing the irregular satellite measurements with reference data. Nevertheless, Crow et al. (2012) discuss the issue with the lack of reference data that represents the same physical quantity as the satellite measures. Problems with on ground measurements compared to satellites are both differences in spatial resolution, for example 50 km compared to point measurements, and the measuring depth as an installed probe measures at a larger depth than 5 cm. Also modelled soil moisture data are uncertain as parameters like precipitation and soil properties affects the outcome. The correlation between satellite measurements, models and in-situ data are therefore often low, or no correlation at all. However, this does not mean that the satellite data is bad. It could depend on not representative in-situ data for large areas, or lack in quality of the modelled data. The uncertainty factor in comparing and validating the results is thus an issue.

Nevertheless, several validation studies and comparisons between ASCAT and SMOS have been performed (Albergel et al., 2012; Fascetti et al., 2014; Lacava et al., 2012; Leroux et al.,

2014; Parrens et al., 2012; Pierdicca et al., 2013). Albergel et al. (2012) implies similar performance of ASCAT and SMOS with an estimated error of $0.08 \text{ m}^3\text{m}^{-3}$. Showing that the soil moisture retrieval capabilities of ASCAT are comparable with SMOS, despite the less suitable C-band measurements compared to the L-band of SMOS. Studies made by Parrens et al. (2012) also confirms this and further enhances the performance by ASCAT as the SMOS satellite are affected by Radio frequency interferences (RFI), which in turn can affect its outcome. The study also state that ASCAT correlates better with in situ observations and is less affected by topography.

After the conversion of the ASCAT saturation index into volumetric soil moisture in the study by Fascetti et al. (2014), the result shows good correlation (0.6) and a small bias of 1.2% between ASCAT and SMOS data. The consistency is dependent on land cover, season and geographical zone. When investigating the influence of land cover, and especially vegetation, areas with forest was disregarded from the SMOS product and the correlation then improved significantly to 0.7 (Fascetti et al., 2014). Also Leroux et al. (2014) finds a correlation close to 0.7 and Pierdicca et al. (2013) a degree of correlation of 0.67 and a small bias of 1.6%. Both Lacava et al. (2012) and Fascetti et al. (2014) concludes that ASCAT best identifies small scale temporal patterns and seasonal variations. While Brocca et al. (2011) implies that the accuracy goal of $0.04 \text{ m}^3\text{m}^{-3}$ is reached by the ASCAT sensor if the SWI is applied.

However, certain differences between the datasets might affect the results. Active and passive microwave sensors are linked in some ways considering surface emission, radar backscattering, and sensitiveness to the same parameters (soil roughness, vegetation and soil permittivity), but their relationship to soil moisture content are different (Pierdicca et al., 2013). The sampling depth differs, were SMOS has a deeper sampling depth, which may affect the temporal variability of soil moisture in relation to precipitation events. Topography, i.e. different slopes, affect the brightness temperatures values and thus the soil moisture retrieval of SMOS. The number of satellite observations that are available also affects the comparing result, as ASCAT has more available observations than SMOS due to the better temporal resolution. Despite the differences in measurement technique and microwave frequency, correlating results, particularly in wet conditions, was found to be consistent (Parrens et al., 2012). Also the result of Pierdicca et al. (2013) show consistency between the estimates of soil moisture between SMOS and ASCAT with the exception of desert areas. The consistency is also lower in association with complex topographic areas and areas with permanent snow cover. The ASCAT satellite is developed from the scatterometers on ERS-1 and ERS-2, and thus is more mature in comparison with other satellite products like SMOS (Wagner et al., 2013). The inclusion of both ASCAT and SMOS satellites in this study was made to validate the soil moisture values, which also showed a good correlation. Although, more research and technical development will further improve the satellite data.

5.4.3 Soil moisture retrievals from satellite data

Soil moisture has a high variability depending on scale and depth, and particular in the top surface layer that is measured by remote sensing techniques, as the top soil layer is affected by evaporation, vertical and lateral redistribution, topography on micro scale and varying soil properties (Wagner et al., 1999). Including soil moisture can thus be problematic. Nevertheless, as soil moisture is fundamental in the distribution of rainfall and infiltration within a catchment, the assimilation of soil moisture data into runoff prediction models can highly improve the estimations.

In opposition to conventional measurements methods, the use of remote sensing in estimating soil moisture content has the advantage that observations can be retrieved over a large area in a short time. The spatial distribution and frequency of the satellites enable daily to sub-daily measurement, and with the development of near real time retrievals, the capabilities of high quality soil moisture values increase.

The launch of specific soil moisture satellites, such as the SMOS satellite and the Soil Moisture Active Passive (SMAP) mission in 2015, with 36 km spatial resolution and 2 days' temporal resolution, demonstrates the importance of including soil moisture data. Other satellites under development are the FengYun-3 and the WindSat Polarimetric Radiometer, that are being employed for soil moisture (Brocca et al., 2017). One promising option is the Sentinel-1 satellites that is a SAR system with high resolution C-band data. The fine spatial resolution of 5-20 meters provides an attractive option for hydrological measurements at the catchment scale. The temporal resolution is 12 days, and with the two-satellites constellation its 6 days. Several studies examine the use of Sentinel-1 data for retrieving soil moisture data, and the results conclude that there is a high potential for global monitoring of surface soil moisture (Gruber et al., 2013; Hornacek et al., 2012; Petropoulos et al., 2015; Wagner et al., 2009). However, the launch of the Sentinel-1 mission was in April 2014, with full functionality in September 2014 and thus not applicable to this study. Although, for future studies in the area the Sentinel-1 mission is likely relevant and with high potential.

5.5 Limitations and possibilities with the methods used

This chapter summarizes the limitations and possibilities with the methods that are used in this study.

5.5.1 Limitations

The limitations of using remote sensing soil moisture data;

- There are some limitations with the use of satellite data to derive soil moisture. At first, the large resolution of 25 and 50 km might limit the ability of detailed small scale application. The measurement depth of 5 cm can be a limitation depending on the purpose of the extraction and the coverage is varying. The northern latitudes of Sweden restrict the use of satellite data as the retrieval errors increases.
- The measurements are sensible to disrupting signals from for example vegetation, water and topography, which might increase the error factor and impact the derived result.
- The use of satellite data is relatively new in these applications and the validation processes are therefore not as developed as desired. More validation of the data is needed to ensure accurate and reliable results.
- The ASCAT satellite has a temporal resolution of 1.5 day, which means that the measurements can be done on the morning one day and in the evening another day. This affects the results, as for example evaporation during the day changes the values. However, with sufficient precipitation data available, this can be taken into account.
- The disaggregated 1 km soil moisture product from ASCAT is an important contribution to the research, however, the reliability of the results can be questioned. Values are only provided if there is a sufficient temporal correlation between regional and local backscatter, and the temporal variations are driven by the 25 km product and then linearly scaled for each grid point. It is therefore usable for the spatial distribution, rather than temporal dynamics, as it uses static parameters. For this study, there were no available measurements for Västera Götaland, which restricted the use.

- Another challenge is the format and data volume, as large data sets and restricted knowledge of file formats might restrain the amount of users

Further, some limitations are identified with the other methods used:

- The radar precipitation data was processed in Matlab before it was imported to ArcMap for visualization. The most accurate precipitation values would have been if the precipitation per 15 minutes was calculated for each catchment. However, this was not possible due to the data format and thus the time needed to do these calculations.
- Neither the soil moisture values for ASCAT 1 km was calculated for the entire catchment due to technical issues and the time limit. For enhanced results, this should be performed.
- The restricted information about the location of road drainage structures smaller than 2 m in Sweden is a limitation to investigations like this. The knowledge about how water and sediment moves within a catchment in relation to the road infrastructure is essential for flood prediction. The reconditioned DEM used in the calculations of sediment connectivity was adjusted to ensure correct flow in relation to roads. However, with the knowledge about existing smaller road drainage structures, the result could have been more precise.

5.5.2 Possibilities

The possibilities identified during the study are presented below;

- The use of satellite data creates abilities to measure soil moisture at a global scale and with limited time needed. There is no need for time-consuming ground measurements and it decreases the costs of measuring.
- The near real time possibilities of satellite data opens up for investigations of for example soil moisture only a few hours after the measurements, which is an important factor when working with forecasting and prevention of flooding.
- The spatial and temporal consistency of space borne sensors creates a huge potential for retrieving reliable soil moisture values.
- With further development of satellites with better resolution and enhanced abilities to measure soil moisture characteristics, the input data quality will increase. Analyzing patterns of dynamic soil moisture will be enhanced with better spatial and temporal resolution and thus lead to more accurate results.
- The development of SedInConnect as a stand-alone open source application for calculating sediment connectivity index, independent from GIS software, creates possibilities and usability. This encourage usage by the scientific community and management authorities. Also no programming knowledge is required which widen the available users of the software. However, there are also the option to use the Connectivity toolbox imported to GIS if that is preferred.
- The sediment connectivity index (IC) is an important contribution to the research as it can be varied with several different input data, weights and targets to adapt it to the specific research aim. The inclusion of sediment connectivity, and in this case the contribution of soil moisture in the estimates of flood risk adds a new factor into the calculations.

CONCLUSION

The sediment connectivity index is a framework to assess temporal and spatial dynamics of sediment and to identify variables and processes to evaluate the connectivity within a catchment. The IC results show that the inclusion soil moisture decrease the IC compared to Cavalli et al. (2013) which takes surface roughness into consideration, but increases the IC compared to the results of Cantone (2016), which takes precipitation, land use and soil type into consideration (Appendix E). This implies further studies in the area to create the most suitable method for identifying factors that contribute to the flood risk.

The results of analyzing PCDs, precipitation and soil moisture show that larger slopes and drainage density in general means higher risk of flooding. Larger catchments might have an enhanced risk of flooding, but the result is uncertain as more locations should be investigated for a more validated result. No conclusion can be drawn from the soil type or land use, as it varies between the flooded areas. The precipitation is the same, however, it can be concluded that more precipitation in most cases give higher soil moisture values. The lack of, or the dimensioning, of road drainage structures seems to have a large impact on the flood risk as more sediment and water can be accumulated at the road-stream intersection.

When choosing a sensor for extracting soil moisture values, the most important sensor characteristics are the spatial-temporal coverage, the radiometric accuracy and multiple-viewing capabilities. The spatial and temporal consistency of space borne sensors creates a potential for retrieving reliable soil moisture values. With an increased availability of satellites with enhanced resolution, the development of the retrieval algorithms and the validation networks, the opportunities for soil moisture data is increasing.

The methods assessed can be used together with other methods to strengthen and validate the results. It also needs to be tested on several different geographical regions as different conditions like soil type, land use, slope, catchment size and drainage density will affect the result and thus the reliability of the methods. Several different remote sensing techniques can be applied to identify the most suitable for extraction of the needed parameters and finally, to adapt the sediment connectivity calculations after the most important factors.

RECOMMENDATIONS

Roads can have an impact on the connectivity of the catchment through induced effects on flow paths, runoff, sediment transport and erosion. It is therefore essential to adapt the maintenance and planning both to increased flows of water, but also to an increase of the amount of roads that affect the natural flood patterns and acts like a barrier. With an increased development of roads more impacts are observed to water levels, flood extent, duration and velocity. At the same time are the implementation of drainage structure to allow water to pass under the roads essential, and also to identify and maintain current structures. Another option might be to increase the elevation of the roads and to create dykes that can protect the road infrastructure. Overall, the infrastructure network need to be constructed to minimize the damage, to avoid sediment and water to reach the roads and be handled as an induced potential of the flood risk.

To be able to prioritize and direct actions towards road sections that are in risk of flooding is important for the adaptation and maintenance. Cost effective protection against sediment and water movements are necessary to ensure a safe and resilient transport system. To look at the dimensioning of the drainage facilities as that could be identified as one contributing factor to the flooding in Kristinehamn is a good way to start. Important is to consider the whole water course and catchment, including all contributing culverts upstream, as can be seen in Östra Ringvägen catchment where several road-stream interactions were affected. The differences in dimensioning and maintenance of the drainage facilities might had an impact, and clogging of culverts and small dimensions affect the flow in the entire catchment. It is thus essential to adapt the dimensioning to future changes, where land use and climatic changes also are included, and not only adapt after simple static corrections.

Furthermore, recommendations are to also focus on the characteristics of the roads as road material, drainage efficiency, construction practices, location and age of the road all affect the flood risk. Soil moisture, temperature, slope, basin geology and precipitation characteristics further enhances the risk. Older roads located at stream intersections, in low land areas with medium slopes have been identified as gathering the most sediment, and thus in high risk of flooding.

To include soil moisture into flood prediction models is an important parameter, and will most likely be included in several future studies. SMHI is currently developing their research about flood risks in cities, and the high resolution radar precipitation data is a part of this project (SMHI, 2017b). The goal is to use the precipitation observations in real time to calculate the current soil moisture locally, and connect this to a detailed and high resolution hydrologic model. In this way can information of how water from a skyfall flows when it reaches the surface in cities be assessed, and thus predict fast increase in flow after heavy precipitation events. To develop the use of high resolution precipitation data and include several other parameters that has been identified as contributing factors to flooding is interesting considering the future increase in heavy precipitation and the increase of urban areas.

REFERENCES

- Albergel, C., de Rosnay, P., Gruhier, C., Muñoz-Sabater, J., Hasenauer, S., Isaksen, L., . . . Wagner, W. (2012). Evaluation of remotely sensed and modelled soil moisture products using global ground-based in situ observations. *Remote Sensing of Environment*, 118, 215-226. doi:10.1016/j.rse.2011.11.017
- Anderson, C., Figa, J., Bonekamp, H., Wilson, J. J. W., Verspeek, J., Stoffelen, A., & Portabella, M. (2012). Validation of backscatter measurements from the advanced scatterometer on MetOp-A. *Journal of Atmospheric and Oceanic Technology*, 29(1), 77-88. doi:10.1175/jtech-d-11-00020.1
- Arvidsson, A. K., Blomqvist, G., Erlingsson, S., Hellman, F., Jägerbrand, A., & Öberg, G. (2012). *Klimatanpassning av vägkonstruktion, drift och underhåll*. Retrieved from VTI rapport 771: https://www.vti.se/sv/Publikationer/Publikation/klimatanpassning-av-vagkonstruktion-drift-och-unde_670640
- Baartman, J. E. M., Masselink, R., Keesstra, S. D., & Temme, A. J. A. M. (2013). Linking landscape morphological complexity and sediment connectivity. *Earth Surface Processes and Landforms*, 38(12), 1457-1471. doi:10.1002/esp.3434
- Baghdadi, N., Aubert, M., & Zribi, M. (2012). Use of TerraSAR-X Data to Retrieve Soil Moisture Over Bare Soil Agricultural Fields. *IEEE Geoscience and Remote Sensing Letters*, May 2012, Vol.9(3), 512-516.
- Barrett, B. W., & Petropoulos, G. P. (2012). Satellite remote sensing of surface soil moisture. In *Petropoulos, G.P. (red) (2014). Remote sensing of energy fluxes and soil moisture content* (pp. 85-120): Boca Raton: CRC Press.
- Bartalis, Z., Naeimi, V., Hasenauer, S., & Wagner, W. (2008). *ASCAT soil moisture product handbook*. Retrieved from ASCAT Soil Moisture Report Series, No. 15, Institute of Photogrammetry and Remote Sensing, Vienna University of Technology, Austria.: https://publik.tuwien.ac.at/files/PubDat_219464.pdf
- Bartalis, Z., Wagner, W., Naeimi, V., Hasenauer, S., Scipal, K., Bonekamp, H., . . . Anderson, C. (2007). Initial soil moisture retrievals from the METOP-A Advanced Scatterometer (ASCAT). *Geophysical Research Letters*, 34(20). doi:10.1029/2007GL031088
- Bates, B. C., Kundzewicz, Z. W., Wu, S., & Palutikof, J. P. (2008). *Climate Change and Water. Technical Paper of the Intergovernmental Panel on Climate Change*. Retrieved from <http://www.ipcc.ch/pdf/technical-papers/climate-change-water-en.pdf>
- Beevers, L., Douven, W., Lazuardi, H., & Verheij, H. (2012). Cumulative impacts of road developments in floodplains. *Transportation Research Part D: Transport and Environment*, 17(5), 398-404. doi:10.1016/j.trd.2012.02.005
- Berg, P., Norin, L., & Olsson, J. (2016). Creation of a high resolution precipitation data set by merging gridded gauge data and radar observations for Sweden. *Journal of Hydrology*, 541, Part A, 6-13. doi:10.1016/j.jhydrol.2015.11.031
- Berthet, L., Andréassian, V., Perrin, C., & Javelle, P. (2009). How crucial is it to account for the antecedent moisture conditions in flood forecasting? Comparison of event-based and continuous approaches on 178 catchments. *Hydrology and Earth System Sciences*, 13(6), 819-831. doi:10.5194/hess-13-819-2009
- Bohuslänningen. (2014-08-21). Regnkaoset i Munkedal. Retrieved from <http://bohuslaningen.se/nyheter/munkedal/1.3370086-regnkaos-i-munkedal>
- Bonn, F., & Dixon, R. (2005). Monitoring flood extent and forecasting excess runoff risk with RADARSAT-1 data. *Natural Hazards*, 35(3), 377-393. doi:10.1007/s11069-004-1798-1

- Borselli, L., Cassi, P., & Torri, D. (2008). Prolegomena to sediment and flow connectivity in the landscape: A GIS and field numerical assessment. *CATENA*, 75(3), 268-277. doi:10.1016/j.catena.2008.07.006
- Bracken, L. J., & Croke, J. (2007). The concept of hydrological connectivity and its contribution to understanding runoff-dominated geomorphic systems. *Hydrological Processes*, 21(13), 1749-1763. doi:10.1002/hyp.6313
- Bracken, L. J., Turnbull, L., Wainwright, J., & Bogaart, P. (2015). Sediment connectivity: a framework for understanding sediment transfer at multiple scales. *Earth Surface Processes and Landforms*, 40(2), 177-188. doi:10.1002/esp.3635
- Brencic, M., Dawson, A., Folkesson, L., Francois, D., & Leitao, T. (2009). Chapter 12. Pollution Mitigation. In A. Dawson (Ed.), *Water in road structures - Movement, drainage & effects* (pp. 283-297). Dordrecht: Springer.
- Brimicombe, A. (2009). *GIS, Environmental Modeling and Engineering* (2 ed.). Boca Raton: CRC Press.
- Brocca, L., Crow, W. T., Ciabatta, L., Massari, C., de Rosnay, P., Enenkel, M., . . . Wagner, W. (2017). A review of the applications of ASCAT soil moisture products. *IEEE Journal of Selected Topics in Applied Earth Observations and Remote Sensing*, 10(5), 2285-2306.
- Brocca, L., Hasenauer, S., Lacava, T., Melone, F., Moramarco, T., Wagner, W., . . . Bittelli, M. (2011). Soil moisture estimation through ASCAT and AMSR-E sensors: An intercomparison and validation study across Europe. *Remote Sensing of Environment*, 115(12), 3390-3408. doi:10.1016/j.rse.2011.08.003
- Brocca, L., Melone, F., & Moramarco, T. (2008). On the estimation of antecedent wetness conditions in rainfall-runoff modelling. *Hydrological Processes*, 22(5), 629-642. doi:10.1002/hyp.6629
- Brocca, L., Melone, F., Moramarco, T., Wagner, W., Naeimi, V., Bartalis, Z., & Hasenauer, S. (2010). Improving runoff prediction through the assimilation of the ASCAT soil moisture product. *Hydrology and Earth System Sciences*, 14(10), 1881-1893. doi:10.5194/hess-14-1881-2010
- Brocca, L., Moramarco, T., Melone, F., Wagner, W., Hasenauer, S., & Hahn, S. (2012). Assimilation of surface- and root-zone ASCAT soil moisture products into rainfall-runoff modeling. *IEEE Transactions on Geoscience and Remote Sensing*, 50(7), 2542-2555. doi:10.1109/TGRS.2011.2177468
- Cantone, C. (2016). *Modelling sediment connectivity in Swedish catchments and application for flood prediction of roads*. (Master), Politecnico di Milano, Milano.
- Cavalli, M., Crema, S., & Marchi, L. (2014). *Guidelines on the Sediment Connectivity ArcGIS Toolbox and stand-alone application*. Retrieved from <http://www.sedalp.eu/download/tools.shtml>
- Cavalli, M., Trevisani, S., Comiti, F., & Marchi, L. (2013). Geomorphometric assessment of spatial sediment connectivity in small Alpine catchments. *Geomorphology*, 188, 31-41. doi:10.1016/j.geomorph.2012.05.007
- Copernicus. (2017). Soil Water Index. Retrieved 2017-06-03 from <http://land.copernicus.eu/global/products/swi>
- Crema, S., Schenato, L., Goldin, B., Marchi, L., & Cavalli, M. (2015). Toward the development of a stand-alone application for the assessment of sediment connectivity. *Rendiconti online della Società Geologica Italiana*, 34, 58-61. doi:10.3301/rol.2015.37
- Croke, J., Mockler, S., Fogarty, P., & Takken, I. (2005). Sediment concentration changes in runoff pathways from a forest road network and the resultant spatial pattern of

- catchment connectivity. *Geomorphology*, 68(3–4), 257-268.
doi:10.1016/j.geomorph.2004.11.020
- Crow, W. T., Berg, A. A., Cosh, M. H., Loew, A., Mohanty, B. P., Panciera, R., . . . Walker, J. P. (2012). Upscaling sparse ground-based soil moisture observations for the validation of coarse-resolution satellite soil moisture products. *Reviews of Geophysics*, 50(2). doi:10.1029/2011RG000372
- Crow, W. T., Bindlish, R., & Jackson, T. J. (2005). The added value of spaceborne passive microwave soil moisture retrievals for forecasting rainfall-runoff partitioning. *Geophysical Research Letters*, 32(18). doi:10.1029/2005GL023543
- Entekhabi, D., Njoku, E. G., O'Neill, P. E., Kellogg, K. H., Crow, W. T., Edelstein, W. N., . . . Van Zyl, J. (2010). The soil moisture active passive (SMAP) mission. *Proceedings of the IEEE*, 98(5), 704-716. doi:10.1109/JPROC.2010.2043918
- EO. (2017). SMOS (Soil Moisture and Ocean Salinity) Mission. Retrieved 2017-04-22 from <https://directory.eoportal.org/web/eoportal/satellite-missions/s/smos#footback20%29>
- Erlingsson, S., Brencic, M., & Dawson, A. (2009). Chapter 2. Water flow theory for saturated and unsaturated pavement material. In A. Dawson (Ed.), *Water in road structures - Movement, drainage & effects* (pp. 23-44). Dordrecht: Springer.
- ESA. (2017). How to obtain SMOS data. Retrieved from https://earth.esa.int/web/guest/missions/esa-operational-eo-missions/smos/content/-/asset_publisher/t5Py/content/how-to-obtain-data-7329 (Retrieved 2017-03-29)
- EUMETSAT. (2010). *H-SAF Product User Manual (PUM). SM-OBS-2 - Small-scale surface soil moisture by radar scatterometer*. Retrieved from <http://hsaf.meteoam.it/documents/PUM/PUM-08.pdf>
- EUMETSAT. (2017). ASCAT Soil Moisture at 25 km Swath Grid – Metop. Retrieved 2017-02-14 from [http://eoportal.eumetsat.int/discovery/Start/DirectSearch/Extended.do?f\(r0\)=EO:EUM:DAT:METOP:SOMO25](http://eoportal.eumetsat.int/discovery/Start/DirectSearch/Extended.do?f(r0)=EO:EUM:DAT:METOP:SOMO25)
- European Commission. (2007). *Green Paper EU: Adapting to climate change in Europe – options for EU action*. Retrieved from Green Paper from the Commission to the Council, the European Parliament, the European Economic and Social Committee and the Committee of the Regions COM(2007)354 final. European Commission, Brussels
- Fascetti, F., Pierdicca, N., Pulvirenti, L., & Crapolicchio, R. (2014, 24-27 March 2014). *ASCAT and SMOS soil moisture retrievals: A comparison over Europe and Northern Africa*. Paper presented at the Microwave Radiometry and Remote Sensing of the Environment (MicroRad), 2014 13th Specialist Meeting on (pp. 10-13). IEEE.
- Fitzjohn, C., Ternan, J. L., & Williams, A. G. (1998). Soil moisture variability in a semi-arid gully catchment: implications for runoff and erosion control. *CATENA*, 32(1), 55-70. doi:10.1016/S0341-8162(97)00045-3
- Fryirs, K. (2013). (Dis)Connectivity in catchment sediment cascades: a fresh look at the sediment delivery problem. *Earth Surface Processes and Landforms*, 38(1), 30-46. doi:10.1002/esp.3242
- Fryirs, K., Brierley, G., Preston, N., & Kasai, M. (2007). Buffers, barriers and blankets: The (dis)connectivity of catchment-scale sediment cascades. *CATENA*, 70(1), 49-67. doi:10.1016/j.catena.2006.07.007

- Gay, A., Cerdan, O., Mardhel, V., & Desmet, M. (2016). Application of an index of sediment connectivity in a lowland area. *Journal of Soils and Sediments*, 16(1), 280-293. doi:10.1007/s11368-015-1235-y
- Geodata. (2015). Geodata download. Retrieved 2017-03-25 from <https://www.geodata.se/geodataportalen/srv/swe/catalog.search;jsessionid=5739B6A294BA2FC61EE4DA7A4BA2369E#/search?resultType=swe-details&type=dataset%20or%20series&from=1&to=20>
- Gruber, A., Wagner, W., Hegyiová, A., Greifeneder, F., & Schlaffer, S. (2013). *Potential of Sentinel-1 for high resolution soil moisture monitoring*. Paper presented at the Geoscience and Remote Sensing Symposium (IGARSS), 2013 IEEE International (pp. 4030-4033). IEEE.
- Hansson, K., Hellman, F., Grauert, M., & Larsen, M. (2010). *Methods to predict and handle flooding on highways. The blue spot concept* (181). Retrieved from <https://trid.trb.org/view.aspx?id=1256261>
- Hassaballa, A. A., Althuwaynee, O. F., & Pradhan, B. (2014). Extraction of soil moisture from RADARSAT-1 and its role in the formation of the 6 December 2008 landslide at Bukit Antarabangsa, Kuala Lumpur. *Arabian Journal of Geosciences*, 7(7), 2831-2840. doi:10.1007/s12517-013-0990-6
- Help, A. (2017). Cell size and resampling in analysis. Retrieved from <http://resources.arcgis.com/en/help/main/10.2/index.html#//018700000006000000>
- Hillel, D. (1998). *Environmental Soil Physics*. San Diego, CA: Academic Press.
- Holgersson, B., Hedlund, T., Ahlroth, S., Frost, C., Rosenqvist, P., & Thörn, P. (2007). *Sverige inför klimatförändringarna - hot och möjligheter* (SOU 2007:60). Retrieved from <http://www.regeringen.se/rattsdokument/statens-offentliga-utredningar/2007/10/sou-200760-/>
- Hornacek, M., Wagner, W., Sabel, D., Truong, H. L., Snoeij, P., Hahmann, T., . . . Doubkova, M. (2012). Potential for high resolution systematic global surface soil moisture Retrieval via change detection using Sentinel-1. *IEEE Journal of Selected Topics in Applied Earth Observations and Remote Sensing*, 5(4), 1303-1311. doi:10.1109/JSTARS.2012.2190136
- HSAF. (2017). Description: SM-OBS-1. Large scale surface soil moisture by radar scatterometer. Retrieved 2017-02-08 from <http://hsaf.meteoam.it/description-sm-obs-1.php>
- HSAF. (no year). *Satellite application facility on support to operational hydrology and water management*. Retrieved 2017-02-08 from <http://hsaf.meteoam.it/>: <http://hsaf.meteoam.it/documents/news/H-SAF-brochure.pdf>
- Hughes, G., Chinowsky, P., & Strzepek, K. (2010). *The costs of adapting to climate change for infrastructure*. Retrieved from Development and climate change discussion paper no 2: http://siteresources.worldbank.org/EXTCC/Resources/407863-1229101582229/DCCDP_2Infrastructure.pdf
- Jones, J. A., Swanson, F. J., Wemple, B. C., & Snyder, K. U. (2000). Effects of roads on hydrology, geomorphology, and disturbance patches in stream networks. *Conservation Biology*, 14(1), 76-85.
- Kalantari, Z., & Folkesson, L. (2013). Road drainage in Sweden: current practice and suggestions for adaptation to climate change. *Journal of Infrastructure Systems* 19, 147-156, [https://doi.org/10.1061/\(ASCE\)IS.1943-555X.0000119](https://doi.org/10.1061/(ASCE)IS.1943-555X.0000119)

- Kalantari, Z., Lyon, S. W., Jansson, P.-E., Stolte, J., French, H. K., Folkesson, L., & Sassner, M. (2015). Modeller subjectivity and calibration impacts on hydrological model applications: An event-based comparison for a road-adjacent catchment in south-east Norway. *Science of The Total Environment* **502**, 315-329, <https://doi.org/10.1016/j.scitotenv.2014.09.030>
- Kalantari, Z., Nickman, A., Lyon, S. W., Olofsson, B., & Folkesson, L. (2014). A method for mapping flood hazard along roads. *Journal of Environmental Management* **133**, 69-77, <https://doi.org/10.1016/j.jenvman.2013.11.032>
- Keesstra, S. D., Kondrlova, E., Czajka, A., Seeger, M., & Maroulis, J. (2012). Assessing riparian zone impacts on water and sediment movement: a new approach. *Netherlands Journal of Geosciences*, *91*(1-2), 245-255.
- Kerr, Y. H. (2007). Soil moisture from space: Where are we? *Hydrogeology Journal*, *15*(1), 117-120. doi:10.1007/s10040-006-0095-3
- Kerr, Y. H., Waldteufel, P., Richaume, P., Wigneron, J. P., Ferrazzoli, P., Mahmoodi, A., . . . Delwart, S. (2012). The SMOS soil moisture retrieval algorithm. *IEEE Transactions on Geoscience and Remote Sensing*, *50*(5), 1384-1403. doi:10.1109/TGRS.2012.2184548
- Kerr, Y. H., Waldteufel, P., Wigneron, J. P., Delwart, S., Cabot, F., Boutin, J., . . . Mecklenburg, S. (2010). The SMOS Mission: New tool for monitoring key elements of the global water cycle. *Proceedings of the IEEE*, *98*(5), 666-687. doi:10.1109/JPROC.2010.2043032
- Koetse, M. J., & Rietveld, P. (2012). Adaptation to climate change in the transport sector. *Transport Reviews*, *32*(3), 267-286. doi:10.1080/01441647.2012.657716
- Kornelsen, K. C., & Coulibaly, P. (2013). Advances in soil moisture retrieval from synthetic aperture radar and hydrological applications. *Journal of Hydrology*, *476*, 460-489. doi:10.1016/j.jhydrol.2012.10.044
- Kron, W., & Berz, G. (2007). Flood disasters and climate change: Trends and options - A (re-)insurer's view. in: Lozán, J. L., Grassl, H., Hupfer, P., Menzel, L., Schönwiese, C-Din: Lozán, J. L., Grassl, H., Hupfer, P., Menzel, L., Schönwiese, C-D. *Global Change: Enough water for all?* (pp. 268-273). Hamburg.
- Lacava, T., Brocca, L., Faruolo, M., Matgen, P., Moramarco, T., Pergola, N., & Tramutoli, V. (2012, 22-27 July 2012). *A multi-sensor (SMOS, AMSR-E and ASCAT) satellite-based soil moisture products inter-comparison*. Paper presented at the Geoscience and Remote Sensing Symposium (IGARSS), 2012 IEEE International (pp.1135-1138). IEEE.
- Lakshmi, V. (2013). Remote Sensing of Soil Moisture. *ISRN Soil Science*, *2013*, 33. doi:10.1155/2013/424178
- Lakshmi, V., Jackson, T. J., & Zehrhuhs, D. (2003). Soil moisture-temperature relationships: results from two field experiments. *Hydrological Processes*, *17*(15), 3041-3057. doi:10.1002/hyp.1275
- Larsson, R. (2008). *Jords egenskaper*. Retrieved from Swedish Geotechnical Institute: <http://www.swedgeo.se/globalassets/publikationer/info/pdf/sgi-i1.pdf>
- Lenderink, G., & van Meijgaard, E. (2008). Increase in hourly precipitation extremes beyond expectations from temperature changes. *Nature Geoscience*, *1*(8), 511-514. doi:10.1038/ngeo262
- Leroux, D. J., Kerr, Y. H., Bitar, A. A., Bindlish, R., Jackson, T. J., Berthelot, B., & Portet, G. (2014). Comparison between SMOS, VUA, ASCAT, and ECMWF soil moisture products

- over four watersheds in U.S. *IEEE Transactions on Geoscience and Remote Sensing*, 52(3), 1562-1571. doi:10.1109/TGRS.2013.2252468
- Lillesand, M. T., Kiefer, W. R., & Chipman, W. J. (2015). *Remote sensing and image interpretation* (7 ed.): Hoboken, N.J: Wiley.
- López-Vicente, M., Quijano, L., Palazón, L., Gaspar, L., & Navas, A. (2015). Assessment of soil redistribution at catchment scale by coupling a soil erosion model and a sediment connectivity index (central spanish pre-pyrenees). *Cuadernos de investigacion geografica*, 41(1), 21. doi:10.18172/cig.2649
- Merlin, O., Chehbouni, A., Kerr, Y. H., & Goodrich, D. C. (2006). A downscaling method for distributing surface soil moisture within a microwave pixel: Application to the Monsoon '90 data. *Remote Sensing of Environment*, 101(3), 379-389. doi:10.1016/j.rse.2006.01.004
- Merlin, O., Walker, J. P., Chehbouni, A., & Kerr, Y. (2008). Towards deterministic downscaling of SMOS soil moisture using MODIS derived soil evaporative efficiency. *Remote Sensing of Environment*, 112(10), 3935-3946. doi:10.1016/j.rse.2008.06.012
- Messenzehl, K., Hoffmann, T., & Dikau, R. (2014). Sediment connectivity in the high-alpine valley of Val Mütschans, Swiss National Park — linking geomorphic field mapping with geomorphometric modelling. *Geomorphology*, 221, 215-229. doi:10.1016/j.geomorph.2014.05.033
- Michielsen, A. (2015). *Modelling flood risk of transport infrastructure based on watershed characteristics*. (Master), Royal Institute of Technology, Stockholm. Retrieved from <http://www.diva-portal.org/smash/get/diva2:845071/FULLTEXT01.pdf>
- Michielsen, A., Kalantari, Z., Steve, L. W., & Liljegren, E. (2016). Predicting and communicating flood risk of transport infrastructure based on watershed characteristics. *Journal of Environmental Management* **182**, 505-518, <https://doi.org/10.1016/j.jenvman.2016.07.051>
- Moran, M. S., Peters-Lidard, C. D., Watts, J. M., & McElroy, S. (2004). Estimating soil moisture at the watershed scale with satellite-based radar and land surface models. *Canadian Journal of Remote Sensing*, 30(5), 805-826. doi:10.5589/m04-043
- Nigel, A., Chunzhen, L., Compagnucci, R., da Cunha, L., Hanaki, K., Howe, C., . . . Döll, P. (2001). *Chapter 4. Hydrology and Water Resources*. Retrieved from IPCC: <http://www.ipcc.ch/ipccreports/tar/wg2/index.php?idp=166>
- Njoku, E. G., Jackson, T. J., Lakshmi, V., Chan, T. K., & Nghiem, S. V. (2003). Soil moisture retrieval from AMSR-E. *IEEE Transactions on Geoscience and Remote Sensing*, 41(2), 215-229. doi:10.1109/TGRS.2002.808243
- Nordlander, H., Löfling, P., & Andersson, O. (2007). *Bilaga B1. Vägverkets rapport till Klimat- och sårbarhetsutredningen – gruppen transporter*. Retrieved from Stockholm: Klimat- och sårbarhetsutredningen SOU 2007:60: <http://www.regeringen.se/49bbad/contentassets/94b5ab7c66604cd0b8842fd6510b42c9/sverige-infor-klimatforandringarna---hot-och-mojligheter-bilagedel-b-forteckning-bilaga-b-28-31-sou-200760>
- Nya Kristinehamnsposten. (2014-08-21). Vattenkaos efter nattens skyfall. Retrieved from <http://nwt.se/kristinehamn/2014/08/21/vattenkaos-efter-nattens-skyfall>
- Olsson, J., & Foster, K. (2013). *Extrem korttidsnederbörd i klimatprojektioner för Sverige*. Retrieved from SMHI Klimatologi 6: http://www.smhi.se/polopoly_fs/1.29658!/Klimatologi_6.pdf

- Parrens, M., Zakharova, E., Lafont, S., Calvet, J. C., Kerr, Y., Wagner, W., & Wigneron, J. P. (2012). Comparing soil moisture retrievals from SMOS and ASCAT over France. *Hydrology and Earth System Sciences*, 16(2), 423-440. doi:10.5194/hess-16-423-2012
- Petropoulos, G. P., Griffiths, H., Dorigo, W., Xaver, A., & Gruber, A. (2013). Surface Soil Moisture Estimation. In: *Petropoulos G.P. (Ed.), Remote Sensing of Energy Fluxes and Soil Moisture Content* (pp. 29-48): Boca Raton: CRC Press.
- Petropoulos, G. P., Ireland, G., & Barrett, B. (2015). Surface soil moisture retrievals from remote sensing: Current status, products & future trends. *Physics and Chemistry of the Earth, Parts A/B/C*, 83–84, 36-56. doi:10.1016/j.pce.2015.02.009
- Pierdicca, N., Pulvirenti, L., Fascetti, F., Crapolicchio, R., & Talone, M. (2013). Analysis of two years of ASCAT-and SMOS-derived soil moisture estimates over Europe and North Africa. *European Journal of Remote Sensing*, 46(1), 759-773. doi:10.5721/EuJRS20134645
- Piles, M., Sánchez, N., Vall-Ilossera, M., Camps, A., Martínez-Fernández, J., Martínez, J., & González-Gambau, V. (2014). A downscaling approach for SMOS land observations: Evaluation of high-resolution soil moisture maps over the Iberian Peninsula. *IEEE Journal of Selected Topics in Applied Earth Observations and Remote Sensing*, 7(9), 3845-3857. doi:10.1109/JSTARS.2014.2325398
- Pulvirenti, L., Chini, M., Pierdicca, N., Guerriero, L., & Ferrazzoli, P. (2011). Flood monitoring using multi-temporal COSMO-SkyMed data: Image segmentation and signature interpretation. *Remote Sensing of Environment*, 115(4), 990-1002. doi:10.1016/j.rse.2010.12.002
- Refice, A., Capolongo, D., Pasquariello, G., D'Addabbo, A., Bovenga, F., Nutricato, R., . . . Pietranera, L. (2014). SAR and InSAR for flood monitoring: Examples with COSMO-SkyMed data. *IEEE Journal of Selected Topics in Applied Earth Observations and Remote Sensing*, 7(7), 2711-2722. doi:10.1109/JSTARS.2014.2305165
- Santinho Faisca, J., Baena, J., Baltzer, S., Gajewska, B., Nousianinen, A., Hermansson, Å., . . . Dawson, A. (2009). Chapter 13. Control of pavement water and pollution prevention. In A. Dawson (Ed.), *Water in road structures - Movement, drainage & effects*. Dordrecht: Springer.
- Saran, S., Sterk, G., Nair, R., & Chatterjee, R. S. (2014). Estimation of near surface soil moisture in a sloping terrain of a Himalayan watershed using ENVISAT ASAR multi-incidence angle alternate polarisation data. *Hydrological Processes*, 28(3), 895-904. doi:10.1002/hyp.9632
- Seneviratne, S. I., Corti, T., Davin, E. L., Hirschi, M., Jaeger, E. B., Lehner, I., . . . Teuling, A. J. (2010). Investigating soil moisture–climate interactions in a changing climate: A review. *Earth-Science Reviews*, 99(3–4), 125-161. doi:10.1016/j.earscirev.2010.02.004
- SGI. (2016). Jordarter. Retrieved 2017-03-10 from <http://www.swedgeo.se/sv/kunskapscentrum/om-geoteknik-och-miljogeoteknik/geoteknik-och-markmiljo/jords-hallfasthet/lera-och-kvicklera/>
- SGU. (2016). *Produkt: Jordarter 1:25 000 - 1:100 000*. Retrieved 2017-03-10 from Geological Survey of Sweden: <http://resource.sgu.se/dokument/produkter/jordarter-25-100000-beskrivning.pdf>
- SMAP. (2017). Soil Moisture - Dirt to Dinner. Retrieved 2017-04-17 from <https://smap.jpl.nasa.gov/classroom-activities/>

- SMHI. (2012). Hur förändras klimatet – Kraftig nederbörd. Retrieved 2017-02-26 from <http://www.klimatanpassning.se/hur-forandras-klimatet/nederbord/kraftig-nederbord-1.21297>
- SMHI. (2017a). Extrem punktnerbörd. Retrieved 2017-04-11 from <http://www.smhi.se/kunskapsbanken/meteorologi/extrem-punktnerbörd-1.23041>
- SMHI. (2017b). Prognoser för översvämningsrisk i städer utvecklas. Retrieved 2017-06-03 from <https://www.smhi.se/forskning/forskningsnyheter/prognoser-for-oversvamningsrisk-i-stader-utvecklas-1.115064>
- SMHI. (2017c). *Öppna Data - Meteorologiska observationer*. Retrieved 2017-04-11 from: <http://opendata-download-metobs.smhi.se/explore/>
- Step-ESA. (2017). Science toolbox exploitation platform. Retrieved 2017-03-29 from <http://step.esa.int/main/download/>
- Styffe, S. (2017-05-19). [Trafikverket].
- Suarez, P., Anderson, W., Mahal, V., & Lakshmanan, T. R. (2005). Impacts of flooding and climate change on urban transportation: A systemwide performance assessment of the Boston Metro Area. *Transportation Research Part D: Transport and Environment*, 10(3), 231-244. doi:10.1016/j.trd.2005.04.007
- Svenska Dagbladet. (2014-08-20). Känsligt läge i översvämningsland. Retrieved from <https://www.svd.se/kansligt-lage-i-oversvamningsland>
- Sveriges Radio. (2014-08-21). Regn och översvämningsdrabbar Värmland. Retrieved from <http://sverigesradio.se/sida/artikel.aspx?programid=83&artikel=5943235>
- SVT. (2014-08-20). Bohusbanan bortsköjd. Retrieved from <https://www.svt.se/nyheter/lokalt/vast/bohusbanan-bortskoljd?>
- SVT. (2014-08-21). Regnkaoset sprider sig. Retrieved from <https://www.svt.se/nyheter/lokalt/vast/regnkaoset-sprider-sig>
- SVT. (2014-10-14). Trumman som ska öppna vägen. Retrieved from <http://www.svt.se/nyheter/lokalt/varmland/trumman-som-ska-oppna-vagen>
- SVTnyheterVärmland. (2014-08-23). E18 avstängd i Karlstad. Retrieved from <https://www.svt.se/nyheter/lokalt/varmland/e18-avstangd>
- Tague, C., & Band, L. (2001). Simulating the impact of road construction and forest harvesting on hydrologic response. *Earth Surface Processes and Landforms*, 26(2), 135-151. doi:10.1002/1096-9837(200102)26:2<135::AID-ESP167>3.0.CO;2-J
- Tarboton, D. G. (1997). A new method for the determination of flow directions and upslope areas in grid digital elevation models. *Water Resources Research*, 33(2), 309-319. doi:10.1029/96WR03137
- Tarolli, P., & Sofia, G. (2016). Human topographic signatures and derived geomorphic processes across landscapes. *Geomorphology*, 255, 140-161. doi:10.1016/j.geomorph.2015.12.007
- Trafikverket. (2015). BaTMan - Bridge and Tunnel Management. Retrieved 2017-05-24 from <https://batman.vv.se/batman/logon/logon.aspx?url=https://batman.vv.se/batman/>.
- Trafikverket. (2016). *Handlingsplan för Trafikverkets klimatanpassningsstrategi. Förkortad version*. Retrieved from http://www.trafikverket.se/contentassets/177558982048461097bf6ede37614630/slutrappport_handlingsplan_klimatanpassning.pdf
- Trevisani, S., & Cavalli, M. (2016). Topography-based flow-directional roughness: potential and challenges. *Earth Surface Dynamics*, 4(2), 343-358. doi:10.5194/esurf-4-343-2016

- Wagner, W., Hahn, S., Figa, J., Albergel, C., de Rosnay, P., Brocca, L., . . . Dorigo, W. (2013). Operations, challenges, and prospects of satellite-based surface soil moisture data services In: *Petropoulos, G.P. (ed.), Remote Sensing of Energy Fluxes and Soil Moisture Content* (pp. 463-488): Boca Raton: CRC Press.
- Wagner, W., Lemoine, G., Borgeaud, M., & Rott, H. (1999). A study of vegetation cover effects on ERS scatterometer data. *IEEE Transactions on Geoscience and Remote Sensing, Vol 37(2)*, 938-948.
- Wagner, W., Lemoine, G., & Rott, H. (1999). A method for estimating soil moisture from ERS scatterometer and soil data. *Remote Sensing of Environment, 70(2)*, 191-207. doi:10.1016/S0034-4257(99)00036-X
- Wagner, W., Pathe, C., Doubkova, M., Sabel, D., Bartsch, A., Hasenauer, S., . . . Löw, A. (2008). Temporal stability of soil moisture and radar backscatter observed by the Advanced Synthetic Aperture Radar (ASAR). *Sensors, 8(2)*, 1174-1197.
- Wagner, W., Sabel, D., Doubkova, M., Bartsch, A., & Pathe, C. (2009). *The potential of Sentinel-1 for monitoring soil moisture with a high spatial resolution at global scale*. Paper presented at the Symposium of Earth Observation and Water Cycle Science.
- Wang, Y., Colby, J. D., & Mulcahy, K. A. (2002). An efficient method for mapping flood extent in a coastal floodplain using Landsat TM and DEM data. *International Journal of Remote Sensing, 23(18)*, 3681-3696. doi:10.1080/01431160110114484
- Wemple, B. C., Swanson, F. J., & Jones, J. A. (2001). Forest roads and geomorphic process interactions, Cascade Range, Oregon. *Earth Surface Processes and Landforms, 26(2)*, 191-204. doi:10.1002/1096-9837(200102)26:2<191::AID-ESP175>3.0.CO;2-U
- Vägverket. (2002). *Ökade vattenflöden - Behov av åtgärder inom väghållningen*. Retrieved from <http://www.trafikverket.se/Foretag/Bygga-och-underhalla/Vag/Tekniska-dokument/Bro-och-tunnel/Bro-och-tunnel---dokument/Okade-vattenfloden---Behov-av-atgarder-inom-vaghallningen/>
- Vägverket. (2008). *VVMB 310 Hydraulisk dimensionering*. Retrieved from Borlänge: https://trafikverket.ineko.se/Files/sv-SE/11208/RelatedFiles/2008_61_vvmb_310_hydraulisk_dimensionering.pdf
- Zhang, F., Zhu, X., & Liu, D. (2014). Blending MODIS and Landsat images for urban flood mapping. *International Journal of Remote Sensing, 35(9)*, 3237-3253. doi:10.1080/01431161.2014.903351

APPENDIX

APPENDIX A. PCD overview.

PCD overview is revised from Michlielsen (2015) with the addition of precipitation from radar measurements (Berg et al., 2016) and ASCAT 25km soil moisture (EUMETSAT, 2017).

Values for Västra Götaland: Precipitation evening of the 19th of August and soil moisture 19th of August.

Values for Värmland: Precipitation the night between 20th – 21st of August and soil moisture 21st of August.

PCD overview		Size	Elevation	Drainage	Channel	TWI	Road	Density	Gravel	Sand	Till	Peat	Clay	Rock	Urban	Agriculture	Grassland	Forest	Water & Wetland	Precipitation	Soil moisture	
		m ²	m	m/ha	Slope	%	m/ha	m/ha	%	%	%	%	%	%	%	%	%	%	%	mm	%	
Västra Götaland	Flooded	1	Högstörpmotet	3362236	108,60	2,60	24,90	28,58	0,39	10,11	18,12	5,43	15,64	52,23	0,00	16,53	14,56	66,49	2,40	28,07	70,73	
		2	Smaröd	18418544	109,83	0,80	28,91	25,68	1,35	4,64	9,36	12,00	17,90	53,23	0,45	16,27	6,39	70,78	6,14	15,99	70,73	
		3	Sälsby	8834056	51,92	0,40	22,34	35,88	0,00	2,61	0,00	0,43	71,47	25,46	6,30	59,12	9,75	24,84	0,00	7,42	52,75	
	Non-Flooded	4	Båtannen	2046056	55,67	1,20	20,22	33,73	0,00	0,00	0,21	0,00	60,12	39,65	5,01	41,18	7,70	46,25	0,00	26,92	50,58	
		5	Alvbacken	41230384	57,24	16,22	0,20	29,83	30,96	0,18	3,03	0,97	0,71	49,37	45,34	3,39	41,75	6,78	47,11	0,54	4,78	52,75
		6	Bro	2131576	63,94	16,11	1,50	24,63	28,26	0,00	0,00	0,00	2,43	27,42	69,87	0,00	17,36	1,00	81,81	0,00	21,06	48,40
		7	Gravöse	3409064	49,88	14,13	0,40	22,06	29,50	0,00	11,68	2,46	2,33	42,50	40,66	2,27	45,08	5,67	46,82	0,00	26,90	70,73
		8	Hällkista	1277272	39,86	11,47	0,40	24,63	30,22	0,00	6,07	4,89	14,04	13,75	59,40	0,05	18,64	24,03	55,59	1,76	42,61	70,73
		9	Holmen	424900	58,96	9,69	3,00	16,76	66,42	1,03	14,42	9,27	0,00	33,24	42,07	0,00	33,68	6,03	60,46	0,00	18,69	70,73
		10	Korpås	935860	65,05	12,51	0,60	25,36	34,30	0,67	11,82	23,37	0,00	38,33	26,11	8,15	35,33	8,35	48,35	0,00	19,55	70,73
		11	Storreberg	12997908	60,66	15,76	1,00	24,47	31,45	0,00	0,00	0,24	0,51	35,77	63,30	0,74	27,89	6,97	61,61	0,25	3,61	50,58
		12	Svätte	1187376	45,86	11,36	0,76	25,57	29,28	0,68	9,05	1,58	3,00	18,42	67,16	0,00	23,42	19,32	57,69	0,00	9,42	59,56
Värmland	Flooded	13	Ileka	6690884	67,01	18,87	0,60	29,19	31,78	0,40	18,45	12,12	1,69	25,62	41,71	13,02	12,22	16,23	58,58	0,00	0,30	72,89
		14	Fintorp	2952964	84,62	22,18	1,70	27,13	28,06	0,00	78,52	1,55	5,97	0,00	13,86	3,15	0,30	16,51	79,69	0,40	0,15	75,58
		15	Väse Gamla E18	6085292	74,58	16,59	1,92	26,97	22,64	0,64	14,45	6,25	7,17	25,47	45,95	0,00	12,62	21,79	61,82	3,81	32,24	77,74
		16	Strandvägen	2004196	98,53	23,84	4,00	20,02	31,98	3,52	7,83	52,48	11,51	1,19	23,05	8,54	0,00	12,19	75,15	3,90	30,89	86,58
		17	Kristinehamn E18	1828916	101,14	23,23	3,58	19,97	28,26	3,96	8,61	49,36	12,51	1,33	23,61	5,74	0,00	13,09	77,03	4,27	20,44	86,58
		18	Lagmansgatan	59689256	130,41	17,28	2,00	29,96	18,09	1,30	2,60	42,30	22,78	9,91	18,07	1,73	4,43	10,07	63,49	20,24	29,09	86,58
		19	Östra Ringvägen	63026964	128,32	17,40	4,40	29,96	19,41	1,28	2,71	42,66	22,20	10,20	18,08	2,74	4,38	10,35	63,22	19,31	24,27	84,59
		20	Skattkärrsmotet	11265216	81,42	19,28	0,90	30,35	19,87	0,22	8,11	18,99	37,46	11,06	24,12	0,40	9,84	10,67	52,96	26,15	14,71	72,89
		21	Solberg	1597188	68,38	19,62	1,40	24,81	20,32	0,00	2,93	22,19	18,31	11,66	45,24	0,00	20,31	15,34	52,59	12,17	46,95	72,89
		22	Silkesta	6433648	75,45	16,85	0,40	29,76	13,97	0,58	7,20	11,92	21,82	12,60	45,76	0,00	10,68	13,17	61,12	14,99	42,66	77,74
		23	Karlabor	22910276	132,78	19,06	1,60	29,36	25,02	2,74	7,43	57,38	12,90	7,02	12,00	2,86	6,19	16,23	69,95	4,78	25,75	86,58
		24	Sorkan	45809944	81,50	17,80	1,00	28,74	20,89	2,07	8,49	33,46	4,61	33,78	17,44	0,10	44,38	14,25	39,18	2,11	27,43	84,59
	25	Väsemotet	10003796	65,30	17,32	0,30	28,14	17,49	0,27	29,90	15,64	31,99	10,03	11,95	1,80	24,27	11,56	39,80	22,66	19,94	84,59	
	26	Björkebol	12607240	140,10	18,52	0,88	29,36	23,44	1,01	5,70	65,31	11,84	4,67	10,55	0,22	5,87	18,70	71,74	3,44	18,58	86,58	
	27	Heden	6656492	131,73	18,27	0,90	25,30	21,25	3,29	7,12	48,26	18,27	8,75	14,08	0,33	1,75	17,14	72,15	8,56	23,37	86,58	
	28	Bymon	2741396	87,95	15,23	1,08	26,53	9,47	0,46	0,87	39,87	9,76	16,44	32,58	0,00	10,94	29,34	57,18	2,69	2,65	72,89	
	29	Gunerud	4318884	80,10	14,18	1,84	17,97	26,03	0,00	17,37	40,95	0,00	9,70	31,98	0,00	14,62	17,08	68,88	0,00	2,71	72,89	
	30	Kapostad	5939888	79,70	16,68	2,10	28,67	14,92	1,70	16,97	28,69	13,69	13,83	25,06	0,00	22,82	14,89	55,19	7,04	3,15	72,89	
	31	Ockna	430520	5,58	5,28	2,10	21,15	22,21	5,95	43,26	13,50	0,00	9,58	28,31	0,00	13,65	2,18	85,36	0,00	1,86	72,89	
	32	Östervik	9384400	98,32	15,84	0,10	25,86	21,77	1,23	3,13	40,47	11,80	22,64	20,54	0,85	12,13	21,76	57,82	7,37	37,80	84,59	
	33	Spånga	409548	86,18	10,37	4,00	17,27	15,77	18,62	2,59	27,32	3,20	0,00	47,16	0,00	0,00	20,45	79,20	0,00	12,57	72,89	

PCD Calculations by Michielsen (2015)

Type	Physical catchment descriptor	Unit	Description	
Topography	1	Catchment size	m ²	The size of the upstream area draining to the road-stream intersection.
	2	Average catchment elevation	m	The DEM raster was clipped to the watershed boundaries and the average elevation within each catchment was then calculated.
	3	Drainage density	m/ha	Drainage density is defined as the total length of streams divided by the area of the watershed. First, the streams were clipped to the watershed boundaries and their total length was calculated [m]. Dividing the total length of the streams by the catchment area [ha] results in the drainage density [m/ha].
	4	Local channel slope	%	The local channel slope was calculated by identifying the elevation [m] at the road-stream intersection (z_1) and at a point 50 m up the stream (z_2). The local channel slope [%] was then calculated as $100 \cdot (z_2 - z_1) / 50$.
	5	Topographical wetness index	ln(m)	The TWI is a measure of water accumulation in a catchment and indicates for each point in the area its capability to develop saturated conditions (Beven, 2012). TWI can be calculated as $TWI = \ln[a(x) / \tan \beta(x)]$, in which $a(x)$ represents the local upslope area draining to a point x per unit contour length of that point x and $\beta(x)$ is the local slope in radians (Beven, 2012). High values of TWI are a result of a large contributing slope area or of a convergence of long slopes to the point (Beven, 2012). Based on this calculation, the resulting TWI raster was clipped to the watershed areas and the maximum TWI of the watershed was noted as PCD.
Roads	6	Road density	m/ha	All roads (including paths and bicycle lanes) and railways were clipped within the boundaries of each watershed and the total length [m] was then calculated. Dividing this result by the catchment area [ha] results in the road density [m/ha].
Soil type	7	Gravel	%	The different soil types in the soil layer (in vector format) were first reclassified into the following main categories: Gravel, sand, till, peat, clay, water, and rock. Next, the layer was clipped to the watershed extent and then converted from vector format to raster format. The percentage of each soil type within each watershed was then calculated and reported as PCD.
	8	Sand	%	
	9	Till	%	
	10	Peat	%	
	11	Clay	%	
Land use	12	Rock	%	The land use data for the study areas was reclassified into five main classes: Urban areas, agriculture, grassland, forest and water bodies and wetland. The share of each land cover type in the catchment area was then calculated.
	13	Urban land	%	
	14	Agriculture	%	
	15	Grassland	%	
	16	Forest	%	
	17	Water bodies and wetland	%	

APPENDIX B. Sediment connectivity index calculations

The calculations of the sediment connectivity index (IC) is either computed by using the *Connectivity Tool* in ArcGIS or the software SedInConnect developed by Crema et al. (2015). Both methods are free and requires the TauDEM tool that is also free of use. Both methods have been tried, however, all calculations used has been performed in SedInConnect 2.3, which has the advantage of being a stand-alone application, open source and not that time consuming. The dialogue window (Figure 18), were the calculations are operated from is easy to use and requires minimum input data. Here the Input DTM raster is chosen, targets and weights specified and the cell size stated. A detailed description can be found below (Cavalli et al., 2014).

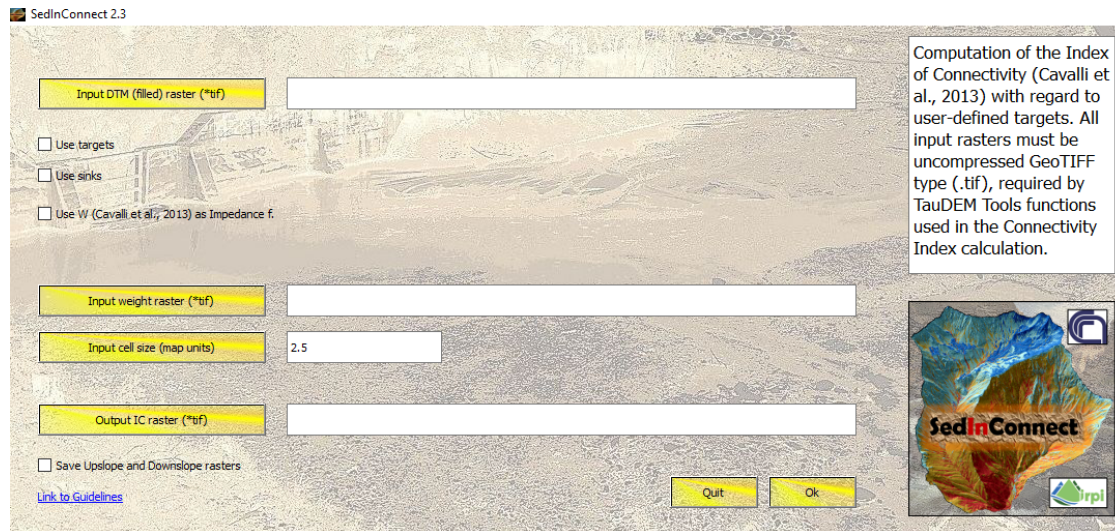


Figure 18. SedInConnect 2.3 dialogue window (Crema et al., 2015)

Input DTM (filled) raster (*.tif): A Digital Elevation model or a Digital Terrain model in TIFF format is used as the base data. To ensure correct results, pits that are depressions from the creation process of the DEM have to be removed. This can be done through Pit Remove in the ArcToolbox → TauDEMtools → Basic-Grid Analysis, to adapt the depressions.

Use Targets: If the calculations want to be focused on a specific target, like a road or catchment outlet, this target feature is applied. The target has to be a raster, however, if a polyline road layer is of interest a buffer can be created around it.

Use sinks: Decoupling of sink-draining areas

Use W (Cavalli et al., 2013 as impedance: This function automatically calculates the roughness index as weighting factor

Input weight raster (*.tif): Input of a weighting layer if another weighting factor is used

Input cell size: The cell size is determined and will be used to process all data. All input data need the same resolution.

Output IC raster (*.tif): Set folder and layer name of the output result.

Preparation of soil moisture layers:

ASCAT 25km

- 1, The soil moisture data from the ASCAT satellite with 25 km resolution has been reclassified to fit into the Sediment connectivity index. The values have been reclassified to present values between 0 and 1 with raster calculator. The original value range is between 0 and 100.
- 2, Then the function Con is used as no values can be 0 in IC calculations. The con is therefore set to $\leq 0,001$, will be 0,001 or else the same value as before
- 3, Then extract by mask to clip the area to the same extent as the DEM layer
- 4, To be able to run the index all input layers must have the same pixel size and the soil moisture layer was therefore resampled to a smaller pixel size. In the resampling process the bilinear approach has been used as it calculates every pixel value from the average of the 4 surrounding pixels. It is therefore suitable for continuous data (Help, 2017).
- 5, For the combination of weighting factors Map Algebra > Raster Calculator has been used with a simple multiplication of the layers

ASCAT 1km

- 1, For the 1km soil moisture the coordinate system had to be changed by using Project raster (WGS84 > Sweref99 TM) (layer name: sm1km_0_111_sw99), then could the extract by Mask (sm1km_mask) and Resampling (Sm1km_resampl2) be done
- 2, In the case of the 1 km soil moisture data there are values that are not valid above 100, by using the tool Set Null the values above 100 is set as NoData before the reclassification to 0-1 is done (Step 1 above)
- 3, Then the step 2,3,4 as above
- 4, To be able to use it in the IC calculations, there cannot be any areas with Nodata. Since the 1 km soil moisture data lack values at some parts the data must be interpolated to fill the gaps. This is done by using the interpolation method Heat Diffusion in-paint in Matlab, as it has better performance than for example IDW, spline and natural neighbor. The Heat Diffusion in-paint uses the DEM to fill the gaps of the soil moisture layer and takes more cells into consideration

IC Calculations

In all calculations, the agree_DEM model with no lakes and corrected for culverts/Sinks are used as INPUT DEM, and the TARGET is the roads (layer: Vagar_buff4m)

Step 1:

- Calculate surface roughness as a weight factor from the standard settings of Cavalli et al 2013 (layer name: Värmland= cavalla_surfrough, Västra Götaland = W_cavalli_rough_vg)
- Outcome: IC calculations from Cavalli et al. 2013 (layer name: Värmland = IC_Cavalli2, Västra Götaland = IC_cavalli_vg)

Step 2

- Use Soil moisture 25km ASCAT as weighting factor (layer name: Värmland= W_SMC_21aug_clip , Västra Götaland = W_SMC_19aug_vg)
- Outcome: IC calculations with Soil moisture 25km (layer name: Värmland = IC_Cavalli_SM, Västra Götaland= IC_SM_19aug_vg)

Step 3

- Combine weight roughness from Cavalli et al., 2013 and weight soil moisture 25 km by multiplication of the weight layers in ArcMap (layer name: Värmland= combined_w_rough_sm , Västra Götaland= W_com_r_sm_vg1)
- Outcome: IC calculations with the combination of weight factors (layer name: Värmland= IC_comb_rough_SM, Västra Götaland= IC_comb_R_SM_vg1)

Step 4 (Soil moisture 1 km)

- Calculate soil moisture from the 1 km ASCAT product. This is only possible for Värmland due to lack of data over Västra Götaland. Use Soil moisture 1km as weighting factor (layer name: W_sm1km)
- Outcome: IC calculations with 1 km soil moisture (layer name: IC_SM_1km_new)

Step 5 (soil moisture 1 km)

- Combine weight roughness from Cavalli et al., 2013 and weight soil moisture 1 km by multiplication of the weight layers in ArcMap (Layer name: W_comb_R_SM1km)
- Outcome: IC calculations with the combination of weight factors (layer name: IC_comb_r_1km)

APPENDIX C. Road drainage constructions from BaTMan (Trafikverket, 2015)

		SWEREF99TM				
		LOCATION	x	y	BaTMan	Google Maps
VÄSTRA GÖTALAND	Flooded	1 Hogstorpstötet	6474655	312167		The road consists of two separate driveways. Two culverts can be identified under one part of the road, and two under the other one, but no outlet can be seen on the other side (Figure 11)
		2 Kråkeröd	6479133	309379		The road is not visible
		3 Småröd	6480988	308678		Nothing can be seen except the railroad that passes underneath
		4 Sälaby	6487562	303768	Steel-soil composite bridge - 3.7m span width - 23m wide - built 1992	
		5 Båthamnen	6482531	305097		Nothing can be seen
	Non-Flooded	6 Älvbacken	6487535	300207	Road bridge - 11,7m span width - 10m wide - Built 1940	
		7 Bjälkebracka	6484990	297071		Nothing can be seen
		8 Bro	6481540	294895	Road bridge (Arch stone bridge) - 5,2m span width - 13m wide - built 1959	
		9 Gravröse	6471709	310282		Nothing can be seen
		10 Hällkista	6472391	308160		Nothing can be seen
		11 Holmen	6466578	316006		Nothing can be seen
		12 Korpås	6467189	315978	Steel-soil composite bridge (Arch stone bridge) - 9m span width - 43m wide	
		13 Skådene	6482457	295375	Road bridge - 4,9m span width - 13m wide - built 1996	
		14 Störreberg	6481962	295116	Road bridge - 4,9m span width - 13m wide - built 1992	
		15 Svälte	6471697	306662		Small culvert can be seen
VÄRMLAND	Flooded	16 Ikea	6583611	409847		A stone culvert can be seen, but it is overgrown (Figure 12)
		17 Fintatorp	6583608	408176		Nothing can be seen
		19 Väse Gamla E18	6587308	432947		Small culvert can be seen
		20 Strandvägen	6577155	448338		Nothing can be seen
		21 Kristinehamn E18	6577328	448641		Culvert can be seen
		22 Rådmandsgatan	6576416	450389	Road bridge (Steel-soil composite bridge) - 4m span width - 25m wide - Built 2012	
		23 Lagmansgatan	6576477	450592		Nothing can be seen. Looks overgrown
		24 Östra Ringvägen	6575815	449806	Road bridge - 5m span width - 1m wide (Old one, before the flooding)	
	Non-Flooded	25 Skattkärrsmotet	6586150	423175	Road bridge (frame bridge) - 14m span width - 12,8m wide	
		26 Solberg	6586253	429774	Road bridge - 29,6m span width - 4,5m wide	
		27 Silkesta	6585449	431031		Culvert can be seen, the dike is well-managed and the culvert is well placed
		28 Karlabron	6575407	450380	Road bridge - 5,3m span width - 16m wide	
		29 Sorkan	6582130	442685	Road bridge (Rigid-frame bridge) - 8,4m span width - 13m wide	
		30 Övre Kvarnmotet	6575717	451542	Road bridge - 3m span width - 54m wide - Somewhat overgrown on pictures	
31 Väsemotet		6583794	435484		Nothing can be seen	
32 Björkebol		6576575	452525	Road bridge (Low built Steel-soil composite bridge) - 3,3m span width - 12,1m wide		
33 Heden		6576245	452296		Culvert can be seen	
34 Bymon		6588526	420836		Snow on images	
35 Gunnerud		6587165	420972		Snow on images	
36 Kappstad	6590884	427395		Nothing can be seen. Looks overgrown		
37 Öckna	6591892	428021		Nothing can be seen. Looks overgrown		
38 Östervik	6579936	447001	Road bridge (circular Steel-soil composite bridge) - 2,2m span width - 56,9m wide - built 1950			
39 Spånga	6588318	426153		The road is located on a high bank with forest upstream and agriculture downstream. No culvert can be seen		

APPENDIX D. Soil moisture values ASCAT 25km, ASCAT 1km and SMOS 50km

The values are the days before, and the first day of the flooding (marked in the table). The flooding in Västra Götaland occurred between 19th – 20th of August 2014 and in Värmland 21st – 25th of August 2014.

Soil moisture	ASCAT 25 km					% Relative soil moisture					SMOS 50km					Unit: m ³ m ⁻³ Volumetric soil moisture											
	16-aug	17-aug	18-aug	19-aug	20-aug	16-aug	17-aug	18-aug	19-aug	20-aug	21-aug	16-aug	17-aug	18-aug	19-aug	20-aug	21-aug	16-aug	17-aug	18-aug	19-aug	20-aug	21-aug				
Västra Götaland	Flooded	1 Hogstorpsmotet	47,48	57,25	61,35	70,73	51,45	61,1	61,1	0,20																	
		2 Smäröd	47,48	57,25	61,35	70,73	51,45	61,1	61,1	0,11																	
		3 Sälaby	32,08	47,77	42,82	52,75	38,79	48,89	48,89	0,11																	
		4 Båthammen	37,16	44,7	41,84	50,58	40,81	57,95	57,95	0,11																	
	Non-Flooded	5 Älvbacken	32,08	47,77	42,82	52,75	38,79	48,89	48,89	0,11																	
		6 Bro	42,23	41,63	40,86	48,4	42,82	67,01	67,01																		
		7 Gravröse	47,48	57,25	61,35	70,73	51,45	61,1	61,1																		
		8 Hällkista	47,48	57,25	61,35	70,73	51,45	61,1	61,1																		
		9 Holmen	47,48	57,25	61,35	70,73	51,45	61,1	61,1	0,20	0,04	0,10															
		10 Korpås	47,48	57,25	61,35	70,73	51,45	61,1	61,1	0,20	0,04	0,10															
		11 Störreberg	37,16	44,7	41,84	50,58	40,81	57,95	57,95																		
		12 Svälte	44,86	49,44	51,11	59,56	47,14	64,01	64,01																		
Värmland	Flooded	13 Ilea	59,15	84,02	72,1	84,1	63,77	72,89	72,89	67,6	87,6	63,8	82,6	82,6	0,35	0,30	0,36	0,35	0,30	0,30	0,49	0,36	0,71	0,71	0,71		
		14 Fintatorp	64,44	80,79	67,7	84,15	65,63	75,58	75,58	56,1	79,1	61,9	69	69	0,35	0,30	0,49	0,36	0,30	0,30	0,44	0,55	0,64	0,64	0,64		
		15 Våse Gamla E18	66,5	79,73	74,5	91,41	69,83	77,74	77,74	72,5		83,1	95	95	0,33	0,30											
		16 Strandvägen	60,7	75,46	64,64	81,54	65,44	86,58	86,58	64,2		72	86,1	86,1													
	Non-Flooded	17 Kristinehamn E18	60,7	75,46	64,64	81,54	65,44	86,58	86,58	63,9		71,5	85,6	85,6													
		18 Lagmansgatan	60,7	75,46	64,64	81,54	65,44	86,58	86,58	45,3		59,4	71,8	71,8													
		19 Östra Ringvägen	67,28	75,46	70,77	90,13	70,67	84,59	84,59	51,1		57,3	69	69													
		20 Skartkärrsmotet	59,15	84,02	72,1	84,1	63,77	72,89	72,89	82,7	100	90	100	100	0,33	0,30	0,44	0,55	0,33	0,30	0,44	0,55	0,64	0,64	0,64		
		21 Solberg	59,15	84,02	72,1	84,1	63,77	72,89	72,89	100	100	100	100	100	0,33	0,30	0,44	0,55	0,33	0,30	0,44	0,55	0,64	0,64	0,64		
		22 Silkesta	66,5	84,02	74,5	91,41	69,83	77,74	77,74	94,7		34,2	41,3	41,3													
		23 Karlabron	60,7	75,46	64,64	81,54	65,44	86,58	86,58	30,5		84,2	100	100	0,33	0,30	0,44	0,55	0,33	0,30	0,44	0,55	0,64	0,64	0,64		
		24 Sorkan	67,28	75,46	70,77	90,13	70,67	84,59	84,59	94,2		79,6	93,4	93,4													
25 Väsemotet	67,28	75,46	70,77	90,13	70,67	84,59	84,59	70,1		88,2	100	100	0,33	0,30	0,44	0,55	0,33	0,30	0,44	0,55	0,64	0,64	0,64				
26 Björkebo	60,7	75,46	64,64	81,54	65,44	86,58	86,58	65,1		72,6	88,2	88,2															
27 Heden	60,7	75,46	64,64	81,54	65,44	86,58	86,58	73,4		82,1	99,7	99,7															
28 Bymon	59,15	84,02	72,1	84,1	63,77	72,89	72,89	92,3	100	98,8	100	100	0,33	0,30	0,44	0,55	0,33	0,30	0,44	0,55	0,64	0,64	0,64				
29 Gunnerud	59,15	84,02	72,1	84,1	63,77	72,89	72,89	74,8	96	80,2	91	91	0,33	0,30	0,44	0,55	0,33	0,30	0,44	0,55	0,64	0,64	0,64				
30 Kappstad	59,15	84,02	72,1	84,1	63,77	72,89	72,89	95,3	100	100	100	100	0,33	0,30	0,44	0,55	0,33	0,30	0,44	0,55	0,64	0,64	0,64				
31 Öckna	59,15	84,02	72,1	84,1	63,77	72,89	72,89	82,2	100	96,6	100	100	0,33	0,30	0,44	0,55	0,33	0,30	0,44	0,55	0,64	0,64	0,64				
32 Östervik	67,28	75,46	70,77	90,13	70,67	84,59	84,59	73,5		73,5	97,2	97,2															
33 Spånå	59,15	84,02	72,1	84,1	63,77	72,89	72,89	82	98,2	84,4	100	100	0,33	0,30	0,44	0,55	0,33	0,30	0,44	0,55	0,64	0,64	0,64				

APPENDIX E. IC results

The results of Cantone (2016) with addition of IC soil moisture (SM) calculations

Name		Flooding	IC _{Cavalli} max	IC _{Cavalli} and AgreeDEM max	IC _Q max	IC _{revised} Q _{linear} max	IC _{revised} Q _{sigmoid} max	IC SM 25km	IC Cavalli and SM 25km	IC SM 1km	IC Cavalli and SM 1km
Västra Götaland	Hogstorpstötet	1	2,39	2,39	1,62	0,68	1,83	2,22	2,21		
	Småröd	1	2,45	2,55	1,71	0,90	0,26	2,38	2,37		
	Säleby	1	2,37	2,37	1,51	0,54	-5,94	2,16	2,15		
	Båthamnen	1	2,25	2,25	1,26	0,52	-0,86	2,05	2,04		
	Älvbacken	0	2,73	2,74	1,80	0,99	-1,30	2,39	2,39		
	Bro	0	2,47	2,47	1,06	0,25	-7,84	2,20	2,19		
	Gravröse	0	2,34	2,34	1,52	0,77	-3,44	2,16	2,15		
	Hällkista	0	2,13	2,17	1,01	0,14	-0,79	1,96	1,95		
	Holmen	0	1,45	1,50	0,65	-0,04	-3,82	1,34	1,33		
	Korpås	0	2,17	2,07	1,37	0,56	-3,90	1,91	1,90		
	Störreberg	0	2,64	2,65	1,49	0,72	-2,87	2,39	2,38		
Svälte	0	2,29	2,33	0,99	0,19	-0,77	2,11	2,10			
Värmland	ikea	1	1,99	2,00	0,95	-1,58	0,59	1,89	1,88	1,91	1,90
	Fintatorp	1	1,84	1,85	0,66	-0,01	0,36	1,74	1,73	1,76	1,75
	VäseGamlaE18	1	2,15	1,54	1,14	-0,46	1,07	0,18	0,12	0,24	0,18
	Kristinehamn Strandvägen	1	1,33	1,41	0,23	0,69	0,00	1,99	1,97	1,98	1,97
	KirstinehamnE18	1	2,03	2,05	0,99	0,00	0,72	-4,18	-4,23	-4,16	-4,21
	Lagmansgatan	1	2,75	2,75	2,15	-0,92	2,09	-5,59	-5,63	-5,59	-5,64
	ÖstraRingvägenF	1	2,00	2,00	0,94	-0,16	0,64	2,69	2,68	2,71	2,70
	Skattkärrstötet	0	2,12	2,13	1,49	0,84	1,32	2,03	2,02	2,07	2,07
	Solberg	0	1,61	1,72	1,39	0,49	1,36	1,63	1,62	1,66	1,65
	Silkesta	0	2,08	2,10	1,69	0,33	1,63	2,01	2,00	2,07	2,06
	Karlabron	0	2,07	2,28	1,30	1,33	1,12	2,25	2,24	2,26	2,25
	Sorkan	0	2,63	2,64	1,95	1,12	1,74	2,57	2,56	2,62	2,61
	Väsestötet	0	2,01	2,01	1,54	0,41	1,48	1,94	1,93	2,00	1,99
	Björkebol	0	2,30	2,31	1,24	0,10	0,98	-4,82	-4,85	-4,83	-4,85
	Heden	0	1,79	1,77	0,81	-0,81	0,70	0,53	0,50	0,42	0,40
	BymonNF	0	1,98	1,99	1,29	-0,21	1,13	1,88	1,87	1,94	1,93
	GunnerudNF	0	1,69	1,70	0,80	0,84	0,43	1,59	1,58	1,67	1,66
	Kappstad	0	2,11	0,95	0,14	0,19	-0,22	0,85	0,83	0,93	0,92
	Öckna	0	1,55	0,59	0,66	0,10	0,32	1,50	1,48	1,54	1,53
	ÖstervikE18NF	0	2,33	2,34	1,53	0,65	1,32	2,27	2,26	2,30	2,29
SpångaNF	0	1,65	1,68	0,98	0,69	0,78	1,58	1,57	1,65	1,64	